ELSEVIER

Chemical Geology 233 (2006) 75–112

CHEMICAL GEOLOGY
INCLUDING
ISOTOPE GEOSCIENCE

www.elsevier.com/locate/chemgeo

Major, trace element and Nd–Sr–Pb–O–He–Ar isotope signatures of shield stage lavas from the central and western Canary Islands: Insights into mantle and crustal processes

A.A. Gurenko [a,*], K.A. Hoernle [a], F. Hauff [a], H.-U. Schmincke [a], D. Han [b], Y.N. Miura [b], I. Kaneoka [b]

[a] *IfM-GEOMAR Leibniz Institute for Marine Sciences, Dynamics of the Ocean Floor, Wischhofstraße 1-3, D-24148 Kiel, Germany*
[b] *Earthquake Research Institute, University of Tokyo, Bunkyo-ku, Tokyo 113-0032, Japan*

Received 19 October 2005; received in revised form 6 January 2006; accepted 14 February 2006

Abstract

The Canary plume is one of the few plumes that can be traced to the core–mantle boundary, making it an excellent location for studying mantle melting dynamics. We performed a comprehensive study of the subaerial shield stage lavas erupted on Gran Canaria, Tenerife, La Gomera and La Palma because these rocks are believed to have been formed by the greatest degree of partial melting of the source and thus can provide direct insights into the origin of plume material and deep crustal recycling. The most primitive picritic to alkali basaltic and basanitic shield stage lavas are moderately enriched in light rare earth elements ($[La/Sm]_n$=2.1–4.6), strongly enriched in Nb and Ta ($[Nb/La]_n$=0.8–1.5, $[Ta/La]_n$=1.3–1.8) and depleted in K and Pb ($[K/La]_n$=0.2–0.7; $[Pb/La]_n$=0.2–0.3), resembling HIMU-type magmas. Fractional crystallization and phenocryst accumulation are processes affecting the compositions of parental magmas. The Sr–Nd–Pb isotope data ($^{87}Sr/^{86}Sr$=0.702966–0.703312, $^{143}Nd/^{144}Nd$=0.512884–0.512929, $^{206}Pb/^{204}Pb$=19.49–20.27, $^{207}Pb/^{204}Pb$=15.59–15.66, $^{208}Pb/^{204}Pb$=39.21–39.81) and the relationship between Sr isotopes in whole rocks and O isotopes in olivine phenocrysts ($\delta^{18}O$=4.3–5.8±0.3‰) argue against extensive magma contamination at crustal depths. Varying, but relatively low, degrees of partial melting (1–10%) of a peridotite source containing 2–20% garnet can explain the Zr/Y range between 6.7 and 10.3 but require unrealistically high amount of garnet (up to 30%) to account for higher (up to 11.8) Zr/Y ratios in the lavas from Gran Canaria. This observation, as well as systematically lower CaO/Al_2O_3 ratios, higher SiO_2 and NiO contents at a given MgO in the Gran Canaria lavas, as compared with those from other Canary Islands, imply melting of a plume probably containing garnet-bearing recycled component in a form of eclogite. The presence of amphibole and/or phlogopite is essential to produce variations in Ba/Nb (3.6–7.7), Ba/Th (51–108), K/La (65–295) and Nb/U (42–85) ratios in the shield stage magmas. We propose a scenario in which the magmas are derived through partial melting of a plume probably containing a recycled component with "ghost" amphibole and/or phlogopite signature; fluid-mobile elements compatible in amphibole and phlogopite could be preferentially lost to the subarc mantle during subduction-related breakdown of these phases. The relationships between He ($^3He/^4He$=5.7–9.3 R_A), Nd, Sr and Pb isotope ratios support the presence of a recycled component in the source of the Canary shield stage magmas. The observed

* Corresponding author. Max-Planck-Institut für Chemie, Abteilung Geochemie, Postfach 3060, D-55020 Mainz, Germany. Tel.: +49 6131 305 304; fax: +49 6131 371 051.
E-mail address: agurenko@mpch-mainz.mpg.de (A.A. Gurenko).

0009-2541/$ - see front matter
doi:10.1016/j.chemgeo.2006.02.016

relatively low $^{40}Ar/^{36}Ar$ isotopic ratios between ~310 and ~450 indicate contamination of plume-derived magmas by atmospheric air.

Keywords: Canary Islands; Mantle plume; Trace elements; Radiogenic isotopes; Noble gases

1. Introduction

One of the major geochemical challenges in understanding dynamics of mantle magmatism is to identify the components involved in, and to evaluate their separate contributions to, the origin of mafic magmas. Primitive, mantle-derived rocks are traditionally used to constrain the composition of their mantle source regions. In contrast to mid-ocean ridge basalts (MORB), whose origin is ascribed to melting of the depleted upper mantle, ocean island basalts (OIB) are believed to be derived from mantle plumes whose roots can often be traced to the lower mantle and even the D″ layer at the core/mantle boundary (e.g., Williams and Garnero, 1996; Revenaugh and Meyer, 1997; Van der Hilst et al., 1997; Williams et al., 1998; Albarède and van der Hilst, 1999; Kellogg et al., 1999; Montelli et al., 2004). Thus, the study of mantle melting and melt transport resulting in mafic OIB magmas is fundamental for understanding the Earth's origin, dynamics of evolution and its current constitution. This information is crucial for understanding global cycling models and for assessing what material and how much is fed into the lower mantle at subduction zones and then returned back to the surface via deep mantle plumes.

The Canary Archipelago is well suited for the study of mantle melting dynamics and the origin of plume material. The Canary Islands exhibit an unusually long magmatic history spanning 20 Ma or more in the eastern Canaries, 12–15 Ma in the central part of the archipelago, and 1–4 Ma on the westernmost islands, representing an age-progressive ~500 km long island chain (e.g., Schmincke and Flower, 1974; Schmincke, 1976, 1982, 1998; Schmincke and Sumita, 1998). Age dating of seamounts northwest of the Canary Islands shows that this age-progressive volcanic chain can be traced back to ~ 70 Ma, consistent with derivation of Canary volcanism from a mantle plume (Geldmacher et al., 2001, 2005). Geophysical observations, such as geoid and seismic tomographic studies, show a low velocity anomaly beneath the Canary Islands, consistent with the presence of a mantle plume (Hoernle et al., 1995; Goes et al., 1999; Montelli et al., 2004). Furthermore, Montelli et al. (2004) have recently demonstrated that the Canary plume is one of the few that can be traced to the core–mantle boundary.

Volcanic rocks from the Canary Islands display an exceptionally large compositional range. Transitional tholeiitic to moderately alkaline basalts and picrites are dominant in the shield-building stage of island growth, whereas olivine nephelinites and basanites are common during the late (post-erosional or rejuvenated) stage of volcanism (Fúster et al., 1968; Ibarrola, 1970; Schmincke, 1982). It is now agreed that geochemical and isotopic signatures of the mafic magmas erupted on the Canary Islands require partial melting of a HIMU-type mantle source, whose origin is attributed to the recycling of <2 Ga old oceanic crust (e.g., Sun, 1980; Hoernle et al., 1991; Hoernle and Tilton, 1991; Marcantonio et al., 1995; Thirlwall, 1997; Hoernle, 1998; Widom et al., 1999; Simonsen et al., 2000; Geldmacher et al., 2001, 2005). Interaction between plume-derived melts and the lithospheric mantle and/or crust complicates the chemistry of the mafic magmas and must be taken into consideration (Hoernle et al., 1991; Thirlwall et al., 1997; Hoernle, 1998; Widom et al., 1999; Gurenko et al., 2001; Hansteen and Troll, 2003; Lundstrom et al., 2003).

Here we present a comprehensive data set including mineral chemistry, whole rock major and trace element compositions, and radiogenic (Sr, Nd, Pb), stable (O) and noble gas isotope data (He, Ar) for mafic lavas from the volcanic shields of two central and two western Canary Islands (Gran Canaria, Tenerife, La Gomera and La Palma). The shield basalts and picrites were selected because, as shown by Wyllie (1988), the greatest degree of partial melting of the plume material occurs during the shield stage of volcanism. We excluded Lanzarote and Fuerteventura, the closest islands to the African continental margin, in order to minimize the effects of contamination from the thick sequence of continental rise sediments (up to 10 km) and from enriched transitional continental to oceanic lithopsheric mantle beneath these islands (Hoernle and Tilton, 1991; Hoernle et al., 1995; Widom et al., 1999).

The focus of this paper is on the compositional diversity and origin of shield stage volcanism on the central and western Canary Islands, which has implications for the composition of the Canary plume. The main questions addressed include whether there is a common

magma source for the magmas erupted on different islands? Are there intra-island, temporal and spatial variations in trace elements and long-lived radiogenic isotope ratios between 15 and 1 Ma and what can these variations tell us about the compositional structure of the Canary plume? Were melt–lithosphere interaction or crustal contamination of the most primitive shield stage lavas significant during magma transfer to the surface? Does noble gas isotope data from the shield stage of volcanism show any evidence of a lower mantle origin for the plume material?

2. Geology and samples

The Canary Archipelago, located off the northwestern African continental shelf, includes seven large volcanic islands (Fig. 1). All islands are underlain by the 155 to 175 Ma old oceanic crust, as indicated by gabbro xenoliths on Lanzarote, Gran Canaria, Tenerife and La Palma (Hoernle, 1998; Schmincke et al., 1998; Neumann et al., 2000). A comprehensive overview of the geology and origin of the Canary Islands is given by Schmincke (1976, 1982), Hoernle and Schmincke (1993a,b) and Schmincke and Sumita (1998). Appendix A briefly summarizes the geological evolution of the four Canary Islands for which we report data in this study.

Rocks (Appendix B) were collected on Gran Canaria (i.e., Agaete, Barrancos de la Palma, Guayedra, Guigui Chico, Tasartico and Montaña de Agüimes), Tenerife (massifs of Teno in the NW and Roque del Conde in the SW), La Gomera (Barrancos de Las Lajas, Valle Gran Rey, Erque, Santiago, Casas de Enchereda, Casas de Juel, Playa de Alojera) and La Palma (Caldera de Taburiente and Barranco de las Angustias). Rocks with <5 vol.% phenocrysts were classified as aphyric. The samples studied are dominantly olivine (Ol)- and

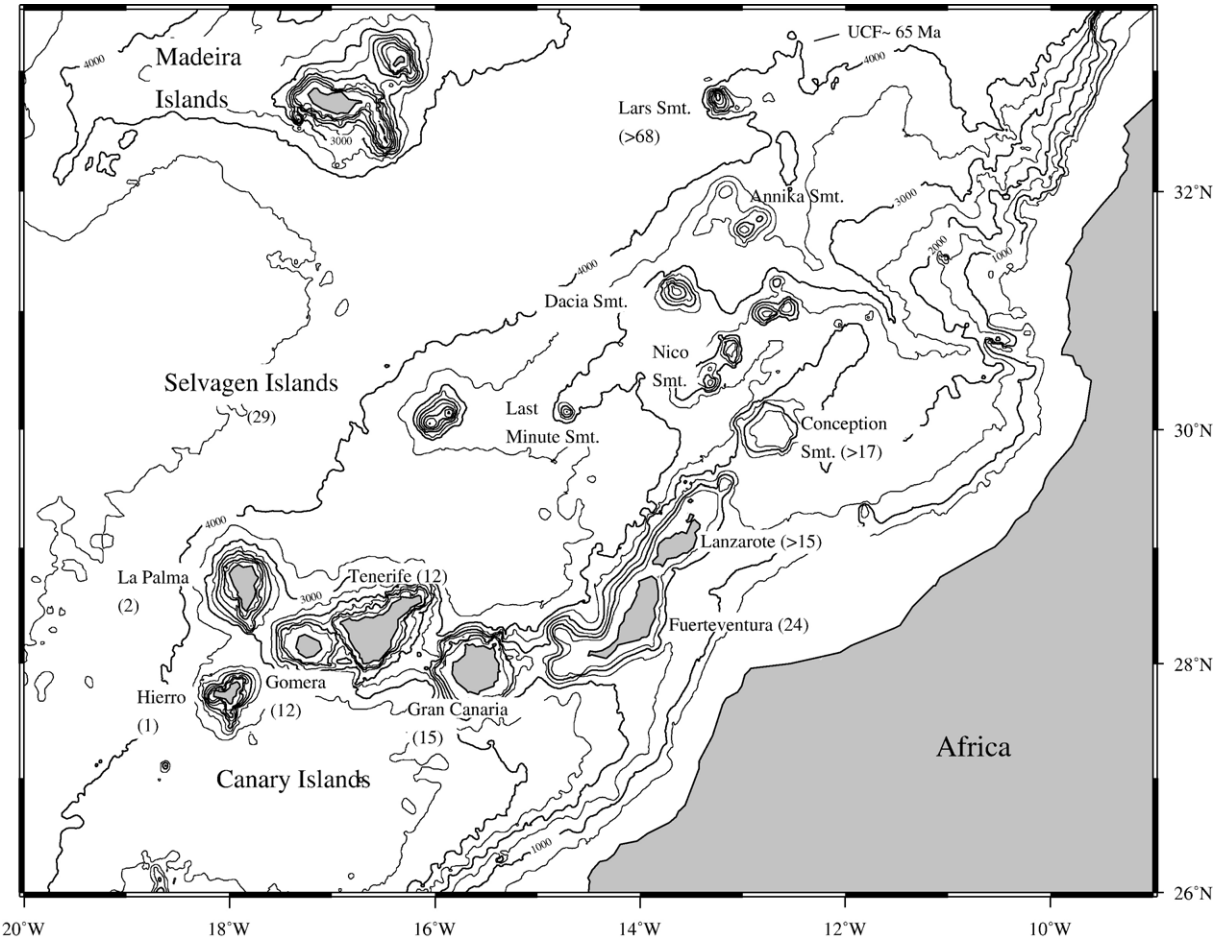

Fig. 1. The position of the Canary Islands relative to the western coast of the African continent (modified after Geldmacher et al., 2001, 2005; Lundstrom et al., 2003). The oldest available ages of the volcanic rocks for each island and dated seamount are shown, which indicate a crude SW to NE progression of increasing age.

clinopyroxene (Cpx)-phyric. Plagioclase (Pl) is more common in the youngest shield basalts of the Hogarzales Formation on Gran Canaria (e.g., Schmincke, 1976; Heuschkel, 1996; Schmincke and Segschneider, 1998). Alteration is often observed macroscopically in the lava flows and represented by veined calcite, chabazite, and unidentified zeolite-like minerals that line and often fill fractures, vesicles, and cavities of the lavas. We emphasize that only the freshest and possibly free from visual signs of alteration fragments of whole rock samples, except for olivine that is often partially altered, were selected for the present study.

Olivine and Cpx phenocrysts (mostly 0.5 to 10 mm in size but in some cases reaching 30–50 mm) occur as individual euhedral to subhedral crystals and their fragments or as glomerocrysts, some with partially resorbed edges. The proportion of Ol relative to Cpx varies, ranging from 10% to 90%. Olivine phenocrysts are fresh to strongly altered. Their alteration varies from a rim of iddingsite, secondary clay minerals along grain boundaries and fractures to a complete replacement by pseudomorphs. Clinopyroxene crystals are typically fresh. Plagioclase (commonly <5 vol.%) forms elongated euhedral crystals, 0.5–1.5 mm long that can be weakly altered along grain boundaries, cleavage planes and fractures. The main alteration product of plagioclase is unidentified. Trace phenocrysts of up to 5 mm large cubic crystals of Cr-spinel and Fe–Ti oxides are also present. The groundmass is holocrystalline to hypocrystalline and is composed of randomly arranged rectangular Pl crystals (mostly 30 to 150 μm in size), subhedral to anhedral Cpx (up to 100 μm in size), rare euhedral to subhedral Ol or pseudomorphs of Ol (up to 50 μm), Fe–Ti oxides and tachylite.

3. Results

3.1. Mineral chemistry

Compositions of olivine, clinopyroxene, plagioclase and spinel phenocrysts, as well as spinel inclusions in Ol and Cpx were analyzed with the Cameca SX-50 electron microprobe at IfM-GEOMAR Leibniz Institute (for further details see Appendix C.1.1); they are summarized in Table 1 and presented in Fig. 2. Olivine phenocrysts are $Fo_{78.1–90.2}$ in basalts from Gran Canaria, $Fo_{72.1–86.3}$ from Tenerife, $Fo_{78.1–87.8}$ from La Gomera, and $Fo_{81.2–87.0}$ from La Palma (Table 1, Fig. 2a). Their Ca-concentrations (0.2–0.5 wt.% CaO; Table 1) are typical for phenocrysts crystallized from basaltic magma rather than being derived from disintegrated mantle peridotites (<0.15 wt.% CaO in early Ol porphyroclasts from peridotite xenoliths from the Canary Islands (Amundsen, 1987; Neumann, 1991; Neumann et al., 1995; Klügel, 1998). The concentrations of Ni (0.06–0.4 wt.% NiO; Table 1) generally decrease with decreasing Fo contents, and the lowest NiO content was observed in olivine $Fo_{72.1}$ from Tenerife. The highest Ni-concentrations found in the most magnesian olivines are similar to those from mantle xenoliths. Most olivines analyzed are normally zoned with >3 mol.% variations in Fo from core to rim, though reversely zoned olivines are also present. Olivines probably experienced only a short contact with the transporting magma prior to eruption, since only the marginal parts of Ol crystals were re-equilibrated after being trapped from a cumulative layer.

Clinopyroxene phenocrysts (*mg*-number [$100 \times Mg/(Mg+Fe_{tot})$ given as atomic ratio, where Fe_{tot} is total iron as FeO] ranges from 73.4 to 90.0) are optically and chemically zoned. Normally zoned crystals are composed of beige or olive Mg-rich augite in the core changing to pinkish Al–Ti-rich augite on the rim; phenocryst rims are compositionally similar to groundmass Cpx. Both TiO_2 (0.6–4.4 wt.%) and Al_2O_3 (1.7–8.6 wt.%) contents vary widely. Clinopyroxenes contain up to 1.3 wt.% Cr_2O_3 and 0.2–0.8 wt.% Na_2O. Similar compositional variations in Cpx phenocrysts were already described for the Miocene shield rocks on Gran Canaria and Tenerife (e.g., Gurenko et al., 1998; Schmincke and Segschneider, 1998; Neumann et al., 1999). Na-salites with low *mg*-number described by Neumann et al. (1999) from Tenerife were not found during this study.

Rare plagioclase phenocrysts range from An_{65} to An_{76} [$An = 100 \times Na_2O/(CaO+Na_2O)$, atomic ratio]. Some individual Pl crystals show normal, reverse or oscillatory zoning. The obtained range of An contents is similar to that described in the Miocene shield rocks on Gran Canaria and Tenerife (Heuschkel, 1996; Schmincke and Segschneider, 1998; Neumann et al., 1999).

Spinel-group minerals, represented by spinel (Sp)–chromite (Crt)–magnetite (Mt)–ulvöspinel (Usp) and ilmenite (Ilm)–hematite (Hmt) solid solutions, are present as (1) numerous opaque inclusions (0.005–0.3 mm in size) in Ol and Cpx phenocrysts, (2) relatively small (0.3–0.7 mm in size) euhedral phenocrysts, and (3) small euhedral to anhedral crystals (0.02–0.05 mm in size) in the groundmass. Most analyzed Sp are inclusions in Ol; only a few Sp crystals from the groundmass were analyzed. Ilmenite is rare and was found in the groundmass of more evolved lavas, which also contain ilmenite in a form of exsolution lamellae in large titanomagnetite crystals. Chemical compositions of Sp inclusions in Ol are presented in Fig. 2b. The

Table 1
Compositional ranges of olivine and clinopyroxene phenocrysts and their hosted spinel inclusions [a]

Sample	Olivine				Clinopyroxene					Spinel and Ti-magnetite				
	N	Fo	CaO	NiO	*N*	$Mg\#_{cpx}$	TiO_2	Al_2O_3	Na_2O	*N*	$Mg\#_{sp}$	$Cr\#_{sp}$	TiO_2	Fe^{2+}/Fe^{3+}
Gran Canaria														
G1264	45	80.6–90.2	0.25–0.47	0.22–0.35	12	79.3–86.2	0.8–1.7	2.2–4.0	0.25–0.39	18	31.5–55.1	49.9–77.9	2.5–8.6	0.8–2.4
G1265	35	80.8–89.7	0.26–0.41	0.22–0.25	4	79.9–87.5	0.7–1.5	1.7–4.1	0.22–0.32	7	34.1–56.3	56.6–74.1	2.6–7.9	1.1–1.9
1545	25	81.5–88.3	0.24–0.42	ND	–	ND	ND	ND	ND	–	ND	ND	ND	ND
1552	33	82.2–88.5	0.24–0.42	0.27–0.35	–	ND	ND	ND	ND	7	33.0–50.5	54.5–71.8	3.3–9.3	1.0–2.1
1553	37	82.4–88.4	0.27–0.42	0.27–0.31	–	ND	ND	ND	ND	16	28.4–45.5	56.8–71.2	1.7–8.3	0.9–1.6
1557	38	81.8–89.8	0.24–0.38	0.25–0.41	–	ND	ND	ND	ND	10	29.6–51.4	47.3–72.6	2.8–11.2	0.9–2.2
1567	27	81.3–87.5	0.24–0.34	ND	–	ND	ND	ND	ND	–	ND	ND	ND	ND
GC98-35	22	80.2–89.1	0.20–0.43	0.22–0.34	8	82.7–86.3	1.0–1.4	2.7–3.9	0.43–0.49	10	25.2–54.6	49.9–72.1	2.6–10.3	1.0–1.6
GC98-43	20	81.5–86.5	0.29–0.38	0.23–0.34	23	78.7–83.3	1.1–1.6	2.9–4.3	0.39–0.46	20	28.6–48.3	56.0–72.8	3.0–9.5	1.0–1.7
GC98-56	58	79.7–84.6	0.24–0.37	0.21–0.39	24	77.8–84.9	1.2–2.0	2.4–4.4	0.38–0.49	13	28.5–38.6	54.4–75.8	3.9–9.5	1.0–1.9
GC98-59	36	78.1–89.5	0.23–0.41	0.24–0.40	16	80.1–87.5	0.7–1.6	1.7–3.9	0.33–0.48	17	25.7–55.2	44.5–74.9	2.2–9.2	1.0–3.0
Tenerife														
TF98-04	70	79.6–85.4	0.21–0.37	0.11–0.34	68	73.7–85.5	1.0–3.5	4.0–8.1	0.38–0.61	12	38.1–52.5	44.1–56.1	2.3–4.6	1.1–1.6
TF98-07	25	79.5–82.8	0.23–0.32	0.15–0.24	16	80.8–83.8	1.1–1.8	4.6–6.2	0.47–0.57	9	31.2–51.4	30.1–41.5	2.4–15.0	1.0–1.3
TF98-16	51	77.4–84.0	0.25–0.35	0.15–0.27	33	80.9–85.3	0.9–1.5	3.8–5.2	0.50–0.59	11	42.7–53.8	41.7–52.2	1.9–4.4	1.1–1.4
TF99-23	40	72.1–86.3	0.26–0.37	0.06–0.27	10	80.6–86.1	0.9–1.7	4.0–6.5	0.53–0.59	9	29.2–50.5	21.9–47.8	3.3–13.2	1.1–2.2
TF99-64	24	80.8–84.3	0.28–0.34	0.16–0.26	10	78.8–84.1	0.9–1.6	4.6–6.4	0.51–0.62	19	31.3–52.6	34.9–48.4	2.8–14.4	1.1–1.9
La Gomera														
LG97-01	12	83.6–84.7	0.27–0.35	0.19–0.29	12	82.8–85.1	1.2–1.5	3.6–4.2	0.42–0.47	11	38.2–48.5	58.2–60.8	4.5–10.3	1.2–1.7
LG97-02	31	83.6–84.7	0.29–0.37	0.15–0.34	38	74.8–87.2	0.8–2.9	2.7–7.3	0.38–0.60	12	33.0–46.8	61.3–65.1	3.6–5.2	1.4–1.7
LG99-11	18	83.3–84.4	0.28–0.33	0.19–0.28	10	75.6–86.0	1.0–3.1	2.7–7.5	0.34–0.55	14	35.9–44.6	37.8–64.3	4.0–15.5	1.1–1.8
LG99-35	65	81.9–85.9	0.25–0.33	0.19–0.39	–	ND	ND	ND	ND	19	42.1–51.1	59.0–61.5	3.2–7.0	1.4–2.2
LG99-65	14	78.8–83.7	0.30–0.38	0.15–0.21	21	78.9–87.9	0.9–2.2	2.5–5.2	0.28–0.39	15	26.6–42.7	37.4–62.9	3.2–12.7	1.0–1.4
LG99-59	20	82.6–87.8	0.32–0.43	0.18–0.33	10	84.7–90.0	0.6–1.2	1.9–3.4	0.35–0.43	6	31.4–55.2	48.1–72.8	2.8–9.4	1.4–1.7
La Palma														
LP97-01	48	82.2–86.2	0.31–0.41	0.13–0.30	13	78.2–87.6	0.9–2.3	3.2–6.4	0.45–0.60	25	44.7–55.3	56.4–66.2	2.0–5.2	1.0–1.4
LP99-13	48	81.2–86.0	0.32–0.40	0.14–0.31	61	79.2–87.4	0.8–2.6	2.8–6.7	0.35–0.79	9	45.0–49.5	57.7–65.3	2.4–4.4	1.1–1.3
LP00-25	16	83.0–86.8	0.29–0.38	0.18–0.28	35	73.4–86.8	1.0–4.4	2.7–8.5	0.33–0.48	14	36.6–49.8	51.4–63.7	2.4–9.6	1.0–1.7
LP00-81	12	80.7–86.5	0.30–0.36	0.18–0.31	63	75.0–87.7	0.8–4.2	2.5–8.6	0.30–0.51	13	30.4–54.6	40.5–64.7	2.8–12.3	1.1–1.4

[a] Individual analyses are available on request; *N*=number of microprobe analyses; concentrations of oxides are given in wt.%; Fo=mol% forsterite; $Mg\#_{cpx}$=clinopyroxene *mg*-number, $100\times Mg/(Mg+Fe_{tot})$, atomic ratio, where Fe_{tot} is total iron as Fe^{2+}; $Mg\#_{sp}$=spinel *mg*-number, $100\times Mg/(Mg+Fe^{2+})$, atomic ratio, where Fe^{2+} was calculated on the basis of spinel stoichiometry; $Cr\#_{sp}$=spinel *cr*-number, $100\times Cr/(Cr+Al)$, atomic ratio; ND=not determined; –=no value.

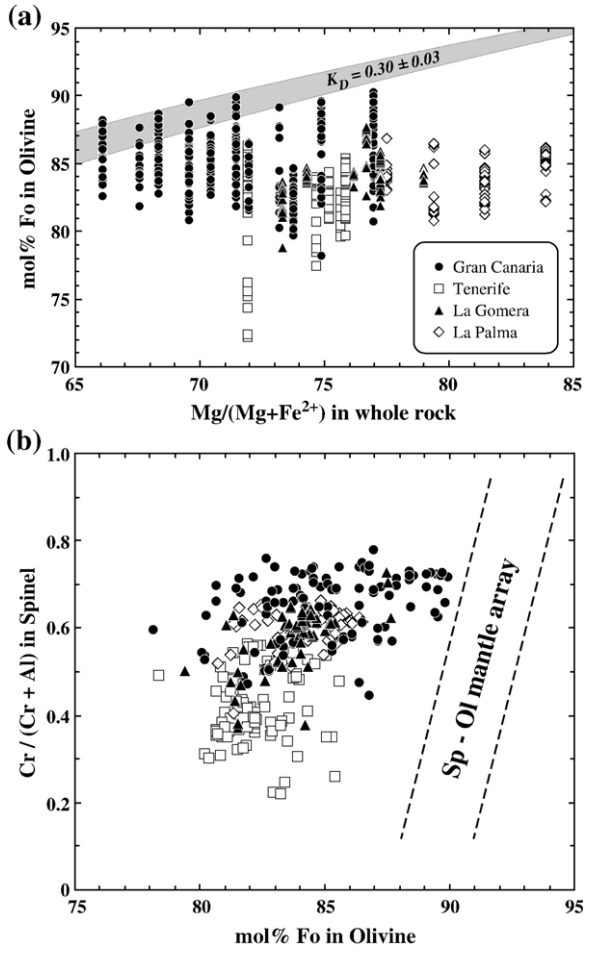

Fig. 2. (a) Composition of olivine phenocrysts (mol.% Fo) shown vs. whole-rock *mg*-number 100×(Mg/(Mg+Fe^{2+}). Except for Gran Canaria, the lavas from other islands contain Ol phenocrysts whose Fo contents are too low to be in equilibrium with whole rock magma compositions. This implies that the lavas have accumulated olivine. *Shaded field* displays the range of equilibrium values of olivine–melt Fe–Mg partition coefficient (K_D=0.30±0.03; Roeder and Emslie, 1970). (b) Cr/(Cr+Al) atomic ratio in spinel inclusions vs. mol.% Fo of host olivine. Spinels from high-Mg olivines on Gran Canaria are closer than other spinels to the Sp–Ol mantle array (Arai, 1987), further indicating their primitive nature. The observed decrease of *cr*-number with decreasing Fo is attributed to abundant Cpx crystallization.

compositional range observed in each particular sample usually spans the range obtained for the Miocene shield lavas in general. Generally, spinel *cr*-number [Cr/(Cr+Al), atomic ratio] decreases and (Fe^{3+}+Ti)-content increases (not shown) with decreasing forsterite in host olivine. A systematic difference in *cr*-number appears to be significant for the samples from different Canary Islands, although they have been trapped by Ol of similar Fo content (Fig. 2b). The Fe^{2+}/Fe^{3+} ratios calculated from spinel stoichiometry range from 0.8 to 3.0 with no systematic difference between the islands.

3.2. Whole rock chemistry

3.2.1. Major elements

Whole-rock major element compositions (for analytical details see Appendix C.1.2) are listed in Table 2 and plotted in Fig. 3. The H_2O and CO_2 contents equivalent to loss on ignition (LOI) and range from 0.25 to 4.64 wt.% H_2O+CO_2. The high (>2 wt.%) LOI result from relatively strong secondary alteration of lavas, very common for subaerial shield stage volcanic rocks on Canary Islands, that could significantly influence some major (e.g., SiO_2, Na_2O) and fluid-mobile trace element concentrations (e.g., Ba/Rb ratio; Hofmann and White, 1983; Halliday et al., 1995). Assuming that H_2O+CO_2 contents could be considered as a proxy for degree of rock alteration, we examined concentrations of major and trace elements, as well as Sr, Nd and Sr isotope ratios for whether they correlate with H_2O+CO_2. We emphasize that no correlations have been observed for any elements and isotopic ratios examined, and the strongest variations of fluid-mobile elements such as Rb, Ba, U, Pb, as well as Th were found in the lavas with <1 wt.% H_2O+CO_2. We conclude therefore that the degree of secondary alteration of the Canary shield stage lavas studied had no significant impact on trace elements and isotopic ratios, being within analytical error of these elements.

The lavas range in composition from tholeiitic basalts and picrites, which are more common on Gran Canaria, through alkali basalts and basanites to tephrites and trachybasalts, which are more abundant on Tenerife, La Gomera and La Palma. Magnesium contents range from 2.9 to 29.8 wt.% MgO and *mg*-number ranges from 40.4 to 91.4. The lavas from Gran Canaria are characterized by generally higher SiO_2 and TiO_2, and lower CaO contents than the other shield basalts at a given MgO (Fig. 4). The other major elements correlate well with MgO contents following the common trends of Ol and Ol+Cpx fractional crystallization and/or phenocryst accumulation.

3.2.2. Trace elements

Trace element concentrations are listed in Table 2 (for analytical details see Appendix C.1.2). Nickel and Cr concentrations decrease with decreasing MgO from 974 to 11 ppm Ni and from 1920 to 27 ppm Cr mostly due to Ol and Cpx fractionation (Fig. 4). Nickel, although being mostly controlled by olivine crystallization, scatters significantly in the lavas with MgO >

Table 2
Whole-rock compositions

Sample	G1264*	G1265	1557	1553	1552	GC59	GC35	GC41	GC43	GC81	GC88
Locality	Gran Canaria										
Major elements, wt.%											
SiO_2	45.65	44.90	46.77	46.54	46.82	44.52	44.70	45.64	45.61	44.54	45.50
TiO_2	2.77	3.35	3.21	3.26	3.53	2.74	3.11	2.87	3.09	2.73	3.48
Al_2O_3	8.35	10.30	9.66	10.52	11.06	8.33	9.19	9.77	10.05	8.72	11.03
Fe_2O_3	13.46	12.92	13.54	13.32	13.12	13.15	13.35	13.11	13.30	13.50	13.30
MnO	0.18	0.18	0.18	0.18	0.17	0.18	0.18	0.17	0.16	0.18	0.17
MgO	18.38	12.40	13.94	12.49	11.73	17.31	14.87	15.02	13.84	16.40	11.25
CaO	9.37	9.90	10.12	11.00	10.65	9.63	10.47	8.33	8.99	8.64	10.66
Na_2O	1.65	2.09	1.93	2.05	2.22	1.66	1.72	1.65	1.67	1.69	2.13
K_2O	0.76	0.96	0.83	0.81	0.97	0.72	0.79	0.71	0.66	0.59	0.97
P_2O_5	0.32	0.40	0.38	0.39	0.41	0.29	0.36	0.33	0.34	0.32	0.43
H_2O	ND	2.90	ND	ND	ND	1.56	1.37	1.78	1.80	2.35	1.93
CO_2	ND	0.29	ND	ND	ND	0.20	0.08	0.09	0.10	1.17	0.16
Total	100.89	100.59	100.56	100.56	100.68	100.26	100.16	99.47	99.61	100.83	101.01
Trace elements, ppm											
V	226	308	296	221	167	280	292	276	306	272	358
Cr	1301	709	979	798	702	1415	981	1000	906	1174	708
Ni	660	383	592	409	385	631	386	448	385	638	271
Rb	12	19	24	25	27	15	17	14	13	18	23
Sr	307	372	436	481	445	319	384	363	371	336	465
Y	29	32	27	27	29	20	22	23	21	18	27
Zr	200	252	241	241	264	195	238	225	232	193	278
Nb	34	42	40	38	44	28	34	31	30	28	40
Ba	163	191	203	209	211	131	150	136	145	117	201
La	22	27	35	36	29	23	28	25	25	24	35
Ce	47	59	75	76	63	52	63	55	55	52	74
Pr	6.1	7.6	9.5	9.6	8.0	6.8	8.2	7.2	7.3	6.7	9.4
Nd	27	34	42	42	36	30	36	32	33	29	41
Sm	5.6	7.0	8.6	8.9	7.5	6.3	7.4	7.2	7.4	6.6	8.4
Eu	1.9	2.3	2.8	2.9	2.5	2.1	2.3	2.4	2.5	2.2	2.7
Gd	5.3	6.4	7.9	8.2	7.1	6.0	6.5	6.7	7.0	6.2	7.8
Tb	0.8	0.9	1.2	1.2	1.0	0.8	0.9	1.0	1.1	0.9	1.1
Dy	3.8	4.8	5.7	5.9	5.2	4.2	4.6	5.1	5.3	4.7	5.6
Ho	0.7	0.8	1.0	1.0	0.8	0.7	0.8	0.9	0.9	0.8	1.0
Er	1.7	2.1	2.6	2.7	2.3	2.0	2.0	2.2	2.5	2.1	2.6
Tm	0.2	0.3	0.3	0.3	0.3	0.2	0.3	0.3	0.3	0.3	0.3
Yb	1.2	1.5	1.9	2.0	1.6	1.4	1.5	1.7	1.7	1.5	1.7
Lu	0.2	0.2	0.2	0.3	0.2	0.2	0.2	0.2	0.2	0.2	0.2
Hf	4.5	5.6	6.9	6.2	5.6	4.9	5.7	5.5	5.8	4.9	6.6
Ta	1.8	2.3	2.8	2.9	2.2	2.0	2.4	2.0	2.0	1.8	2.8
Pb	ND	ND	ND	ND	ND	1.8	2.3	ND	ND	ND	ND
Th	2.2	2.7	3.5	3.2	2.7	2.2	2.6	2.2	2.3	2.3	3.6
U	0.6	0.7	0.9	0.9	0.8	0.6	0.7	0.7	0.6	0.6	0.8
$(La/Sm)_n$	2.5	2.4	2.6	2.5	2.4	2.3	2.4	2.2	2.1	2.3	2.6
$(Nb/La)_n$	1.5	1.5	1.1	1.0	1.5	1.2	1.2	1.2	1.2	1.2	1.1
$(Ta/La)_n$	1.4	1.5	1.4	1.4	1.3	1.5	1.5	1.4	1.4	1.3	1.4
$(K/La)_n$	0.7	0.7	0.5	0.4	0.7	0.6	0.6	0.6	0.5	0.5	0.5
$(Pb/La)_n$	–	–	–	–	–	0.3	0.3	–	–	–	–
Ba/Nb	4.8	4.5	5.1	5.5	4.8	4.7	4.4	4.4	4.8	4.2	5.0
Ba/Th	74.1	70.7	58.0	65.3	78.1	59.5	57.7	61.8	63.0	50.9	55.8
K/La	287	295	197	187	278	260	234	236	219	204	230
Zr/Nb	5.9	6.0	6.0	6.3	6.0	7.0	7.0	7.3	7.7	6.9	7.0
Zr/Y	6.9	7.9	8.9	8.9	9.1	9.8	10.8	9.8	11.0	10.7	10.3
Nb/U	56.7	60.0	44.4	42.2	55.0	46.7	48.6	44.3	50.0	46.7	50.0

(continued on next page)

Table 2 (*continued*)

Sample	G1264*	G1265	1557	1553	1552	GC59	GC35	GC41	GC43	GC81	GC88
Locality	Gran Canaria										
Trace elements, ppm											
Ce/Pb	–	–	–	–	–	28.9	27.4	–	–	–	–
Nd/Pb	–	–	–	–	–	16.7	15.7	–	–	–	–
Sample	GC56	GC58	TF2	TF4	TF7	TF9	TF16	TF64	TF67	TF23	TF51
Locality			Tenerife								
Major elements, wt.%											
SiO_2	44.38	44.70	44.52	43.17	44.51	44.21	44.20	43.50	44.01	44.98	43.36
TiO_2	3.03	3.31	2.36	2.38	2.32	3.01	2.21	2.34	3.30	2.82	4.00
Al_2O_3	8.10	8.89	8.35	9.08	9.34	13.24	9.95	9.71	12.99	10.58	14.01
Fe_2O_3	14.60	14.65	11.58	13.43	12.85	13.54	13.29	13.20	13.12	12.04	14.65
MnO	0.18	0.18	0.15	0.17	0.17	0.18	0.18	0.18	0.17	0.16	0.18
MgO	17.08	15.51	15.42	17.42	15.63	10.29	15.86	16.19	8.73	12.61	7.91
CaO	8.03	8.99	13.88	10.23	12.06	10.81	11.01	11.75	13.49	13.48	12.49
Na_2O	1.43	1.61	0.90	1.32	1.74	2.08	1.55	1.30	2.40	1.84	2.34
K_2O	0.73	0.68	0.41	0.59	0.61	0.94	0.62	0.58	0.95	0.64	0.97
P_2O_5	0.33	0.37	0.23	0.31	0.29	0.45	0.32	0.29	0.57	0.36	0.44
H_2O	1.31	0.64	1.67	2.13	0.34	0.79	0.75	1.81	1.06	1.15	0.95
CO_2	0.16	0.13	0.18	0.10	0.04	0.05	0.04	0.35	0.04	0.08	0.05
Total	99.36	99.66	99.65	100.31	99.90	99.59	99.96	101.20	100.83	100.72	101.35
Trace elements, ppm											
V	271	291	261	258	242	300	232	269	344	292	452
Cr	1371	1277	738	1237	1006	429	1175	974	326	888	260
Ni	540	427	268	460	282	186	367	363	117	253	108
Rb	15	13	6	12	14	22	15	16	21	24	28
Sr	399	439	334	372	405	610	414	512	670	515	790
Y	18	22	16	17.2	15	23	21.9	21	25	22.5	24
Zr	213	244	117	142	130	215	158	141	257	200	263
Nb	33	35	19	26.1	29	48	37.1	39	45	45.9	74
Ba	191	157	136	146	152	254	209	232	276	217	265
La	27	29	17	21	24	39	31	31	43	32	62
Ce	60	63	36	45	49	80	57	62	91	68	116
Pr	7.8	8.2	4.4	5.8	6.0	9.6	7.1	7.1	11.1	8.2	12.3
Nd	35	36	20	25	26	41	30	29	45	35	46
Sm	7.4	7.8	4.7	5.3	5.5	8.1	5.8	5.7	8.8	7.2	8.5
Eu	2.4	2.5	1.6	1.7	1.9	2.7	1.9	1.9	3.0	2.2	2.8
Gd	6.7	7.1	4.5	4.9	5.4	7.8	5.6	5.5	8.6	6.6	8.2
Tb	1.0	1.0	0.7	0.7	0.8	1.1	0.8	0.8	1.1	0.9	1.1
Dy	4.8	5.1	3.4	3.7	3.9	5.6	4.0	4.1	5.6	4.9	5.7
Ho	0.8	0.8	0.6	0.6	0.7	1.0	0.7	0.7	1.0	0.8	1.0
Er	2.0	2.1	1.5	1.7	1.6	2.5	1.9	1.8	2.4	2.1	2.6
Tm	0.2	0.3	0.2	0.2	0.2	0.3	0.2	0.2	0.3	0.3	0.3
Yb	1.4	1.5	1.1	1.3	1.1	1.9	1.5	1.4	1.7	1.6	1.9
Lu	0.2	0.2	0.1	0.2	0.2	0.3	0.2	0.2	0.2	0.2	0.3
Hf	5.7	6.0	3.0	4.3	3.8	5.1	4.0	4.0	5.5	4.8	6.1
Ta	2.2	2.3	1.4	2.0	2.0	3.4	2.5	2.7	4.0	3.1	6.4
Pb	ND	ND	ND	1.7	ND	ND	2.4	ND	ND	2.1	ND
Th	2.5	2.7	1.3	1.9	2.0	3.2	2.8	3.4	3.2	3.0	4.5
U	0.7	0.7	0.3	0.4	0.5	0.9	0.7	0.8	0.8	0.8	1.3
$(La/Sm)_n$	2.3	2.3	2.3	2.5	2.7	3.0	3.4	3.4	3.1	2.8	4.6
$(Nb/La)_n$	1.2	1.2	1.1	1.2	1.2	1.2	1.2	1.3	1.0	1.4	1.2
$(Ta/La)_n$	1.4	1.4	1.4	1.7	1.5	1.5	1.4	1.5	1.6	1.7	1.8
$(K/La)_n$	0.5	0.5	0.5	0.6	0.5	0.5	0.4	0.4	0.4	0.4	0.3
$(Pb/La)_n$	–	–	–	0.3	–	–	0.3	–	–	0.2	–
Ba/Nb	5.8	4.5	7.2	5.6	5.2	5.3	5.6	5.9	6.1	4.7	3.6
Ba/Th	76.4	58.1	104.6	76.8	76.0	79.4	74.6	68.2	86.3	72.3	58.9

Table 2 (*continued*)

Sample	GC56	GC58	TF2	TF4	TF7	TF9	TF16	TF64	TF67	TF23	TF51
Locality			Tenerife								
Trace elements, ppm											
K/La	224	195	200	233	211	200	166	155	183	166	130
Zr/Nb	6.5	7.0	6.2	5.4	4.5	4.5	4.3	3.6	5.7	4.4	3.6
Zr/Y	11.8	11.1	7.3	8.3	8.7	9.3	7.2	6.7	10.3	8.9	11.0
Nb/U	47.1	50.0	63.3	65.3	58.0	53.3	53.0	48.8	56.3	57.4	56.9
Ce/Pb	–	–	–	26.5	–	–	23.8	–	–	32.4	–
Nd/Pb	–	–	–	14.7	–	–	12.5	–	–	16.7	–

Sample	LG1	LG2	LG6	LG11	LG35	LG50	LG53	LG58	LG59	LG65	LG66
Locality	La Gomera										
Major elements, wt.%											
SiO_2	43.17	42.99	44.16	44.21	42.69	45.75	43.61	45.47	43.29	44.72	44.54
TiO_2	2.71	1.99	3.24	2.46	2.27	2.94	2.95	2.34	2.32	2.81	3.18
Al_2O_3	10.14	7.31	10.16	9.21	8.75	13.50	10.53	8.62	8.32	10.12	9.36
Fe_2O_3	13.66	13.04	12.66	13.28	14.47	13.49	13.18	11.63	12.16	12.60	13.58
MnO	0.18	0.18	0.17	0.17	0.18	0.17	0.17	0.17	0.18	0.17	0.17
MgO	16.14	20.53	11.91	17.75	20.74	9.20	14.23	14.24	16.79	13.50	12.42
CaO	10.05	9.29	14.03	10.13	8.26	9.88	12.36	12.76	11.77	12.58	13.08
Na_2O	1.65	1.09	1.48	1.63	1.86	3.33	2.04	1.24	0.85	1.32	1.88
K_2O	0.59	0.46	0.46	0.57	0.69	1.08	0.70	0.59	0.21	0.73	0.79
P_2O_5	0.38	0.36	0.47	0.35	0.39	0.71	0.41	0.35	0.33	0.36	0.57
H_2O	1.57	2.08	1.96	0.57	0.37	0.44	0.28	2.91	4.43	1.73	0.69
CO_2	0.13	0.33	0.21	0.03	0.01	0.04	0.07	0.34	0.21	0.07	0.07
Total	100.36	99.65	100.91	100.36	100.66	100.53	100.53	100.66	100.84	100.71	100.33
Trace elements, ppm											
V	237	180	334	222	232	275	306	261	234	284	309
Cr	1077	1265	541	1420	1457	392	906	974	987	762	867
Ni	406	542	211	554	822	250	313	321	395	231	296
Rb	13	14	12	15	15	27	18	16	6	16	19
Sr	607	461	497	528	423	763	531	307	248	430	616
Y	20	15	25	18	18	29	21	20	20	24	24
Zr	167	132	244	140	152	301	193	150	159	208	237
Nb	35	35	44	35	35	60	50	34	31	46	45
Ba	187	210	206	193	186	333	218	197	127	204	220
La	29	31	36	26	24	54	36	25	27	36	39
Ce	64	66	78	54	52	106	73	53	56	75	83
Pr	7.8	7.9	9.7	6.8	6.5	12.3	8.6	6.4	6.8	8.6	10.3
Nd	34	33	42	29	28	50	36	28	29	36	45
Sm	7.3	6.5	8.3	6.1	6.0	9.7	7.3	5.7	6.2	7.2	8.9
Eu	2.4	2.2	2.7	2.1	2.0	3.2	2.4	1.9	1.9	2.4	2.9
Gd	5.9	5.9	7.7	5.6	5.4	9.1	6.7	5.6	5.4	6.9	8.4
Tb	0.8	0.8	1.0	0.8	0.8	1.3	0.9	0.8	0.8	0.9	1.1
Dy	4.4	4.0	5.3	4.0	3.8	6.3	4.7	4.1	3.9	4.9	5.4
Ho	0.8	0.7	0.9	0.7	0.6	1.1	0.8	0.7	0.7	0.9	0.9
Er	1.9	1.7	2.3	1.7	1.6	2.7	1.9	1.8	1.7	2.2	2.2
Tm	0.2	0.2	0.3	0.2	0.2	0.3	0.2	0.2	0.2	0.3	0.3
Yb	1.3	1.1	1.6	1.2	1.3	1.9	1.4	1.3	1.3	1.7	1.5
Lu	0.2	0.2	0.2	0.2	0.2	0.3	0.2	0.2	0.2	0.2	0.2
Hf	4.5	4.2	5.8	3.7	3.8	6.0	4.7	3.7	4.0	5.3	5.2
Ta	2.6	2.3	3.2	2.2	2.4	4.1	3.3	2.2	2.2	3.2	3.1
Pb	1.5	ND	ND	ND	1.6	ND	ND	ND	1.4	ND	ND
Th	2.2	2.8	3.0	2.0	2.1	4.8	3.0	2.1	2.5	3.4	2.8
U	0.6	0.7	0.8	0.6	0.6	1.3	0.8	0.4	0.4	0.8	0.7
$(La/Sm)_n$	2.5	3.0	2.7	2.7	2.5	3.5	3.1	2.8	2.7	3.1	2.8

(continued on next page)

Table 2 (*continued*)

Sample	LG1	LG2	LG6	LG11	LG35	LG50	LG53	LG58	LG59	LG65	LG66
Locality	La Gomera										
Trace elements, ppm											
$(Nb/La)_n$	1.2	1.1	1.2	1.3	1.4	1.1	1.4	1.4	1.1	1.3	1.1
$(Ta/La)_n$	1.6	1.3	1.6	1.5	1.7	1.3	1.6	1.5	1.4	1.6	1.4
$(K/La)_n$	0.4	0.3	0.3	0.4	0.6	0.4	0.4	0.5	0.2	0.4	0.4
$(Pb/La)_n$	0.2	–	–	–	0.2	–	–	–	0.2	–	–
Ba/Nb	5.3	6.0	4.7	5.5	5.3	5.6	4.4	5.8	4.1	4.4	4.9
Ba/Th	85.0	75.0	68.7	96.5	88.6	69.4	72.7	93.8	50.8	60.0	78.6
K/La	169	123	106	182	239	166	161	196	65	168	168
Zr/Nb	4.8	3.8	5.5	4.0	4.3	5.0	3.9	4.4	5.1	4.5	5.3
Zr/Y	8.4	8.8	9.8	7.8	8.4	10.4	9.2	7.5	8.0	8.7	9.9
Nb/U	58.3	50.0	55.0	58.3	58.3	46.2	62.5	85.0	77.5	57.5	64.3
Ce/Pb	42.7	–	–	–	32.5	–	–	–	40.0	–	–
Nd/Pb	22.7	–	–	–	17.5	–	–	–	20.7	–	–

Sample	LP1	LP7	LP8	LP13	LP14	LP25	LP43	LP46	LP47	LP48	LP81
Locality	La Palma										
Major elements, wt.%											
SiO_2	40.88	44.24	43.89	42.32	42.89	42.91	41.74	41.20	42.79	42.67	42.25
TiO_2	1.51	2.64	3.01	2.13	2.50	2.72	3.91	4.07	4.01	3.29	2.36
Al_2O_3	4.86	9.38	10.95	6.89	8.09	9.09	12.97	12.30	15.12	11.65	7.73
Fe_2O_3	14.34	12.48	12.38	13.06	12.97	12.78	15.20	14.31	14.55	14.15	13.01
MnO	0.18	0.17	0.17	0.17	0.17	0.17	0.19	0.19	0.19	0.18	0.17
MgO	29.83	14.39	11.07	22.55	19.92	17.69	9.03	9.98	6.14	12.29	20.24
CaO	5.79	13.40	13.48	9.55	10.32	10.71	11.86	12.86	10.72	11.90	10.36
Na_2O	0.80	1.36	1.70	0.90	0.83	1.20	2.95	2.48	3.57	1.95	0.93
K_2O	0.49	0.71	0.94	0.58	0.69	0.81	0.89	1.27	1.58	1.05	0.66
P_2O_5	0.24	0.29	0.43	0.28	0.34	0.37	0.55	0.66	0.68	0.41	0.31
H_2O	0.50	1.58	1.42	1.60	2.01	1.61	0.65	0.66	0.43	0.55	0.55
CO_2	0.04	0.43	1.04	0.30	0.32	0.19	0.00	0.01	0.03	0.00	0.00
Total	99.46	101.07	100.48	100.31	101.05	100.23	99.91	99.96	99.80	100.07	98.55
Trace elements, ppm											
V	152	298	341	221	236	260	418	419	374	342	239
Cr	1920	826	456	1616	1328	1339	412	422	110	547	1459
Ni	974	252	137	772	613	444	187	136	60	226	624
Rb	12	17	26	16	15	21	14	32	38	27	17
Sr	545	436	549	351	450	475	722	878	989	632	407
Y	19	19	22	15	20	19	27	27	30	23	16
Zr	146	173	215	123	133	171	281	259	328	220	144
Nb	22	30	45	28	35	38	56	59	67	50	32
Ba	168	220	266	172	237	236	341	453	462	331	216
La	26	26	34	21	25	31	43	48	57	38	25
Ce	56	58	71	43	51	60	89	96	119	77	51
Pr	6.9	7.1	8.4	5.2	6.2	7.4	11.5	11.2	14.1	9.1	6.4
Nd	30	30	36	22	27	31	48	46	56	39	28
Sm	6.4	6.1	7.7	4.9	5.6	6.9	9.3	9.7	11.0	7.9	5.8
Eu	2.2	2.0	2.5	1.5	1.9	2.0	2.7	2.9	3.2	2.4	1.7
Gd	6.0	5.8	7.1	4.3	5.3	5.9	7.9	8.0	8.9	7.1	4.6
Tb	0.8	0.8	1.0	0.6	0.7	0.8	1.1	1.1	1.2	0.9	0.7
Dy	4.1	4.2	5.3	3.2	3.7	4.2	5.4	5.8	6.6	5.2	3.7
Ho	0.7	0.7	0.9	0.5	0.6	0.7	1.0	1.0	1.1	0.8	0.6
Er	1.7	1.8	2.3	1.3	1.6	1.7	2.2	2.5	2.8	2.0	1.5
Tm	0.2	0.2	0.3	0.2	0.2	0.2	0.3	0.3	0.4	0.3	0.2
Yb	1.2	1.3	1.7	1.0	1.1	1.4	2.0	1.7	2.3	1.6	1.2
Lu	0.2	0.2	0.2	0.1	0.2	0.2	0.2	0.3	0.3	0.2	0.2
Hf	3.9	4.8	5.4	3.2	3.7	4.6	6.4	6.0	7.4	5.5	4.0

Table 2 (*continued*)

Sample	LP1	LP7	LP8	LP13	LP14	LP25	LP43	LP46	LP47	LP48	LP81
Locality	La Palma										
Trace elements, ppm											
Ta	2.3	2.1	3.1	1.8	2.2	2.7	3.9	4.1	4.8	3.5	2.2
Pb	ND	ND	ND	1.3	ND	2.0	3.1	2.5	3.8	2.0	1.6
Th	2.0	2.1	2.9	1.8	2.2	2.7	3.7	5.0	5.3	3.5	2.2
U	0.6	0.6	0.7	0.5	0.6	0.7	1.0	1.2	1.4	1.0	0.7
$(La/Sm)_n$	2.6	2.7	2.8	2.7	2.8	2.8	2.9	3.1	3.3	3.0	2.7
$(Nb/La)_n$	0.8	1.1	1.3	1.3	1.4	1.2	1.3	1.2	1.2	1.3	1.3
$(Ta/La)_n$	1.5	1.4	1.6	1.5	1.5	1.5	1.6	1.5	1.5	1.6	1.5
$(K/La)_n$	0.4	0.5	0.5	0.5	0.5	0.5	0.4	0.5	0.5	0.5	0.5
$(Pb/La)_n$	–	–	–	0.2	–	0.2	0.2	0.2	0.2	0.2	0.2
Ba/Nb	7.6	7.3	5.9	6.1	6.8	6.2	6.1	7.7	6.9	6.6	6.8
Ba/Th	84.0	104.8	91.7	95.6	107.7	87.4	92.2	90.6	87.2	94.6	98.2
K/La	156	227	230	229	229	217	172	220	230	229	219
Zr/Nb	6.6	5.8	4.8	4.4	3.8	4.5	5.0	4.4	4.9	4.4	4.5
Zr/Y	7.7	9.1	9.8	8.2	6.7	9.0	10.4	9.6	10.9	9.6	9.0
Nb/U	36.7	50.0	64.3	56.0	58.3	54.3	56.0	49.2	47.9	50.0	45.7
Ce/Pb	–	–	–	33.1	–	30.0	28.7	38.4	31.3	38.5	31.9
Nd/Pb	–	–	–	16.9	–	15.5	15.5	18.4	14.7	19.5	17.5

Concentrations of major and trace elements in the shield-building stage lavas from Gran Canaria, Tenerife, La Gomera and La Palma. H_2O and CO_2 contents equivalent to loss on ignition (LOI) and in some lavas exceed 2% due to secondary rock alteration that is very common for the Canary Islands shield stage lavas. Element ratios are given normalized to primitive mantle composition (Hofmann, 1988). Compositions of the samples labeled with (*) are taken from Hoernle and Schmincke (1993a); Fe_2O_3=total iron, ND=not determined, –=no value.

10 wt.% (i.e., from 229 to 592 ppm at ca. 14 wt.% MgO; panel with Ni in Fig. 4). This is unlikely to be an analytical artifact since similar variations were obtained by both XRF and ICP-MS methods and could not be related to different degrees of Ol accumulation in the individual rock samples that result in Ni–MgO increasing coherently. We believe that the observed NiO scatter in whole rocks represents true variations in the melt. The shield stage lavas from Gran Canaria are characterized by systematically higher Ni contents for a given MgO content compared to samples from other islands of the Canary archipelago.

The concentrations of incompatible trace elements such as Rb, Sr, Y, Zr, Nb, Ba increase with decreasing MgO and are largely controlled by fractional crystallization (Fig. 4). As is the case with Ni, the Gran Canaria lavas are characterized by systematically higher concentrations of Zr and Y and lower concentrations of Ba and Sr at a given MgO content compared to the lavas from other islands. The other incompatible elements show no clear inter-island differences. Because these compositional signatures were reproduced in different laboratories, they are unlikely to represent a bias due to the different analytical methods employed.

The rocks are moderately enriched in light rare earth elements (LREE), most showing pronounced Nb and Ta enrichment when normalized to primitive mantle (Fig. 5) and K and Pb depletion common for HIMU-type mafic rocks ($(La/Sm)_n$=2.1–4.6, $(Nb/La)_n$=0.8–1.5, $(Ta/La)_n$=1.3–1.8, $(K/La)_n$=0.2–0.7, $(Pb/La)_n$=0.2–0.3 (Table 2). Shield basalts from the Canary Islands have Nb/U=37–85 and Ce/Pb=24–43 and Nd/Pb=13–23 (Table 2). These ratios overlap and extend to higher values than those reported for global MORB and OIB magmas (Nb/U=47±10, Ce/Pb=25±5 and Nd/Pb=24±5; Hofmann et al., 1986; Rehkämper and Hofmann, 1997) and determined for the primitive Earth's mantle (Nb/U≈30, Ce/Pb≈9; Hofmann, 1988) and upper continental crust (Nb/U≈9, Ce/Pb≈3; Taylor and McLennan, 1985).

3.2.3. Sr, Nd, Pb and O isotopes

The Sr–Nd–Pb and O isotopic data are summarized in Table 3 (for analytical details see Appendix C.1.3). In the Sr–Nd isotope diagram (Fig. 6), the shield stage lavas from different islands show an elongated field subparallel to the $^{87}Sr/^{86}Sr$-axis exhibiting a relatively wide Sr isotopic range ($^{87}Sr/^{86}Sr$=0.702966–0.703312) accompanied by a restricted range of Nd isotope ratios ($^{143}Nd/^{144}Nd$=0.512884–0.512929). The lavas from Tenerife and La Palma are characterized by stronger HIMU signature (i.e., high time-integrated $\mu=^{238}U/^{204}PB$ ratios; Zindler and Hart, 1986) in coordinates $^{87}Sr/^{86}Sr$ vs. $^{143}Nd/^{144}Nd$ ratios and correspond to the reference fields of Tenerife and the western Canaries (Hoernle and Tilton, 1991; Hoernle et al., 1991; Simonsen et al., 2000 and references therein), while

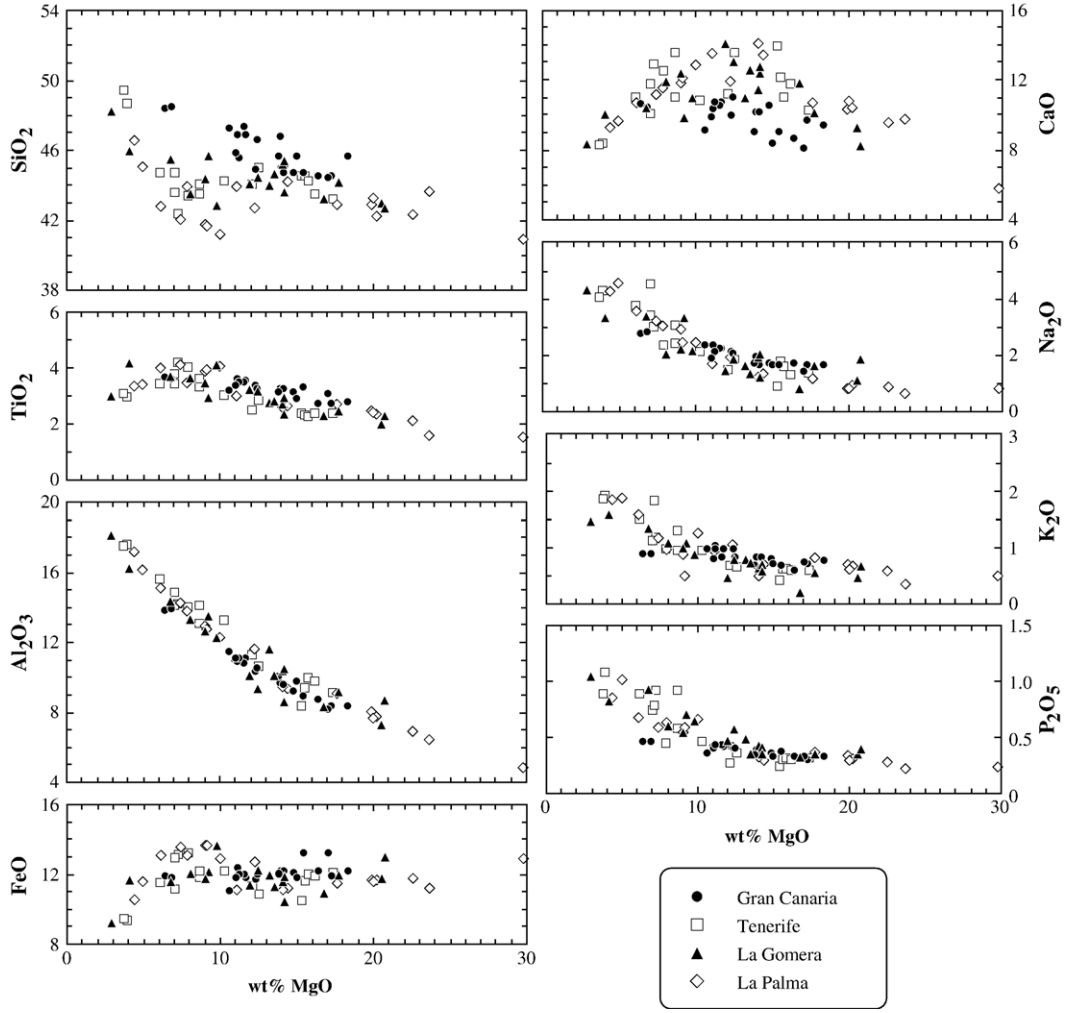

Fig. 3. Major element variation diagrams illustrating the compositions of the shield basalts on Gran Canaria, Tenerife, La Gomera and La Palma, as a function of MgO contents. The Gran Canaria shield basalts generally have lower CaO but higher SiO_2 and TiO_2 contents than the other shield basalts at a given MgO. The other elements correlate well with MgO, following fractional crystallization–phenocryst accumulation trends.

the Gran Canaria rocks tend to plot in a restricted field to the right of the HIMU end-member, similar to the compositions previously reported for Gran Canaria by Cousens et al. (1990), Hoernle et al. (1991), Thirlwall et al. (1997) and Abratis et al. (2002) (Fig. 6). The lavas from La Gomera show intermediate isotopic compositions and plot between Tenerife–La Palma and Gran Canaria lavas, exhibiting a correlation between Nd and Sr isotopes ($R^2=0.75$).

The lead isotopic ratios (total range in $^{206}Pb/^{204}Pb=19.49–20.27$, $^{207}Pb/^{204}Pb=15.59–15.66$, $^{208}Pb/^{204}Pb=39.21–39.81$; Fig. 7) correspond, except for one the most radiogenic sample from Tenerife (TF51, aphyric basalt from Roque del Conde massif; $^{206}Pb/^{204}Pb=20.27$, $^{207}Pb/^{204}Pb=15.65$, $^{208}Pb/^{204}Pb=39.81$; reproduced twice; Table 3), to those previously reported for the Canary Islands (e.g., Cousens et al., 1990; Hoernle and Tilton, 1991; Hoernle et al., 1991; Thirlwall et al., 1997; Simonsen et al., 2000; Abratis et al., 2002). We have no clear explanation for the Pb isotopic composition of TF51, which has more radiogenic Pb isotope ratios than all other lavas reported thus far from the Canary Islands.

Except for two samples from Gran Canaria that plot above the Northern Hemisphere Reference Line (NHRL; Hart, 1984) on the $^{207}Pb/^{204}Pb$ vs. $^{206}Pb/^{204}Pb$ diagram (Fig. 7a), the other shield stage lavas from Tenerife, La Gomera and La Palma form a positively correlated trend slightly below and subparallel to the NHRL ($^{208}Pb/^{204}Pb$ vs. $^{206}Pb/^{204}Pb$ diagram; Fig. 7b), extending from the composition of a seismic low-velocity region of upwelling mantle (i.e.,

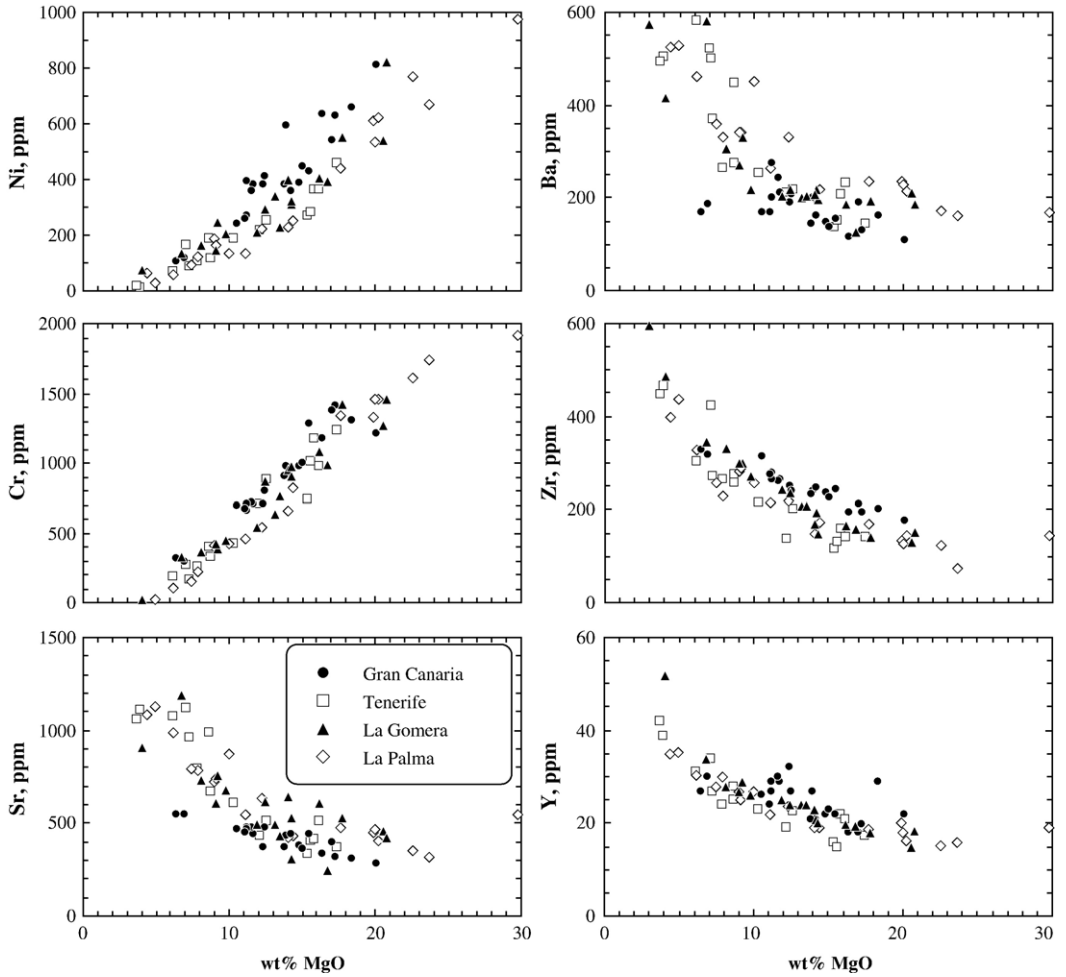

Fig. 4. Trace element vs. MgO variation diagrams for the shield stage lavas on Gran Canaria, Tenerife, La Gomera and La Palma. All trace elements follow fractional crystallization trends. Ni and Cr concentrations decrease with decreasing MgO, since they are compatible in Ol and Cpx, respectively, while the other trace elements demonstrate incompatible behavior. Nickel and Zr in the Gran Canaria shield lavas tend to be higher and Ba and Sr lower for a given MgO content compared to lavas from other islands.

LVC—low-velocity composition; Hoernle et al., 1995) to less radiogenic Pb isotopic compositions. On a diagram of $^{206}Pb/^{204}Pb$ vs. $^{87}Sr/^{86}Sr$ isotope ratios, the Tenerife, La Gomera and La Palma shield lavas extend from the LVC component towards DMM (Fig. 7c). Samples from La Gomera exhibit good positive correlations of $^{206}Pb/^{204}Pb$ vs. $^{207}Pb/^{204}Pb$ ($R^2=0.94$), $^{208}Pb/^{204}Pb$ ($R^2=0.996$) and $^{87}Sr/^{86}Sr$ ($R^2=0.64$) and a negative correlation of $^{206}Pb/^{204}Pb$ vs. $^{143}Nd/^{144}Nd$ ($R^2=0.88$), consistent with mixing between LVC and DM sources. Although the Gran Canaria lavas fall on the same trend as those presented by other islands on the $^{206}Pb/^{204}Pb$ vs. $^{143}Nd/^{144}Nd$ diagram (Fig. 7d), they generally show higher $^{87}Sr/^{86}Sr$, $^{207}Pb/^{204}Pb$ and $^{208}Pb/^{204}Pb$ at a given $^{206}Pb/^{204}Pb$, extending towards the composition of pelagic sediments or EM2 component, as described previously by Hoernle et al. (1991), Thirlwall et al. (1997), and Abratis et al. (2002).

Strontium, Nd and Pb isotopes show no systematic relationships with trace element concentrations and ratios for the lavas from each particular island (Fig. 8), as demonstrated for example of Tenerife by Simonsen et al. (2000) and Abratis et al. (2002). Although the behavior of trace elements and Sr, Nd and Pb isotopes is complex, we observe a crude positive trend of $^{87}Sr/^{86}Sr$ with Zr/Nb ratios (Fig. 8b) and a crude inverse correlation between $^{206}Pb/^{204}Pb$ with Zr/Nb ratio (Fig. 8d). These trends cannot be explained by crustal assimilation but could be by mixing of different plume and/or lithospheric mantle components.

The O isotopic ratios were analyzed in 10 olivine separates from shield stage basalts from Gran Canaria,

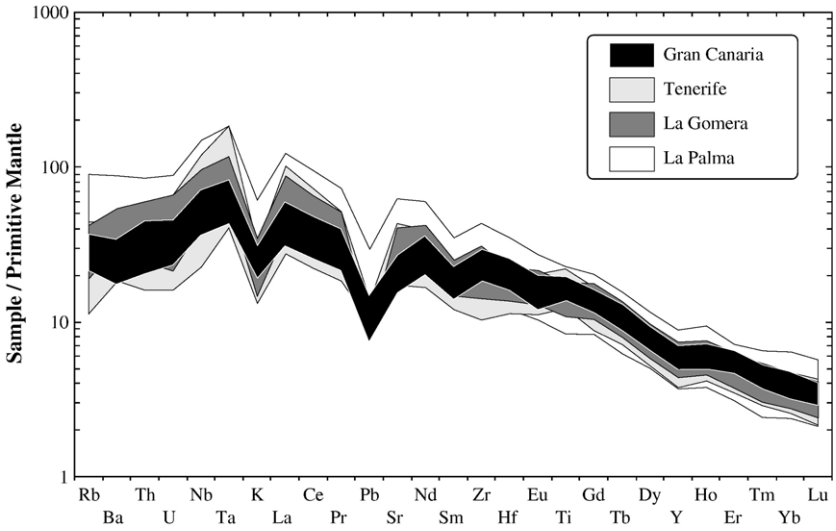

Fig. 5. Multi-element diagrams showing concentrations of trace elements in the shield stage lavas on Canary Islands normalized to primitive mantle (Hofmann, 1988). Significant K and Pb minimums in the trace element patterns are common in mafic HIMU-type rocks.

Tenerife and La Gomera. The $\delta^{18}O$ values (from 4.3 to 5.8±0.3‰, 2σ; Table 3) are in the range of values previously determined in olivines from Gran Canaria, Canary Islands, and São Miguel, Azores (4.6–5.3‰; Thirlwall et al., 1997; Widom and Farquhar, 2003). The $\delta^{18}O$ values show a crude inverse correlation with $^{86}Sr/^{87}Sr$ (Fig. 9) and a crude positive correlation with $^{143}Nd/^{144}Nd$ isotopic ratios (Table 3). No clear relationships exist with Pb or noble gas isotopic ratios, except for the samples from Tenerife showing positive correlations of $\delta^{18}O$ values with Pb isotopes (R^2=0.68 for $^{206}Pb/^{204}Pb$, 0.99 for $^{207}Pb/^{204}Pb$ and 0.5 for $^{208}Pb/^{204}Pb$ ratios).

3.2.4. Noble gases

The noble gas abundances and isotopic compositions are listed in Table 4 (for analytical details see Appendix C.1.4). The $^3He/^4He$ ratios range from 5.7 to 9.3 R_A, where R_A represents $^3He/^4He$ ratio of the atmosphere and is equal to 1.4×10^{-6}. Lavas from Gran Canaria, Tenerife and La Gomera have $^3He/^4He$ ratios similar or somewhat lower than those of typical MORB (8±1 R_A; Fig. 10a); their $^3He/^4He$ ratios are in agreement with the data reported for historical and Quaternary lavas on the Canary Islands (5.6–7.9 R_A; Graham, 2002 and references therein). Two picritic lavas collected within the Caldera de Taburiente on La Palma (7.7 and 9.3 R_A) agree well with previously reported data for lavas (6.3 to 8.9 R_A) and for one geothermal cold spring (9.5 R_A) (Hilton et al., 2000). Very similar $^3He/^4He$ ratios (up to 9.6 R_A) were found in the volcanic–hydrothermal discharges inside the Taburiente Caldera by Pérez et al. (1994) and between 6.0 and 8.1 R_A in the cold springs in and around the Teide volcano on Tenerife (Pérez et al., 1996). $^3He/^4He$ ratios in younger lavas from La Palma and El Hierro are systematically higher compared to the eastern Canary Islands (Graham, 2002), while Pliocene lavas on La Gomera show nearly the full range presently known for the Canary Islands volcanic rocks (5.5–9.3 R_A).

The $^{40}Ar/^{36}Ar$ ratios cover a relatively narrow range from 306 to 447, being only slightly higher than the atmospheric value ($^{40}Ar/^{36}Ar$=295.5±0.5; compilation by Porcelli et al., 2002) (Fig. 10b). These values are low compared to those of typical mantle-derived samples (e.g., Kaneoka, 1983; Ozima and Podosek, 1983; Allègre et al., 1986) but are very close to the $^{40}Ar/^{36}Ar$ ratios found in the Afar basalts by Marty et al. (1993). In contrast to helium that has a relatively low abundance in the atmosphere due to its escape, the heavy noble gases do accumulate over the Earth's history. Hence, later contamination of mantle-derived magmas by atmospheric heavy noble gases could be widespread (e.g., Farley and Craig, 1994; Ballentine and Barfod, 2000; Graham, 2002; Kaneoka et al., 2002 and references therein). This process can partially or completely erase the original source signature recorded in the rocks and minerals. Several factors could result in low $^{40}Ar/^{36}Ar$ values observed in most Canary samples:

1. Air contamination during laboratory handling (e.g., Ballentine and Barfod, 2000). We consider this option as unlikely, since all olivine samples were

Table 3
Nd, Sr, Pb and O isotopic composition of selected shield stage lavas on Canary Islands [a]

Sample	$^{87}Sr/^{86}Sr$	$^{143}Nd/^{144}Nd$	$^{206}Pb/^{204}Pb$	$^{207}Pb/^{204}Pb$	$^{208}Pb/^{204}Pb$	Δ7/4 [b]	$\delta^{18}O$ [c] olivine	$\delta^{18}O$ [d] melt
Gran Canaria								
G1262*	0.703260(16)	0.512915(5)	19.527	15.619	39.288	1.1	ND	–
G1265*	0.703267(17)	0.512898(14)	19.549	15.621	39.307	1.1	ND	–
GC35	0.703234(7)	0.512906(7)	19.663	15.611	39.399	− 1.1	4.9	5.3
GC59	0.703312(7)	0.512917(6)	19.571(1)	15.602(0)	39.309(1)	− 1.0	ND	–
Tenerife								
TF4	0.702998(7)	0.512916(11)	19.930(2)	15.618(1)	39.637(0)	− 3.3	5.1	5.5
TF7	0.702966(7)	0.512924(6)	19.872(2)	15.620(2)	39.564(0)	− 2.5	5.3	5.7
TF9	0.703034(4)	0.512907(5)	19.729(2)	15.616(1)	39.420(3)	− 1.4	ND	–
TF16	0.702988(7)	0.512924(9)	19.891(2)	15.627(1)	39.525(0)	− 2.0	5.8	6.2
TF64	0.703004(7)	0.512889(10)	19.711(1)	15.613(1)	39.433(3)	− 1.5	ND	–
TF23	0.703066(6)	0.512904(4)	19.650(1)	15.604(1)	39.285(2)	− 1.7	4.3	4.7
TF51	0.703088(4)	0.512919(5)	20.269(1)	15.648(1)	39.802(2)	− 4.0	ND	–
TF51rep	ND	ND	20.265(1)	15.650(1)	39.809(2)	− 3.8	ND	–
La Gomera								
LG1	0.703115(8)	0.512903(10)	19.874(3)	15.626(2)	39.542(5)	− 2.0	4.9	5.3
LG11	0.703123(5)	0.512896(9)	19.878(3)	15.629(3)	39.548(6)	− 1.7	5.0	5.4
LG35	0.703051(6)	0.512929(9)	19.567(3)	15.592(3)	39.212(6)	− 2.0	5.0	5.4
LG50	0.703115(8)	0.512908(8)	19.732(1)	15.606(1)	39.409(1)	− 2.4	ND	–
LG53	0.703057(7)	0.512917(5)	19.774(1)	15.623(1)	39.431(3)	− 1.2	ND	–
LG58	0.703149(7)	0.512904(8)	19.816(1)	15.615(1)	39.477(2)	− 2.4	5.4	5.8
LG59	0.703189(7)	0.512898(9)	19.923(4)	15.640(3)	39.616(9)	− 1.1	4.4	4.8
LG65	0.703171(6)	0.512890(7)	20.042(3)	15.655(3)	39.733(6)	− 0.9	ND	–
La Palma								
LP1	0.703087(7)	0.512897(5)	19.492(1)	15.598(1)	39.249(3)	− 0.6	ND	–
LP13	0.703050(6)	0.512884(5)	19.835(4)	15.611(3)	39.609(8)	− 3.0	ND	–
LP25	0.703068(7)	0.512893(4)	19.833(1)	15.613(1)	39.617(2)	− 2.8	ND	–
LP47	0.703040(8)	0.512895(6)	19.834(1)	15.608(1)	39.644(3)	− 3.3	ND	–
LP48	0.703056(8)	0.512898(6)	19.866(2)	15.611(1)	39.640(3)	− 3.3	ND	–
LP81	0.703062(7)	0.512886(4)	19.893(3)	15.614(2)	39.667(6)	− 3.3	ND	–

[a] Isotopic compositions of samples labeled with (*) are taken from Hoernle et al. (1991). Sr–Nd–Pb isotopic compositions were determined from a separate split of the same powders, as used for major and trace element analyses. Prior to sample dissolution the powders were leached in hot 6N HCl for 1 h and thereafter repeatedly rinsed in 18.2 MΩ water. For O isotope determinations, handpicked olivine separates cleaned in 10% HF-solution and then in ultrasonically in distilled water were used. Sr, Nd and Pb isotope ratios were measured on a Finnigan® MAT 262 thermal ionization mass spectrometer (TIMS) at IFM-GEOMAR, operating in static multicollection for Sr and Pb and dynamic multicollection for Nd. Sr and Nd isotopic ratios were normalized within run to $^{86}Sr/^{88}Sr=0.1194$ and $^{146}Nd/^{144}Nd=0.7219$. The longterm reproducibility of NBS 987 is $^{87}Sr/^{86}Sr=0.710249\pm22$ (2 sigma, $N=160$) and $^{143}Nd/^{144}Nd=0.511844\pm11$ (2 sigma, $N=68$) for La Jolla. NBS 981 values ($N=110$) are $^{206}Pb/^{204}Pb=16.899\pm7$, $^{207}Pb/^{204}Pb=15.437\pm9$, $^{208}Pb/^{204}Pb=36.529\pm27$ and are corrected to those of Todt et al. (1996). Errors (given in parentheses) refer to the least significant digits and are 2-sigma mean within-run precision. Replicate analyses yielded an external reproducibility better than 0.05% per a.m.u. (atomic mass unit) for Pb and <0.000015 for $^{143}Nd/^{144}Nd$ and $^{87}Sr/^{86}Sr$.

[b] Δ7/4 represents vertical deviation in $^{207}Pb/^{204}Pb$ ratios from the Northern Hemisphere Reference Line (NHRL) (Hart, 1984).

[c] Oxygen isotopic compositions are given in permil units (‰) and defined relative to the Standard Mean Ocean Water (SMOW).

[d] Calculated values assuming a melt–olivine fractionation of 0.36±0.11‰ (Eiler et al., 2000).

subjected to acid leaching before analysis preventing the low $^{40}Ar/^{36}Ar$ ratios to be caused by atmospheric contamination.

2. Atmospheric signature inherited during underplating, eruption or magma storage. This includes magma contamination by seawater or groundwater-rich fluids, as well as shallow depth assimilation of altered oceanic crust. Taking into account that crystallization of olivine phenocrysts probably occurred at relatively high pressures (ca. 3–7 kbar and even higher; Gurenko et al., 1996, 1998; Nikogosian et al., 2002), corresponding to minimum depths of 10–20 km, the impact of surface contamination on the isotopic composition of olivine is unlikely. On the other hand, magma contamination during underplating is a process capable of significantly decreasing $^{40}Ar/^{36}Ar$ ratios. Kaneoka et al. (2002) examined noble gases in olivines from Loihi basalts using four-

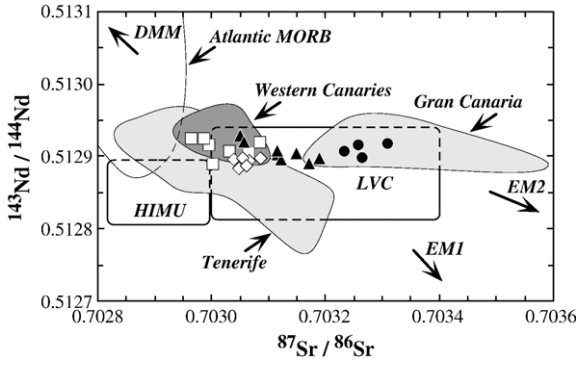

Fig. 6. Sr vs. Nd isotope diagram for the Canary Islands subaerial shield stage lavas. In this figure and Figs. 8 and 9, the reference fields for Gran Canaria and Tenerife shield rocks are taken from Hoernle et al. (1991), Thirlwall et al. (1997), Simonsen et al. (2000); the field of *Western Canaries* is taken from Hoernle and Tilton (1991) and Hoernle et al. (1991); the compositions of DMM, HIMU, EM1 and EM2 mantle components (Zindler and Hart, 1986). The LVC from Hoernle et al. (1995) is low-velocity component ubiquitous beneath the eastern Atlantic, Europe and the western Mediterranean.

stage stepwise heating (i.e., 600, 1000, 1500 and 1900 °C) and found the $^{40}Ar/^{36}Ar$ ratios below 500 in 600 and 1000 °C fractions, while the higher $^{40}Ar/^{36}Ar$ ratios up to 2660 were observed in 1500 and 1900 °C fractions only. These authors claim that low $^{40}Ar/^{36}Ar$ ratios of <500 might be due to decrepitating low-density secondary fluid inclusions that are liberated at 1000 °C. Since our data represent a bulk analysis of noble gases extracted during crushing, the origin of relatively low $^{40}Ar/^{36}Ar$ ratios due to fluid inclusion decrepitation is very likely.

3. Source composition. A low-$^{40}Ar/^{36}Ar$ signature of the recycled material is still under debate. If seawater, the most probable source of atmospheric Ar, is dehydrated during subduction, Ar remaining in the slab may have quite variable and even high $^{40}Ar/^{36}Ar$ ratios due to addition of radiogenic ^{40}Ar with time. However, Marty et al. (1993) ascribed low Ar isotopic ratios in Afar basalts to a deep component in the mantle (e.g., recycled oceanic crust) less degassed in

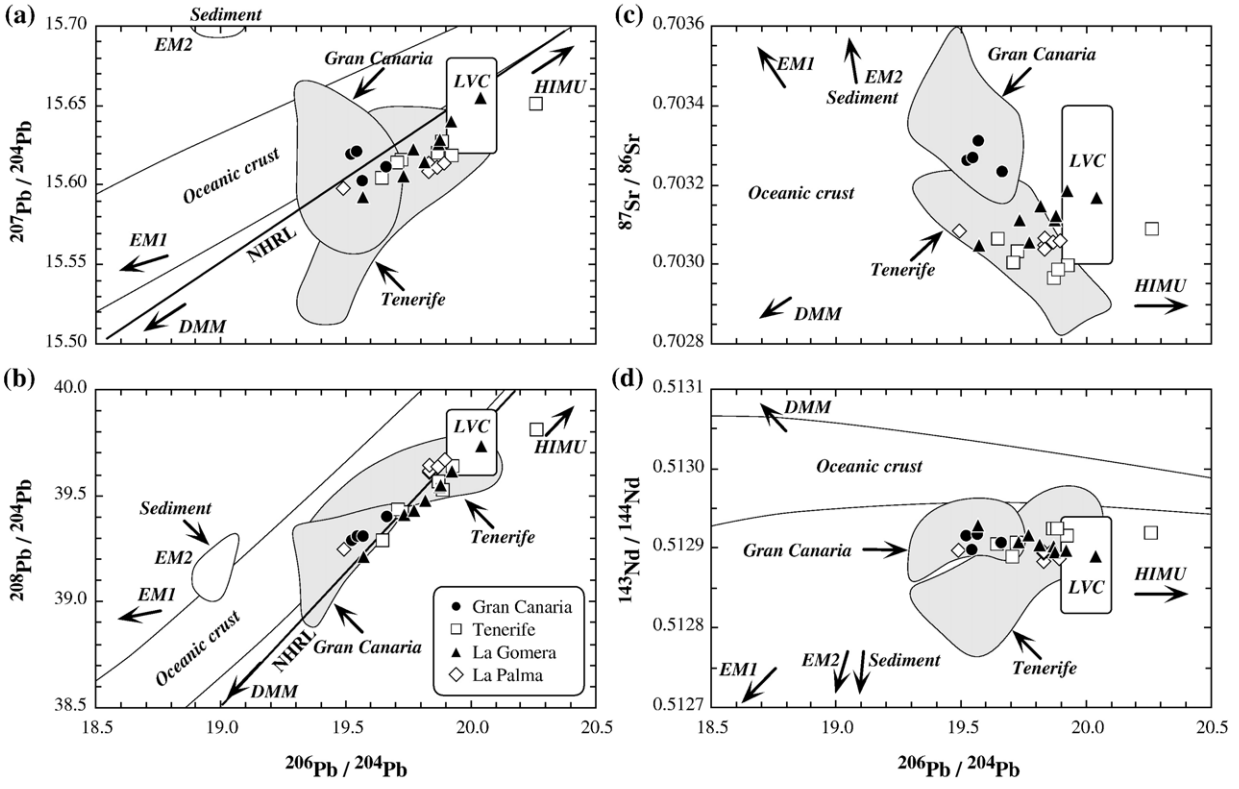

Fig. 7. $^{206}Pb/^{204}Pb$ ratios verses (a) $^{207}Pb/^{204}Pb$, (b) $^{208}Pb/^{204}Pb$ (c) $^{87}Sr/^{86}Sr$, and (d) $^{143}Nd/^{144}Nd$ ratios for the shield stage rocks on the Canary Islands. NHRL = Northern Hemisphere Reference Line from Hart (1984). The fields of local sediments (*Sediment*) and Layer 2 and Layer 3 pillow lavas, sheet flows, dikes and gabbros (*Oceanic Crust*) are based on the data from Hoernle et al. (1991) and Hoernle (1998). Data sources for the other reference fields are the same as in Fig. 6.

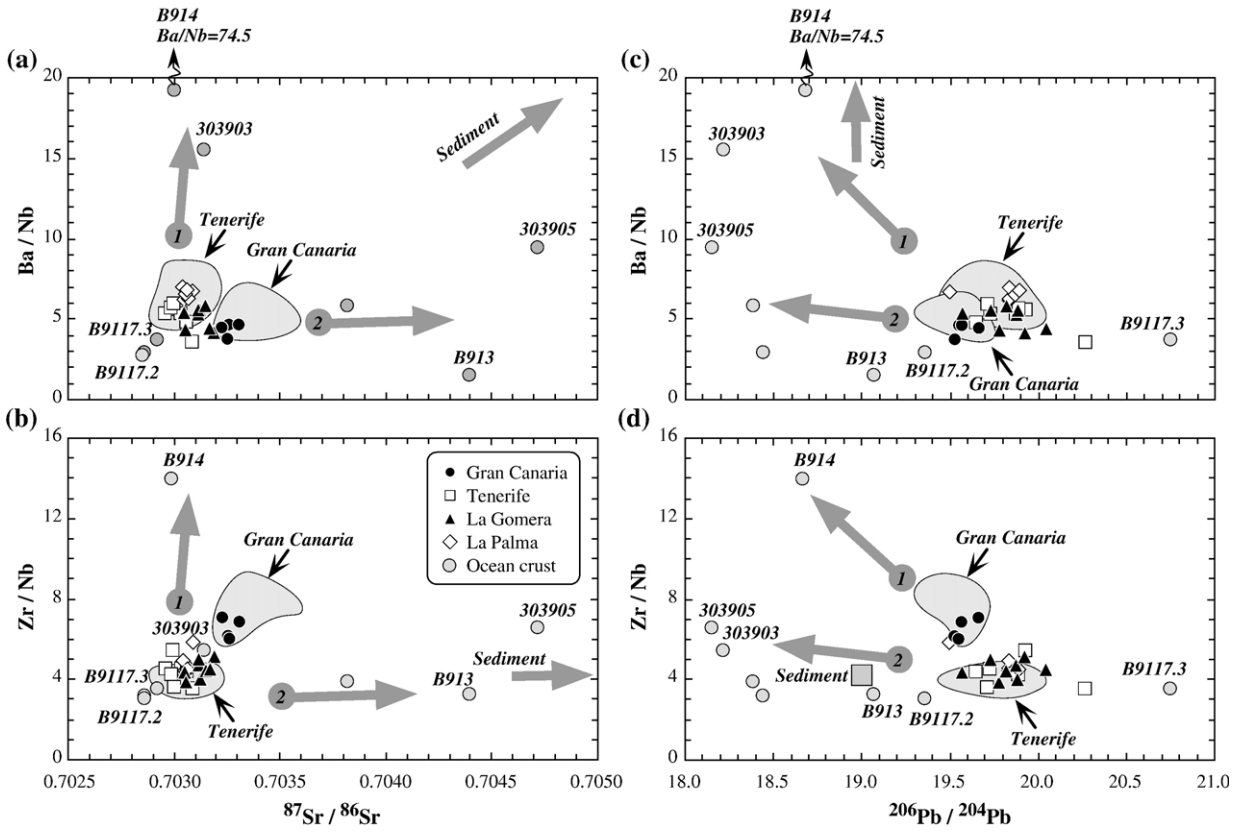

Fig. 8. Relationships between trace elements and radiogenic isotopes in the Canary Islands shield stage lavas. (a) Ba/Nb and (b) Zr/Nb plotted against $^{87}Sr/^{86}Sr$ ratios, and (c) Ba/Nb and (d) Zr/Nb against $^{206}Pb/^{204}Pb$ ratios. Data sources for reference fields are the same as in Fig. 6. The 1 and 2 shaded arrows demonstrate possible contamination trends of presumably uncontaminated magma with hydrothermally altered oceanic crust and sediments (Hoernle et al., 1991; Hoernle, 1998). These trends could potentially explain Ba/Nb vs. Sr and Pb isotope variations in the shield lavas but fail to account for Zr/Nb-isotope relationships and do not support crustal assimilation, either sedimentary or igneous (see text). The B913, B914, B9117.2, B9117.3, 303903 and 303905 labels are ocean crust sample numbers, as given in Hoernle (1998).

^{36}Ar than a MORB source. Furthermore, Sarda (2004) suggested that the atmospheric air signature observed in many MORB and OIB samples could also be of deep mantle origin via recycling. We, therefore, do not exclude the possibility that the low $^{40}Ar/^{36}Ar$ ratios found in some of the Canary Island shield lavas could potentially result from a crustal component transported into the magma source region via subduction and then returned to the surface via a mantle plume.

Because of high analytical uncertainty, only the $^{20}Ne/^{22}Ne$ isotopic ratios are presented in Table 4. They range from 9.0 to 10.3 and are very close to the atmospheric value of 9.80±0.08 (compilation by Porcelli et al., 2002). On the basis of the existing data, it remains also unclear whether near-atmospheric $^{20}Ne/^{22}Ne$ isotope ratios found in the Canary Island shield lavas (a) resemble a mantle source signature, (b) represent contaminated atmospheric Ne resulting from decrepitated secondary fluid inclusions in Ol phenocrysts, or (c) reflect low intrinsic concentrations of Ne in Ol separates, also proposed by Hanyu et al. (1999).

4. Discussion

The compositional signatures of the Canary shield stage magmas ranging from picrites, olivine tholeiites, alkali basalts and basanites to tephrites and trachybasalts may reflect (a) variable bulk chemical composition of the mantle source(s), (b) variations in residual mineralogy, (c) different partial melting parameters, (d) melt–lithospheric mantle interaction and finally (e) magma differentiation and contamination within the crust (e.g., Schmincke, 1982; Hoernle and Tilton, 1991; Hoernle et al., 1991; Hoernle and Schmincke,

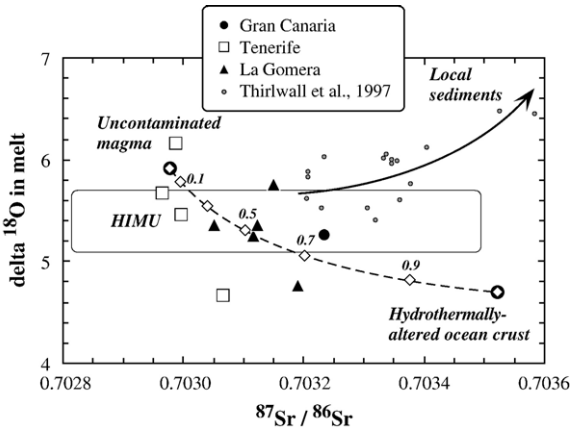

Fig. 9. $\delta^{18}O$ vs. $^{87}Sr/^{86}Sr$ isotope ratios from this study overlap the field for HIMU (Widom and Farquhar, 2003), consistent with derivation of the magmas from recycled oceanic crust. The data from the shield basalts in this study form a crude inverse correlation. The decrease in $\delta^{18}O$ with increasing $^{87}Sr/^{86}Sr$ is not consistent with assimilation of sediments, which have high $\delta^{18}O$ and $^{87}Sr/^{86}Sr$, or reasonable amounts of hydrothermally altered Jurassic oceanic crust beneath the Canary Islands. The following end-member compositions are used to calculate binary mixing between extreme components providing possibly uncontaminated plume-derived magma and hydrothermally altered oceanic crust compositions: *Uncontaminated magma*, $\delta^{18}O=5.9‰$, $^{87}Sr/^{86}Sr=0.70298$, Sr=409 ppm (average of TF7 and TF16 samples; Table 3); *Hydrothermally altered ocean crust*, $\delta^{18}O=4.7‰$, $^{87}Sr/^{86}Sr=0.70352$, Sr=123.4 ppm (average of HAT B 914, B 9117.2 and 303905 samples; Hoernle, 1998; Hansteen and Troll, 2003). Assimilation of hydrothermally-altered ocean crust appears to be an implausible explanation of the observed compositional range in the Miocene lavas, since unrealistically large amounts of contaminant (up to 70 wt.%) are required. Data from Thirlwall et al. (1997) from the Gran Canaria shield basalts form a positive trend on the diagram, extending from the data from this study and the HIMU field towards sediments. Reference fields of *HIMU*-type rocks are from Widom and Farquhar (2003). The HIMU-range of 4.7–5.3‰ by Widom and Farquhar (2003) represents O isotopic composition of olivines that we converted to "melt equivalents" assuming $\Delta_{melt\text{-}ol}=0.36‰$ (Eiler et al., 2000). Similarly, the clinopyroxene $\delta^{18}O$ values (4.9–6.8‰) by Thirlwall et al. (1997) were converted to "melt equivalents" assuming $\Delta_{melt\text{-}cpx}=0.4‰$ (e.g., Kyser et al., 1981; Vroon et al., 2001 and references therein).

1993a,b; Marcantonio et al., 1995; Thirlwall et al., 1997; Hoernle, 1998; Widom et al., 1999; Simonsen et al., 2000; Geldmacher et al., 2001; Gurenko et al., 2001; Abratis et al., 2002; Hansteen and Troll, 2003; Lundstrom et al., 2003). All processes listed above can act independently or together with other processes, contributing variably to magma genesis in space and time. Our main focuses here are to evaluate the contribution of each particular process to the formation of the mafic lavas from Gran Canaria, Tenerife, La Gomera and La Palma, and to determine whether or not there is a systematic difference between the islands over the 15 Ma time interval of volcanic shield construction.

4.1. Fractional crystallization and accumulation of phenocrysts

The most primitive shield stage magmas of the Canary Islands are picritic and are believed to have formed at pressures of ~ 30 kbar (ca. 100 km deep) within the garnet stability field at temperatures between 1500 and 1600 °C (Schmincke, 1982; Hoernle and Schmincke, 1993a; Gurenko et al., 1996, 1998). Chemical variations in the shield stage lavas are often attributed to crystal fractionation processes (e.g., Schmincke, 1976, 1982; Hoernle and Schmincke, 1993a; Neumann et al., 1999 and references therein). The lavas with MgO contents higher than 12–14 wt.% collected during this study are strongly phyric. Most of the lavas, except those from Gran Canaria with *mg*-numbers ranging from 66 to 71, contain Ol phenocrysts whose Fo contents are too low to be in equilibrium with bulk-rock composition (Fig. 2a). Since most olivines have compositions less forsteritic than expected for olivine in equilibrium with the bulk rocks based on $K_D=0.30\pm0.03$ (the distribution coefficient of Fe and Mg between Ol and silicate melt at atmospheric pressure; Roeder and Emslie, 1970; Fig. 2a), some of the Ol-bearing rocks, in particular those collected on Tenerife, La Gomera and La Palma, must have a cumulative origin and their bulk chemical compositions (crystals and matrix) may not represent that of the liquid. Furthermore, significant scatter in CaO contents in the rocks with MgO >7 wt.% observed mostly in lavas from Tenerife and La Gomera suggests that clinopyroxene was also accumulated. Modal proportions of Ol and Cpx in the whole rocks do not reflect those expected for Ol–Cpx cotectic crystallization.

Strong variations in SiO_2 at a given MgO content suggest the existence of a compositional spectrum of parental mantle-derived magmas ranging from transitional tholeiitic basalts to basanites (Fig. 3) to be coupled with chemical composition of the source. An alternative explanation of the common presence of alkali basalts and basanites in association with more Si-rich, "transitional" basalts in the La Palma shield was proposed by Nikogosian et al. (2002) who employed fractionation of clinopyroxene at high (~ 12 kbar) pressures to produce alkali magma compositions from more Si-rich parental melts. We consider this mechanism as potentially possible but having limited implication for the genesis of shield stage lavas on the Canary Islands. The reason is the existence of a thermal barrier

Table 4
Noble gas isotopic composition of olivine phenocrysts

Sample	Weight (g)	^{3}He (cm^3STP/g)	^{4}He (cm^3STP/g)	^{3}He/^{4}He (R/R_A)	Error (2σ)	^{20}Ne (cm^3STP/g)	^{20}Ne/^{22}Ne	Error (2σ)	^{40}Ar (cm^3STP/g)	^{38}Ar/^{36}Ar	Error (2σ)	^{40}Ar/^{36}Ar	Error (2σ)
Gran Canaria													
GC59	1.0083	3.510e−14	3.484e−09	7.26	1.03	5.826e−12	9.14	0.54	1.102e−08	0.1882	0.0013	422	28
GC35	1.0106	3.689e−15	3.979e−10	6.69	2.55	5.326e−12	ND	ND	7.566e−09	0.1886	0.0010	364	25
Tenerife													
TF4	1.0331	1.940e−14	2.068e−09	6.92	1.20	2.252e−12	9.57	1.29	8.068e−09	0.1893	0.0016	358	24
TF7	0.6100	1.854e−14	1.217e−09	6.64	1.63	1.636e−11	9.01	0.29	2.301e−08	0.1884	0.0017	382	10
TF16	0.9583	1.736e−14	1.374e−09	8.64	1.77	1.938e−11	9.77	0.30	4.776e−08	0.1886	0.0009	306	4
TF23	0.8202	2.430e−14	2.078e−09	6.85	1.28	9.047e−12	10.32	0.54	1.258e−08	0.1894	0.0013	414	12
La Gomera													
LG1	1.0110	1.545e−14	1.708e−09	6.53	1.03	1.997e−11	ND	ND	2.386e−08	0.1881	0.0010	315	4
LG35	1.0075	1.046e−14	1.328e−09	5.67	1.04	1.329e−11	9.83	0.25	1.975e−08	0.1885	0.0012	447	9
LG59	0.4666	2.036e−13	8.266e−09	8.21	0.90	2.115e−11	9.74	0.44	4.705e−08	0.1937	0.0012	379	6
La Palma													
LP1	1.0485	1.182e−13	1.158e−08	7.65	0.68	3.707e−11	9.22	0.09	4.210e−08	0.1893	0.0016	362	5
LP13	1.0138	1.064e−12	8.276e−08	9.31	0.59	1.297e−11	9.69	0.40	6.352e−08	0.1886	0.0010	–	–

Handpicked olivine separates were leached in 2N HNO_3, then ultrasonically cleaned in acetone and ethanol and dried at 120 °C. $R/R_A = {}^{3}He/{}^{4}He$ ratios normalized to the atmospheric value of 1.39×10^{-6} (analyst H. Dan, Earthquake Research Institute, University of Tokyo, Japan); – = no value.

in the system "quartz–nepheline–olivine–diopside" that precludes evolution of Si-saturated magmas towards alkali basaltic compositions due to mineral fractionation at lower than 8 kbar pressures (Yoder and Tilley, 1962; O'Hara, 1968). We emphasize, however, that the existing data for differentiation depths of relatively Si-rich, tholeiitic and transitional shield stage magmas on Gran Canaria are restricted to relatively low pressures (<8 kbar, mostly around 3–5 kbar; e.g., Hoernle and Schmincke, 1993a; Gurenko et al., 1996, 1998). Thus, it seems unlikely that most rather primitive Canary shield stage lavas (>8 wt.% MgO) resembling alkali basalts and basanites were produced in accordance with the Nikogosian et al. (2002) model.

Major and trace element variations plotted against MgO (Figs. 3 and 4) indicate that the main process affecting magma composition was fractional crystallization of Ol ± Sp and then Ol + Cpx ± Sp, as follows from continuously increasing Al_2O_3 content and a change from increasing to decreasing CaO at ~ 12–14 wt.% MgO with decreasing MgO content. No or only minor Pl fractionation occurred, as follows from the negative trends of Al_2O_3 and Sr vs. MgO, and the lack of a negative Eu-anomaly in the trace element patterns (Fig. 5). Crystallization of spinel was followed by crystallization of Fe–Ti oxides causing sharp coherent decreases of TiO_2 and FeO in the melt at ~ 7–8 wt.% MgO (Fig. 3). No apatite crystallization is observed even in relatively evolved magmas (incompatible behavior of P_2O_5; Fig. 3). We emphasize that although the absolute concentrations of incompatible trace elements may have been significantly affected by Ol–Cpx crystallization–accumulation processes, the ratios of incompatible element concentrations (especially of those having similar solid–melt distribution coefficients) will reflect the ratios in the parental melts and consequently of source components (mantle or crustal) contributing to magma generation.

4.2. Discrimination between mantle and crustal contributions

The extent of minor crustal contamination of ascending Canary mafic magmas has been debated extensively (e.g., Thirlwall et al., 1997; Hoernle, 1998; Widom et al., 1999; Gurenko et al., 2001; Hansteen and Troll, 2003). Therefore, our first step is to assess whether contamination processes have affected the composition of the most primitive lavas studied here. The existing trace element, radiogenic and stable isotope compositions can provide strong constraints on crustal contamination of the shield stage volcanic rocks.

The components of the crust underlying Canary Islands include Miocene through Jurassic marine sediments, unaltered and hydrothermally altered Jurassic MORB-type igneous crust and Miocene (and possibly older) to Recent intraplate igneous rocks. Samples from the different parts of the crust have

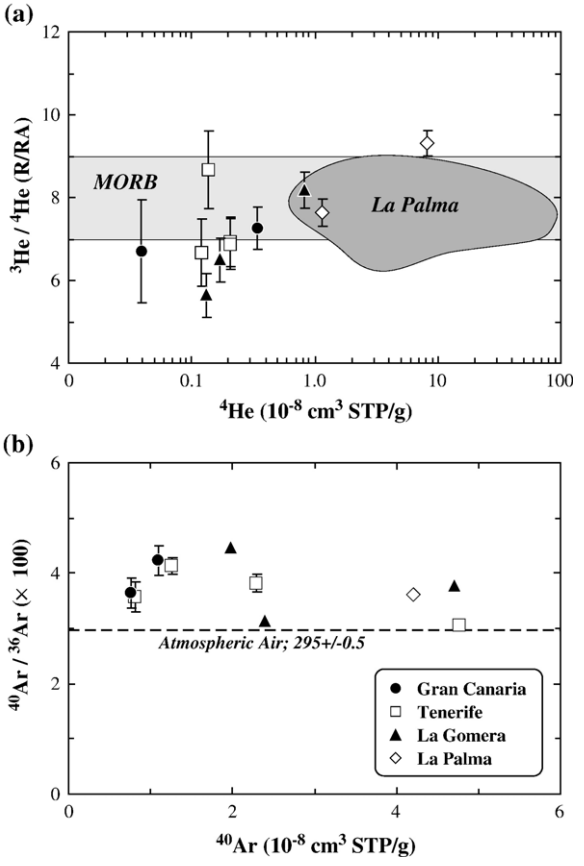

Fig. 10. He and Ar concentrations and isotopic compositions in olivine phenocrysts: (a) ^{3}He/^{4}He ratios vs. ^{4}He concentrations, (b) ^{40}Ar/^{36}Ar ratios vs. ^{40}Ar concentrations. The average ^{3}He/^{4}He ratio of MORB (8±1 R_A) and the ^{40}Ar/^{36}Ar ratio of atmospheric air (295.5±0.5) are taken from Porcelli et al. (2002). The field of La Palma compositions is taken from Hilton et al. (2000). The olivine phenocrysts have ^{3}He/^{4}He ratios close to, or slightly lower, than that of MORB. The ^{40}Ar/^{36}Ar ratios are slightly higher than the atmospheric value. These ^{3}He/^{4}He and ^{40}Ar/^{36}Ar ratios are typical for HIMU-like OIB magmas. Error bars represent ±2σ analytical uncertainty. If not shown, the error bars are similar or smaller than the size of the symbols.

been studied in detail (e.g., Hoernle et al., 1991; Schmincke et al., 1998; Hoernle, 1998; Neumann et al., 2000; Hansteen and Troll, 2003). Oceanic sediments have isotopic compositions that differ significantly from those of the Canary Island magmas (average composition of local sediment is 616 ppm Sr, ^{87}Sr/^{86}Sr=0.71243, 16.9 ppm Nd, ^{143}Nd/^{144}Nd=0.51199, 12.1 ppm Pb, ^{206}Pb/^{204}Pb=18.97, ^{207}Pb/^{204}Pb=15.71, ^{208}Pb/^{204}Pb=39.16; Hoernle et al., 1991; Hoernle, 1998). Addition of a sediment component to the Canary magmas would drive their compositions towards higher ^{87}Sr/^{86}Sr, Δ7/4Pb and Δ8/4Pb and lower ^{143}Nd/^{144}Nd ratios. Cousens et al. (1990) and Hoernle et al. (1991) considered the absence of a negative 207/204Pb–206/204Pb correlation as an evidence of no interaction of Gran Canaria shield magmas with crustal rocks and marine sediments. Thirlwall et al. (1997) have shown, however, that a number of basaltic lavas representing the shield stage on Gran Canaria do not plot collinearly with NHRL but are perpendicular to it in the 207/204Pb–206/204Pb space. The negative 207/204Pb–206/204Pb correlation extending towards local Atlantic sediments was interpreted as a strong evidence for crustal contamination control on the Pb isotopic composition. We emphasize that the lavas studied here, except for two samples from Gran Canaria (G1262 and G1265 from Hoernle et al., 1991), plot below and sub-parallel to NHRL, indicating that these samples have experienced minimal contamination, probably less than 2% sediments even in G1262 and G1265 (Fig. 7).

The altered igneous parts of the ocean crust (pillow lavas, sheet flows, dikes and possibly upper gabbroic portions of the crust) beneath the Canary Islands extend to higher ^{87}Sr/^{86}Sr ratios, have elevated ^{207}Pb/^{204}Pb and ^{208}Pb/^{204}Pb relative to ^{206}Pb/^{204}Pb ratios, but have similar Nd isotopic ratios compared to unaltered MORB and strongly varying incompatible trace element concentrations and ratios (Figs. 7 and 8; Hoernle, 1998). Contamination by different parts of the altered oceanic crust with contrasting Sr isotopic composition could potentially explain the relationships between Ba/Nb and ^{87}Sr/^{86}Sr and ^{206}Pb/^{204}Pb ratios observed for the Canary shield lavas in general (trends 1 and 2 could explain somewhat elevated Ba/Nb ratios of La Palma and lower Ba/Nb ratios of Gran Canaria lavas, respectively; Fig. 8a, c), higher ^{87}Sr/^{86}Sr and ^{207}Pb/^{204}Pb ratios in the Gran Canaria rocks in general (Fig. 7a,b), but it is inconsistent with a single positive Zr/Nb vs. ^{87}Sr/^{86}Sr trend in Fig. 8b and a negative Zr/Nb vs. ^{206}Pb/^{204}Pb relationship in Fig. 8d (where Gran Canaria lavas follow trend 1 but not trend 2 as in Fig. 8a,b). Assimilation of the lower, unaltered portions of the ocean crust (gabbros and ultramafic cumulates) also cannot explain the differences in the composition of the shield stage rocks. In summary, the relationships between trace element and isotopic ratios do not support crustal assimilation of either sedimentary or igneous rocks.

On the radiogenic isotope correlation diagrams (Fig. 8), it is clear that at least two types of sources are needed to explain the composition of the shield stage lavas. Lavas from Tenerife, Gomera and La Palma have HIMU-type compositions, extending from the LVC component towards N-MORB. Lavas from Gran Canaria could be generated by mixing of LVC and EM-type components. Hoernle et al. (1991) have suggested that the HIMU-type component is located

within the plume and reflects mixing between recycled hydrothermally altered oceanic crust in the plume and N-MORB from the asthenosphere. Thirlwall (1997) showed that isotopic arrays similar to that formed by the La Palma, La Gomera and Tenerife shield lavas can be generated by young (<2 Ga) recycled ocean crust and therefore involvement of a depleted asthenospheric component is not required. The isotopic composition of the shield stage lavas on Gran Canaria has been attributed to the Canary plume (Cousens et al., 1990). The more EM-type composition of the shield basalts on the eastern Canary Islands has also been explained through interaction of the Canary plume with LVC-type composition with enriched material in the lower lithosphere and possibly uppermost asthenosphere, ultimately derived from the African/American subcontinental lithospheric mantle during breakup of Pangaea (Hoernle et al., 1991; Hoernle and Tilton, 1991; Hoernle et al., 1995; Widom et al., 1999). In particular, one of the Hoernle et al. (1991) major arguments for placing the EM signatures in the lithosphere was the correlation between *mg*-number and Sr–Nd–Pb isotopic ratios in the Pliocene lavas from Gran Canaria. This correlation does not exist for the Miocene shield volcanic rocks, however. The Pliocene EM component can still reside in the lithosphere. But this does not preclude, however, the Miocene EM component being also from the plume, as argued by Hoernle (1998) and Hoernle et al. (2002).

The relationships between Sr and O can provide additional constraints on the degree of crustal contamination. Since the equilibrium fractionation factor for O isotopes between basaltic melt and olivine ($\Delta_{\text{melt-ol}}$) is in the range of 0.19–0.58‰ (average $\Delta_{\text{melt-ol}}=0.36\pm0.11$; Eiler et al., 2000), the composition of olivine phenocrysts (4.3–5.8±0.3‰, 2σ) gives the equilibrium δ^{18}O values for the magmas of 4.7 to 6.2‰ (Table 3, Fig. 9). The δ^{18}O values extend from values lower than those typical for MORB (5.7±0.2‰) and OIB magmas (5.5±0.5%; Harmon and Hoefs, 1995) to slightly higher values. The data reported here covers the lower end of the δ^{18}O range previously reported for Gran Canaria shield basalts i.e., 4.9–8.0‰ in Cpx phenocrysts (Thirlwall et al., 1997) corresponding to a range of 5.3–8.4‰ in the melts assuming $\Delta_{\text{melt-cpx}}=0.4$ (e.g., Kyser et al., 1981; Vroon et al., 2001 and references therein) and 5.0–8.2‰ in melt inclusions (Gurenko et al., 2001).

The O and Sr isotope data presented in this study from the Canary shield lavas straddle the HIMU field from Widom and Farquhar (2003) and show a weak inverse correlation (Fig. 9). The decrease of δ^{18}O with increasing ^{87}Sr/^{86}Sr is unlikely to have resulted from magma contamination at crustal depths, as previously proposed for the Gran Canaria shield lavas (e.g., Thirlwall et al., 1997; Gurenko et al., 2001; Hansteen and Troll, 2003). Some of the basalts and gabbros from the crust beneath Gran Canaria are characterized by relatively low δ^{18}O values (3.3–5.1‰) at varying to somewhat elevated ^{87}Sr/^{86}Sr ratios (0.7029–0.7047) (Hoernle, 1998; Hansteen and Troll, 2003). Assimilation of such gabbros could drive the composition of the hybrid magmas towards lower δ^{18}O and higher ^{87}Sr/^{86}Sr values. If we assume that presumably "uncontaminated" magma has a δ^{18}O of 5.9‰ (average "melt" value obtained from TF7 and TF16; Table 3) and minimum ^{87}Sr/^{86}Sr of 0.70298, the binary mixing of such magma with hydrothermally altered portions of Layer 2 and 3 (pillow lavas, sheet flows, dikes and gabbros; average δ^{18}O=4.7‰ and ^{87}Sr/^{86}Sr=0.70352; Hoernle, 1998; Hansteen and Troll, 2003) would require assimilation of unrealistically large amounts of crust, up to 70 wt.% (Fig. 9) that is not supported by Pb isotopes, as discussed above. A less extreme magma with lower δ^{18}O and higher ^{87}Sr/^{86}Sr values than those used for calculation of the mixing line in Fig. 9 or hydrothermally altered compositions with higher δ^{18}O and lower ^{87}Sr/^{86}Sr values would require even more pronounced degrees of contamination. We therefore do not consider crustal assimilation as a likely explanation for the observed variations in Sr and O isotopes. We emphasize that contamination of the shield stage magmas at crustal depths could be important in some samples but does not control the differences in radiogenic and stable isotopic composition observed in the Canary shield basalts studied here.

4.3. Implications for source composition

Hernandez-Pachero and Ibarrola (1973), Schmincke (1982, 1998), Hoernle et al. (1991, 1995), Abratis et al. (2002), and Lundstrom et al. (2003) have postulated major changes in source composition across the Canary archipelago. Variations of highly incompatible trace element ratios, especially of those elements having similar or close bulk solid–melt distribution coefficients for mantle peridotite mineral association (e.g., Ba/Nb, La/Nb, Nb/U, Ba/Th, Ce/Pb) are usually used to evaluate the proportion of mixing end-members, either representing mantle reservoirs or crustal components since these elements do not fractionate significantly during partial melting of mantle assemblages containing olivine, two pyroxenes, garnet and/or spinel or during fractional crystallization (e.g., Hofmann et al., 1986;

Weaver, 1991). The correlations of $^{87}Sr/^{86}Sr$ with incompatible trace element ratios in the Canary shield stage lavas suggest that the variation of these element ratios reflects mixing between different components in the source region rather than the processes of magma evolution during underplating. When considering the Gran Canaria shield stage lavas, the more radiogenic Sr and less radiogenic $^{206}Pb/^{204}Pb$ isotope ratios are coupled with relatively low Ba/Nb (4.2–5.8) and Ba/Th ratios (51–78) and high K/La (187–295) and Zr/Nb (5.9–7.7) ratios, as compared to the other islands with Ba/Nb=3.6–7.7, Ba/Th=51–108, K/La=65–239 and Zr/Nb=3.6–6.6 (Fig. 8; Tables 2 and 3). In contrast to Gran Canaria, the lavas from La Palma are characterized by elevated Ba/Nb (5.9–7.7) and Ba/Th ratios (84–108) at less radiogenic Sr and more radiogenic $^{206}Pb/^{204}Pb$ isotopic composition. Their other trace element (e.g., K/La, Zr/Nb) and isotopic characteristics are similar to those of Tenerife and La Palma (Fig. 8). The Tenerife and La Gomera lavas are characterized by stronger variations of Ba/Nb and Ba/Th ratios at varying Sr isotopic compositions, overlapping with Gran Canaria and La Palma (Fig. 8). In summary, the three younger (3–12 Ma) western island (Tenerife, La Gomera and La Palma) shields have distinct trace element and isotope ratios compared to the older (13–15 Ma) easternmost island in this study (Gran Canaria), as is most clearly illustrated on the $^{206}Pb/^{204}Pb$ vs.$^{87}Sr/^{86}Sr$ isotope correlation diagram (Fig. 7c). We therefore suggest that the source(s) of the older, eastern Canary Island shield stage lavas (i.e., Gran Canaria) are distinct from those of the younger, western Canary Islands, either reflecting a temporal change in the composition of the plume or a difference in the composition of the lithosphere beneath the eastern vs. western Canary Islands (Hoernle and Tilton, 1991; Hoernle et al., 1991, 1995; Abratis et al., 2002; Lundstrom et al., 2003).

Variations of Zr/Y ratios (broad range 6.7–11.8) suggest different proportions of garnet in the mantle source rather than variation in the degree of partial melting. Despite our previous discussion demonstrating chemical and isotopic variability of the source rocks, presence of garnet in the magma source can be examined, while assuming melting of a single source composition whose trace element concentrations would have been controlled in the first order by the presence of garnet rather than by mixing of chemically diverse components. Modeling of partial (i.e., batch) melting (Shaw, 1970; Table 5) of a peridotite with initial concentrations of Zr and Y, as those of primitive mantle (Hofmann, 1988) has shown that the observed Zr/Y range could be produced by low degrees of partial melting (1% to 10%) with the amount of garnet ranging from 2% to 20% (Fig. 11a). Similar low degrees of melting (0.5 to 2%) were inferred for the Tenerife shield lavas by Simonsen et al. (2000) who considered Zr/Nb ratios in the whole rocks. We emphasize that the obtained degrees of partial melting are very sensitive to the mineral–melt partition coefficients, melting reaction modes and initial source composition used in the

Table 5
Mineral–melt partition coefficients, phase proportions and melt reaction coefficients used in modeling of peridotite partial melting

Element		Ol	Opx	Cpx	Sp	Gt	Amph	Phlog
Partition coefficients [a]								
Ba		5.0e−6	6.0e−6	0.0003	0	0.0007	0.16	3.68
Th		5.2e−5	0.0056	0.014	0	0.0014	0.0039	0.0014
La		0.0002	0.0031	0.054	0.0006	0.001	0.055	0.028
Sm		0.0009	0.0037	0.27	0.0006	0.625	0.32	0.0059
Zr		0.001	0.012	0.26	0.07	0.505	0.127	0.017
Y		0.0082	0.015	0.47	0.004	5.42	0.52	0.018
Phase proportions and melt reaction coefficients [b]								
Sp–Gt Lherz	*	0.55	0.25	0.16	0.02	0.02	–	–
	**	−0.10	0.25	0.61	0.04	0.20	–	–
Gt Lherz	*	0.54	0.17	0.09	–	0.20	–	–
	**	0.10	0.18	0.30	–	0.42	–	–
Gt–Amph–Phlog	*	0.60	0.20	0.10	–	0.05	0.04	0.01
Lherz	**	0.10	0.18	0.30	–	0.28	0.10	0.04

[a] Mineral–melt partition coefficients for Ol, Opx, Cpx are taken from the compilations by Halliday et al. (1995), for Sp and Gt—from Gurenko and Chaussidon (1995), for Amph and Phlog—from LaTourrette et al. (1995) and Halliday et al. (1995).

[b] Phase proportions (*) and melt reaction coefficients (**) in the source for Sp–Gt peridotite are taken modified after Kinzler and Grove (1992) and Gurenko and Chaussidon (1995), for Gt peridotite—from Kelemen et al. (1993), and for Gt–Amph–Phlog peridotite—modified after McKenzie and O'Nions (1991), Kelemen et al. (1993) and Class and Goldstein (1997).

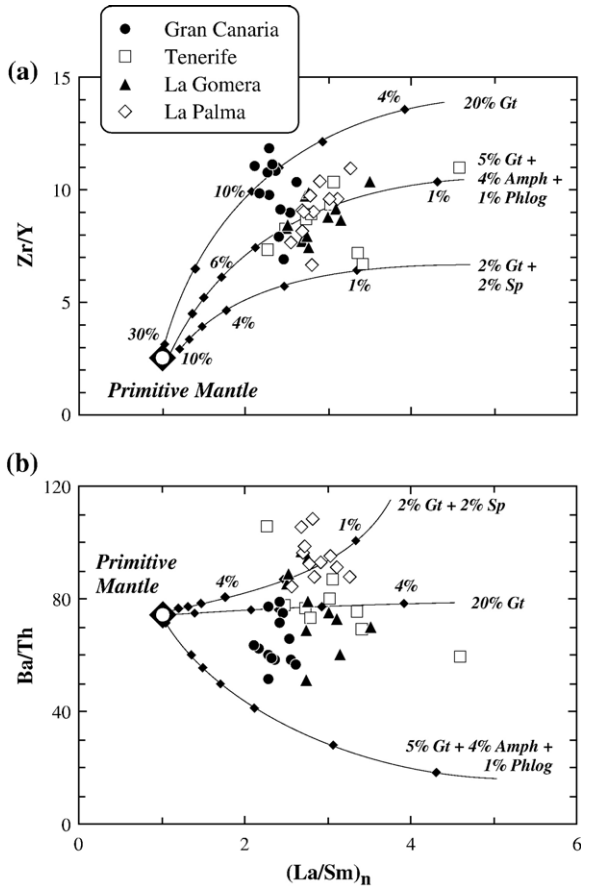

Fig. 11. Diagrams of (a) Zr/Y vs. $(La/Sm)_n$ and (b) Ba/Th vs. $(La/Sm)_n$ in the Canary shield stage lavas demonstrating the effect of partial melting of a peridotite source with varying amounts of garnet. *Solid lines* represent melt compositions resulting from batch melting (Shaw, 1970) of peridotite corresponding in composition to primitive mantle (Hofmann, 1988). Mineral–melt partition coefficients, phase proportions and melt reaction coefficients used are given in Table 5. We emphasize that the positions of melting curves and estimated melting degrees are very sensitive to the values of the partition coefficients used in the modeling. The purpose of this figure is to demonstrate the effect of source mineral composition on the variation of Zr/Y and Ba/Th ratios in the whole rocks but not to quantitatively constrain the degree of partial melting.

calculations. These may explain the observed discrepancies between our results and those of Simonsen et al. (2000).

Some of the elevated Zr/Y ratios (up to 11.8) at relatively low $(La/Sm)_n$ of 2.1–2.6 of the Gran Canaria shield rocks require, however, assumption of unrealistically high amounts of garnet (more than 30%) in the source, which we consider to be unlikely. Furthermore, melting of a single source composition but containing varying proportions of amphibole, phlogopite and garnet in the source can probably account for the broad ranges of Ba/Th (Fig. 11b), but not for the variations observed in other trace element concentrations and ratios (i.e., Ba/Nb, K/Nb, K/La, Sr/Nb; not shown). Therefore, as in the case of radiogenic isotopic data, we come to the conclusion that derivation from the heterogeneous garnet-bearing plume source or melt–lithosphere interaction (discussed below) do represent more plausible explanations for the observed variable to high Zr/Y and other trace element ratios, as it was also shown by Hoernle and Tilton (1991), Hoernle et al. (1991, 1995), Abratis et al. (2002), and Lundstrom et al. (2003). These and previous results imply that melting conditions beneath the Canary archipelago and the composition of the source region vary strongly in the scale of more than ~ 500 km long island chain and more than 15 Ma long magmatic history being maximal beneath Gran Canaria and decreasing towards Tenerife, La Gomera and La Palma. Finally, such intra-island variations may suggest that the scale of heterogeneity appear to be narrower than the dimension of a single island.

4.4. Melt–lithosphere interaction or crustal recycling?

Similar bulk peridotite–melt partition coefficients for Ba, Th, Nb, K and La preclude significant fractionation between these elements during melting and crystallization in the absence of exotic accessory phases. The presence of amphibole and/or phlogopite in association with garnet, ilmenite and zircon in the source of the Canary magmas previously suggested by Schmincke and Flower (1974), Hoernle and Schmincke (1993b), Neumann et al. (1999), Wulff-Pedersen et al. (1999), and Lundstrom et al. (2003) could significantly fractionate Ba, Nb and K from other incompatible elements due to relatively high amphibole–melt and phlogopite–melt partition coefficients for Rb, Ba, Nb and K (e.g., LaTourrette et al., 1995 and compilations in Halliday et al., 1995; White, 1997). Stability of amphibole and phlogopite directly in the melting region of a mantle plume is questionable, however. Class and Goldstein (1997) have shown that the temperatures within the upwelling plume and asthenosphere appear to be too high for amphibole and phlogopite to be stabile as residual phases. Therefore, the processes involving amphibole and/or phlogopite to explain the origin of the Canary shield magmas should probably be restricted to the lithospheric mantle only, as suggested by Lundstrom et al. (2003) in the case of Holocene lavas. We examined the Lundstrom et al. (2003) hypothesis in application to the Canary shield stage rocks. On a plot of Nb vs. Nb/U ratios (Fig. 12), the Canary shield stage

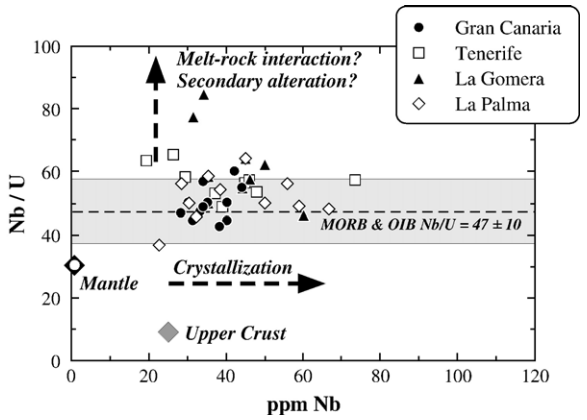

Fig. 12. Nb/U ratios plotted against Nb concentrations in the whole rocks. *Mantle*=primitive mantle composition from Hofmann (1988), *Upper crust*=composition of Upper Continental Crust from Taylor and McLennan (1985), *Shaded field* represents the Nb/U ratio of 47±10 in MORB and OIB from Hofmann et al. (1986).

lavas largely overlap the field for MORB and OIB from Hofmann et al. (1986) but extend to higher Nb/U at low Nb concentration. Except for two extreme samples from La Gomera, all other lavas show Nb/U ratios ranging from 41 to 65, insignificantly exceeding the range of Nb/U ratios of 47±10 suggested for MORB and OIB magmas by Hofmann et al. (1986). Partial removal of U by secondary alteration could also explain somewhat elevated Nb/U ratios exceeding the MORB and OIB range, as well as those in the two Miocene shield stage rocks from La Gomera. Therefore, it is not absolutely necessary to employ the model of melt–lithosphere interaction with older intrusive rocks or amphibole-rich veins suggested by Lundstrom et al. (2003) in the case of the Canary shield stage rocks.

An alternative scenario to explain the variations in (Ba, K, Nb, Zr)/(La, U, Th) ratios could be partial melting of a plume source containing recycled crustal material with "ghost" amphibole or phlogopite. Though amphibole and phlogopite are unlikely to be residual phases in the upwelling plume (Class and Goldstein, 1997), we still need to explain the variations in Ba/Nb (3.6–7.7), Ba/Th (50.8–107.7), K/La (65–295) and Nb/U (42.2–85.0) ratios observed in the Canary shield stage magmas (Table 2). We suggest that amphibole and phlogopite might have been broken down during the subduction process. As a consequence, the fluid-mobile elements compatible in these phases would have been preferentially lost from the subducting oceanic crust to the subarc mantle, causing K, Rb, Ba depletions of the subducting material relative to other incompatible elements. Similar mechanism was employed by Foley et al. (2002) in order to explain relatively low Nb/Ta and Zr/Sm ratios in early continental crust, as compared to those of primitive mantle and mid-ocean ridge basalts. Based on the new experimental trace-element partitioning data, Foley et al. (2002) have suggested that formation of the early continental crust was likely controlled by melting of amphibolites in the subduction-zone environments rather than by melting of eclogite or magnesium-rich amphibolites in the lower part of thick oceanic crust. We qualitatively follow this process "further in depth", suggesting that partial melting of such "amphibole-" or "phlogopite-exhausted" recycled oceanic crust within the plume could generate melts displaying relative depletion in K, Rb and Ba on multi-element diagrams (Fig. 5). The incompatible element patterns of melts formed due to melting of such K-, Rb- and Ba-exhausted and then recycled, ocean crust will appear to be similar to those formed with residual amphibole and phlogopite in the source. In conclusion, we propose that the relative depletion in K, Rb and Ba in the Canary shield lavas does not reflect derivation through melting of sources with amphibole and/or phlogopite in the residuum but may be a signature inherited by the ocean crust during subduction.

Another issue is to understand why the Gran Canaria shield stage lavas geochemically differ from the shield lavas on the other three western islands as can be seen in $^{87}Sr/^{86}Sr$ vs. $^{206}Pb/^{204}Pb$ (Fig. 7c) or Ba/Nb and Zr/Nb vs. $^{87}Sr/^{86}Sr$ and $^{206}Pb/^{204}Pb$ diagrams (Fig. 8). As shown by Hoernle and Tilton (1991), Hoernle et al. (1991, 1995), Abratis et al. (2002), and Lundstrom et al. (2003), such variations could be interpreted as reflecting either heterogeneity in the plume source or contamination with EM components in the lithosphere or their combination. Here we present additional evidence suggesting that the recycling of crustal material might have played an essential role. Indeed, recycling of the oceanic crust would result in formation of eclogite. Partial melting of the eclogite during plume ascent and the reaction of eclogite-derived, Si-rich melts with the peridotite mantle that finally results in transformation of peridotite to pyroxenite (Sobolev et al., 2005). Modeling of Zr/Y vs. $(La/Sm)_n$ ratios (Fig. 11a) requires much higher amount of garnet in the source (up to 30%; see above), than is usually expected in garnet peridotite, whereas melting of eclogite (or pyroxenite) derived from recycled ocean crust could also produce the observed garnet signature in the melt. In this context, the Sobolev et al. (2005) model can also account for relatively lower CaO contents (Fig. 3, CaO vs. MgO panel) and CaO/Al_2O_3 ratios (not shown) in the Gran Canaria shield lavas, as well as their higher SiO_2 and

NiO contents (SiO_2 vs. MgO and NiO vs. MgO panels in Figs. 3 and 4) at a given MgO, thereby suggesting higher pyroxenite/eclogite vs. peridotite ratio in the source rocks of the Gran Canaria shield stage lavas compared to those erupted on Tenerife, La Gomera and La Palma.

4.5. He and Ar isotope signature of the Canary shield stage lavas

Trace element and isotopic signatures of the mafic magmas erupted on the Canary Islands require partial melting of a time-integrated high U/Pb (HIMU)-type mantle source, whose origin is attributed to the recycling of <2 Ga old oceanic crust (Sun, 1980; Cousens et al., 1990; Hoernle et al., 1991; Hoernle and Tilton, 1991; Marcantonio et al., 1995; Thirlwall et al., 1997; Abratis et al., 2002). The relationships between He, Nd, Sr and Pb isotopes in the Canary shield stage lavas are shown in Fig. 13. Our present He isotopic data plot very close to the reference fields of HIMU-type lavas (St. Helena; Graham et al., 1992) in the $^{3}He/^{4}He$ vs. $^{86}Sr/^{87}Sr$ and $^{143}Nd/^{144}Nd$ diagrams (Fig. 13a,b) and also tend to the St. Helena HIMU field in the He–Pb isotope space (Fig. 13c). In order to explain strong variations of $^{3}He/^{4}He$ ratios in many OIB magmas in comparison to significantly lower $^{3}He/^{4}He$ ratios anticipated for old recycled crust, several models of diffusive exchange of helium between recycled material and ambient mantle have been invoked (e.g., Hanyu and Kaneoka, 1997). Considering He and Pb isotopes in the most extreme samples of La Palma, Hilton et al. (2000) concluded that the presence of ancient recycled material producing an excess of both radiogenic He and Pb isotopes is very probable. However, we have no independent evidence supporting the presence of such a plume component in the Canary shield-building stage; more data are required to further constrain the noble gas isotopic signature of the mantle beneath the Canary Islands.

It is well known that MORB magmas have high $^{40}Ar/^{36}Ar$ ratios, generally above 10 000 with the highest values of about 40 000 reported for the MAR popping rocks (Burnard et al., 1997) and glassy basalts from the Mid-Atlantic Ridge (Marty and Humbert, 1997; see also the compilation by Graham, 2002). The highest $^{40}Ar/^{36}Ar$ ratios (up to 8300) obtained for the ocean island basalt glasses are from Loihi Seamount (Trieloff et al., 2000), while Farley and Craig (1994) obtained a maximum of $^{40}Ar/^{36}Ar = 8000$ for olivine phenocrysts from Juan Fernandez, a high $^{3}He/^{4}He$ hotspot. For the Canary samples studied, the $^{40}Ar/^{36}Ar$ ratios range from ~ 310 to ~ 450, likely indicating the effect of

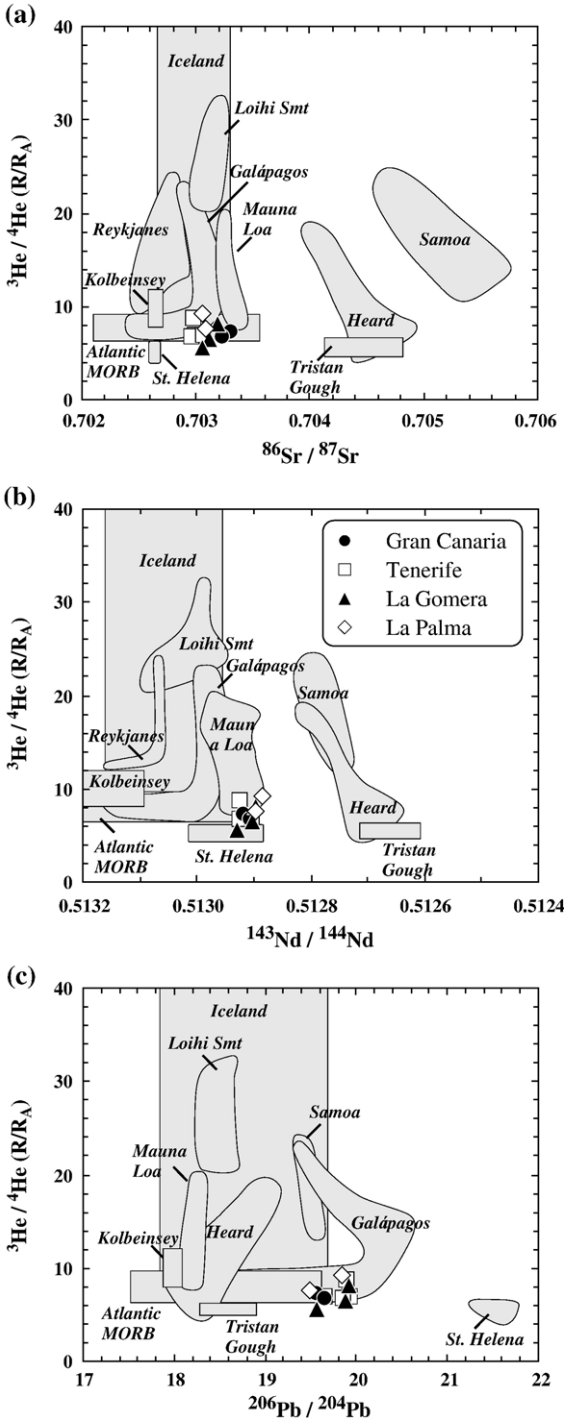

Fig. 13. (a) He–Sr, (b) He–Ne, and (c) He–Pb isotopic relationships for olivine phenocrysts (He isotopes) vs. whole-rock lavas (Sr–Nd–Pb isotopes) from the shield stage rocks on Gran Canaria, Tenerife, La Gomera and La Palma. Reference fields for mid-ocean ridge and ocean island basalts are taken from Graham (2002 and references therein).

contamination by atmospheric air of plume-derived magmas. The origin of the "atmospheric" argon in the Canary rocks is however unclear and, as discussed above, could represent either a signature of the mantle source, containing recycled oceanic crust or contaminated argon from seawater involved in shallow depth hydrothermal circulations and released during decrepitation of secondary fluid inclusions in Ol phenocrysts.

5. Summary and concluding remarks

The HIMU isotopic signature in many OIB magmas is commonly attributed to mantle plumes originating at the core–mantle boundary or D" layer, probably carrying material of deeply subducted oceanic crust (Morgan, 1971; Hofmann and White, 1982; Kellogg et al., 1999; Albarède and van der Hilst, 1999). Although many hotspot tracks are no larger than 200–400 km wide, suggesting that upwelling regions are relatively narrow features i.e., a few hundred kilometers or less (e.g., Hauri et al., 1994), there are a number of geophysical observations, such as geoid and topographic anomalies, as well as seismic tomography studies (e.g., Anderson et al., 1992; Hoernle et al., 1995; Morgan et al., 1995; Moore et al., 1998) indicating that at least the upper portion of the upwelling regions can be significantly larger. In particular, Hoernle et al. (1995) have shown that the volcanism of the eastern Atlantic, northern Africa, western Mediterranean and central Europe may be related to a large region of mantle upwelling, possibly consisting of multiple smaller plume-like structures. Melt production rate estimated for the Canary Islands (0.01–0.03 km^3/year, Hoernle and Schmincke, 1993a) is considerably lower than that of Hawaii (0.16 km^3/year; Watson and McKenzie, 1991). Thus, the origin of the Canary Islands melting anomaly from a voluminous Hawaii-like mantle plume is unlikely. Hoernle et al. (1991) and Hoernle and Schmincke (1993b) proposed a model for Gran Canaria, and Thirlwall et al. (2000) have confirmed this model for Tenerife, which suggests that the magmas of the Canary Islands might have been generated by partial melting of a swarm of small (~50–150 km diameter) blobs upwelling in the upper mantle. As these HIMU-type blobs rise through the uppermost asthenospheric mantle, they migrate from the southwest to the northeast beneath the Canary Archipelago, possibly as a result of upper mantle flow or lithospheric drag. The large-scale, low-velocity thermal anomaly spreading at the base of, or within, the upper mantle (Hoernle et al., 1995) may represent a feeding source for the Canary hotspot and the hotspots located northward (e.g., Madera and Selvagen islands) and southward (Cape Verde archipelago). During ascent through the upper mantle, the component of the depleted astenospheric MORB mantle could be admixed into the ascending blobs, affecting at different scales the composition of the resulting magmas. The last is evident from increasing proportion of DMM component in some magmas erupted on the westernmost Canary Islands and Madeira (Geldmacher and Hoernle, 2000; Abratis et al., 2002). Magma fractionation accompanied by contamination at crustal depths appears to be very probable, especially on Gran Canaria, where assimilation of crustal material was reported by Thirlwall et al. (1997), Gurenko et al. (2001), and Hansteen and Troll (2003).

The results of the present study agree well with the existing models of the Canary plume origin. Primary magmas are picritic and believed to have formed at pressures of ~ 30 kbar (ca. 100 km deep), within the garnet stability field, and temperatures between 1500 and 1600 °C (Schmincke, 1982; Hoernle and Schmincke, 1993a; Heuschkel, 1996; Gurenko et al., 1996, 1998). Even the most primitive, Mg-rich lavas are characterized by significant chemical heterogeneity, ranging from picrites, tholeiites and transitional basalts (primarily erupted on Gran Canaria) to alkali basalts and basanites (more abundant on Tenerife, La Gomera and La Palma). The chemical compositions of the whole rocks and their minerals show that fractional crystallization of olivine, clinopyroxene and spinel group minerals, with no or minor crystallization of plagioclase and Fe–Ti oxides, is a major process affecting the composition of the parental magmas. Many picritic rocks with MgO contents higher than 15–20 wt.% could have accumulated significant amounts of olivine, clinopyroxene and, to a lesser extent, plagioclase, so that their whole rock compositions no longer represent the chemical composition of the liquid. Because of the existence of a thermal barrier in the system quartz–nepheline–olivine–diopside at pressures below 8 kbar, it seems unlikely that the evolved alkali basalt–basanite lavas originated from more Si-rich primitive tholeiitic to transitional basalts due to significant clinopyroxene fractionation at depths, as proposed by Nikogosian et al. (2002). The compositional spectrum of lavas is believed to reflect that of parental magmas.

Although most of the lavas studied have accumulated olivine, clinopyroxene, and in lesser extent, plagioclase and Fe–Ti oxides, the observed ratios of incompatible elements, especially those having similar solid–melt distribution coefficients, may reflect relative element concentrations of parental magmas. Contamination at shallow crustal depths can significantly affect

the composition of the Canary shield stage lavas. However, our present radiogenic, stable and noble gas isotopic data have shown that crustal contamination had a minimal impact on their compositions, if present at all. Correlations between isotope ratios and highly incompatible trace element ratios further suggest that the trace element ratios are characteristic of the magma source (s). The trace element concentrations and ratios of the Canary shield lavas resemble HIMU-like OIBs. The observed intra-island heterogeneity in the shield stage rocks was shown to result from multiple partial melting parameters and from variations in the chemical composition and mineralogy (e.g., variable amounts of garnet) of the mantle source. Modeling of partial melting shows that varying melting degrees (1% to 10%) and amounts of garnet (up to 20%) in the lherzolite source (resembling primitive mantle with respect to La, Sm, Zr and Y concentrations) can partially account for the compositional spectrum of the erupted lavas. We propose, however, that the differences in chemical composition (e.g., in Ba/Nb, Ba/Th, Zr/Nb, K/La and Sr isotope ratios) between the older, eastern Canary Island (Gran Canaria, 15–8.5 Ma) and the younger islands located to the west (Tenerife, La Gomera and La Palma, ca. 1–12 Ma) reflects chemical heterogeneity of the source existing in the scale of ~500 km long island chain and ~15 Ma long magmatic history.

The presence of amphibole and/or phlogopite is essential to significantly fractionate Ba, Nb and K from other incompatible elements, producing the observed range in Ba/Nb (3.6–7.7), Ba/Th (51–108), K/La (65–295) and Nb/U (42–85) ratios. Since amphibole or phlogopite are unlikely to be residual phases in the upwelling plume or asthenospheric mantle and because we did not find evidence for significant assimilation of lithospheric amphibole, we propose that the relative depletion of K, Rb and Ba in the Canary shield lavas reflects depletion of these elements in recycled oceanic crust in the plume source. In accordance with this scenario, fluid-mobile elements compatible in amphibole and phlogopite might have been preferentially lost to the subarc mantle during subduction-related breakdown of these phases.

Helium isotopic composition coupled with Sr, Nd, and Pb isotope data on the Canary shield stage lavas are consistent with the presence of recycled oceanic crust in their plume source, in agreement with the previously proposed HIMU-like signature of the Canary shield lavas. The observed relatively low $^{40}Ar/^{36}Ar$ ratios ranging from ~310 to ~450 likely indicate contamination of plume-derived magmas by atmospheric air.

Acknowledgements

We thank H.-O. Schneider for technical assistance with electron microprobe analyses, S. Vetter for assistance in carrying out the Sr–Nd–Pb isotopic analyses, M. Sumita and A. Klügel for providing us with five samples from the Gran Canaria, La Gomera and La Palma lava shields. Useful criticism provided by formal reviews by Cornelia Class, Sujoy Mukhopadhyay and one anonymous referee significantly improved this paper. The work was supported by grants from the Deutsche Forschungsgemeinschaft (Schm 250/64-1 and 64-2) and by the Max Planck Society during manuscript preparation. The Museum of Natural History, Washington, DC, kindly provided us with standards for electron microprobe analysis. [**RLR**]

Appendix A

A.1. Geologic overview of Gran Canaria, Tenerife, La Gomera and La Palma

The subaerial eruptive history of Gran Canaria located in the central part of the Canary Island chain is subdivided into three periods: (1) Miocene (~15–8.5 Ma); (2) Pliocene (~5.5–1.5 Ma); and (3) Quaternary (~1.5 Ma to present) (e.g., Hoernle and Schmincke, 1993a,b). The oldest subaerially exposed lavas, belonging to the Guigui, Hogarzales and Mogan formations (15–13.4 Ma), range in composition from picrite, tholeiite and alkali basalt to peralkaline rhyolite. The Fataga and Tejeda formations (13.4–8.6 Ma) consist predominantly of trachytes and phonolites, and rare basanites and nephelinites. The oldest unit within the Pliocene phase (E1 Tablero formation, ca 5.5 Ma) is characterized by a wide range of mafic volcanic rocks (nephelinites, rare hawaiites), while the Roque Nublo group (~4.1–3.5 Ma) consists of a complete suite of alkali basalt through trachyte and basanite to phonolite. The volcanic rocks of the Llanos de la Pez formation (~3.2–1.8 Ma) range primarily from alkali basalts to nephelinites and mugearites, while the Quaternary and more recent lavas (~1.8–0 Ma) are dominantly basanites and nephelinites, with rare alkali basalts and local tephrites.

The Tenerife shield lavas form three deeply eroded massifs: Teno (6.7–4.5 Ma) in the NW part of the island, Anaga (6.0–3.5 Ma) in the NE, and Roque del Conde (11.9–3.8 Ma) in the SW (Ancochea et al., 1990; Thirlwall et al., 2000; Guillou et al., 2004; Walter et al., 2005). The exposed rocks are dominated by olivine-rich alkali basalts, but more evolved phonolitic lavas and pyroclastic deposits are also present in the upper parts of

the volcanic sequences (e.g., Fúster et al., 1968; Ancochea et al., 1990). A large volcanic complex in the central part of Tenerife, the Las Cañadas edifice (ca. 3.3 to 0.2 Ma; Martí et al., 1994; Fúster et al., 1994), consists mostly of basanitic to phonolitic lavas and pyroclastic rocks (Ancochea et al., 1990). The dorsal ridge between the Las Cañadas edifice and the Anaga massif formed primarily through basanitic eruptions between 0.6 and 0.9 Ma. The top of the Las Cañadas edifice has been destroyed through several caldera collapses (Martí et al., 1994, 1997) or more likely through giant land slides (Navarro and Coello, 1989; Carracedo, 1994, 1996; Walter and Schmincke, 2002). Subsequent eruptions of basanites to phonolites have formed the Teide–Pico Viejo volcanic complex inside the Las Cañadas "caldera" (Ablay et al., 1998). Both the Teide–Pico Viejo complex and several flank vents were active during historical time (Ancochea et al., 1998).

La Gomera is one of the Canary Islands, together with Fuerteventura and La Palma, whose basal complex is exposed on land. Although the stratigraphy of the island has only been partially reconstructed (e.g., Cendrero, 1971; Cubas, 1978; Cantagrel et al., 1984), five main geological units have been distinguished: (1) the basal complex (<12 Ma; Abdel-Monem et al., 1971; Cantagrel et al., 1984; van den Bogaard, personal communication, 2005), which consists of ultramafic to syenitic plutonic rocks, poorly preserved lavas of basaltic and trachytic composition, tuffs and sediments, intruded in many places by a dense dike swarm; (2) trachyte–phonolite intrusive series (~ 9 Ma) cut by trachytic–phonolitic and basaltic dikes; (3) old basaltic series (~ 12 to 5.9 Ma; Abdel-Monem, 1971; Cantagrel et al., 1984; van den Bogaard, personal communication, 2005), containing three subunits: (a) lower, highly altered olivine+augite±plagioclase-phyric basaltic lava flows separated by an unconformity from (b) basaltic agglomerates and overlain by (c) upper old basalts; (4) horizontal sub-recent lavas (~ 5.2 to 2.8 Ma) presented by mostly aphyric to slightly phyric basaltic to trachybasaltic lava flows; and (5) "Los Roques" series (4.6–3.9 Ma) composed of phonolitic and trachytic subvolcanic intrusives and lava flows.

La Palma, historically the most active volcano of the Canary Islands, consists of three main geological units (e.g., Middlemost, 1970; Hernandez-Pacheco, 1971; Schmincke, 1976, 1982; Staudigel and Schmincke, 1984; Ancochea et al., 1994; Carracedo et al., 1999): (1) the basal complex (~ 3–4 Ma), composed of a Pliocene seamount sequence and a plutonic complex, uplifted and tilted to their present position by later intrusive activity (Staudigel and Schmincke, 1984); (2) the older volcanic series (1.7–0.4 Ma), including the Taburiente shield volcano, the Cumbre Nueva and the Bejenado edifice; and (3) the Cumbre Vieja volcanic series (~ 0.1 Ma to present) forming the southern half of the island. The basal complex exposed on the bottom of the Caldera de Taburiente is made up of plutonic ultramafic to alkali gabbroic and syenitic rocks intruded by innumerable dikes of mostly basaltic composition and overlain by pillow lavas, submarine breccias and dikes exposed along the canyon walls (Hernandez-Pacheco, 1971; Staudigel and Schmincke, 1984). Beginning at the base, the older volcanic series consists of thick clastic deposits, olivine- and augite-phyric picrite and ankaramite lavas, trachybasalts interbedded with abundant pyroclastic rocks (Hernandez-Pacheco, 1971). The Cumbre Vieja volcanic association consists dominantly of basanitic lava flows, cinder cones and several phonolitic plugs. Most historic eruptions are zoned displaying chemical and mineralogical heterogeneity and often carrying abundant mantle and crustal xenoliths during the final eruptive phase (e.g., Neumann and Wulff-Pedersen, 1997; Klügel et al., 1999, 2000).

Appendix B

B.1. Sample location

B.1.1. Gran Canaria

G1264	Barranco Guigui Chico, Ol–Cpx-phyric basalt (Hoernle and Schmincke, 1993a).
G1265	Barranco Guigui Chico, Ol–Cpx-phyric basalt (Hoernle and Schmincke, 1993a).
1552	Barranco Guigui Chico, Ol–Cpx-phyric basalt (provided by H.-U. Schmincke).
1553	Barranco Guigui Chico, Ol–Cpx-phyric basalt (provided by H.-U. Schmincke).
1557	Barranco Guigui Chico, Ol–Cpx-phyric basalt (provided by H.-U. Schmincke).
GC59	27°56′49″N, 15°49′34″W; Playa de Guigui, Barranco Guigui Chico, the first lava flow above sea level; moderately altered Ol–Cpx-phyric basaltic lava.
GC35	28°05′21″N, 15°42′10″W; Agaete, the road N810 from San Nicolas to Agaete, between the 39th and 40th km-posts. Very fresh Ol–Cpx-phyric basaltic lava containing abundant dunite xenoliths of cumulative origin.
GC41	28°05′17″N, 15°42′08″W; Agaete, the road N810, ca. 50 m from the 40th to the 41st km-post. This sample is similar to GC35 but containing no xenoliths.
GC43	28°04′58″N, 15°42′36″W; Playa de Sotavento, Barranco de Guayedra, the road N810 near the 42nd km-post, small road going to the beach; slightly altered Ol–Cpx-phyric basalt taken from the second lava flow above sea level.
GC81	28°04′39″N, 15°42′28″W; Barranco de la Palma, the road N810, between the 43rd and 44th km-posts, sequence of slightly to strongly altered Ol–Cpx-phyric basalts. The

sample represents the most fresh lava just below bedding conglomerates.

GC88 27°55′47″N 15°47′39″W; Barranco de Tasartico, the road cut ca. 100 m above the town of Tasartico, visually fresh Ol–Cpx-phyric basaltic lava flow.

GC56 Montaña de Agüimes, fresh Ol–Cpx–Pl-phyric basalt (provided by M. Sumita).

GC58 Montaña de Agüimes, similar to GC56 (provided by M. Sumita).

B.1.2. Tenerife

B.1.2.1. Massif Teno

TF2 28°17′56″N 16°49′26″W; Degollada de Cherfe, the road from Santiago del Teide to Masca; fresh Ol–Cpx-phyric basalt.

TF4 28°18′39″N, 16°50′38″W; south slope of the El Tablero mountain, road cut outside Masca towards to Buenavista; slightly altered Ol–Cpx-phyric picritic basalt.

TF7 28°15′20″N 16°49′00″W; Montaña del Angel, Risco de Lara, N820 between the 90th and 91st km-posts outside the town of Chío towards to Santiago del Teide; fresh Ol–Cpx-phyric picritic basalt.

TF9 28°18′12″N 16°49′38″W; Degollada de la Mesa; viewpoint on the road from Santiago del Teide to Masca; fresh Ol–Cpx-phyric basalt.

TF16 28°18′40″N 16°49′09″W; Cumbre de Bolico, small field road towards the radar station turning left from N820 between the 79th and 80th km-posts; slightly altered Ol–Cpx-phyric picritic basalt.

TF64 28°19′26″N 16°51′08″W; Cumbre del Carrizal, in the road cut between the towns of Masca and Buenavista; slightly altered Ol–Cpx-phyric picritic basalt.

TF67 28°21′51″N 16°53′00″W; Barranco de Tamargo near the Roque del Anden, the road connecting Faro del Teno and the town of Buenavista; fresh Ol–Cpx basalt.

B.1.2.2. Roque del Conde

TF23 28°07′10″N 16°41′00″W; Barranco del Rey, the base of Roque Imoque Suárez, waterfall locality; fresh Ol–Cpx-phyric basalt.

TF51 28°07′25″N 16°41′13″W; steep lava flows near the top of Roque Imoque Suárez; fresh, nearly aphyric basalt containing only 1–3 vol.% of Ol and Cpx–phenocrysts.

B.1.3. La Gomera

LG1 Degollada de Peraza, viewpoint on the road TF713, a small tourist trail down to Barranco de La Laja; fresh Ol–Cpx-phyric picrite representing the upper old basalt series right below the unconformity (provided by A. Klügel).

LG2 The same locality, another fresh lava flow of Ol–Cpx-phyric picrite (provided by A. Klügel).

LG6 28°07′19″N 17°12′12″W; a small road to Monte el Cedro connecting the TF711 and TF713 roads, ca. 15 m below Mirador de El Rejo; moderately altered Ol–Cpx-phyric basalt.

LG11 28°05′57″N 17°10′57″W; Degollada de Peraza, the same locality, as described for samples LG1 and LG2, ca. 50 below the unconformity separating the older and younger basaltic series, fresh Ol–Cpx-phyric picrite.

LG35 28°07′29″N 17°09′09″W; a small field road towards Casas de Enchereda and Casas de Juel turning left from the TF711 road between Hermigua and San Sebastian (near the 8th km-post); very fresh Ol–Cpx-phyric picrite.

LG50 28°07′36″N 17°08′46″W; similar field road; fresh, aphyric to slightly phyric basalt containing ~ 3–5% of broken Ol crystals and numerous peridotite and gabbro xenoliths.

LG53 28°09′15″N 17°09′23″W; similar field road, between Riscos de Juel and Roque Caraballo, ca. 500 m behind Casas de Juel; very fresh Ol–Cpx-phyric basalt.

LG58 28°09′45″N 17°20′02W; Playa de Alojera, beach outcrop of a very thick sequence of lavas representing the lower old basaltic suite; vesicular Ol–Cpx basalt, Ol is partially altered, Cpx remains fresh.

LG59 28°09′45″N 17°20′02W; similar locality, more fresh Ol- and Cpx-phyric picritic dike.

LG65 28°05′52″N 17°15′18W; Barranco del Erque, small field road towards the villages of Erque and Erquito; very fresh Ol–Cpx-phyric basalt representing the upper old series.

LG66 28°03′53″N 17°12′48″W; Barranco de Santiago, near small town of El Cabezo, upper old basaltic series composed of altered lava flows bedded by pyroclastic deposits; altered Ol–Cpx basalt.

B.1.4. La Palma

B.1.4.1. Inner part of the Caldera de Taburiente

LP1 Barranco de las Angustias, old cumulative picrite (>0.6 Ma) containing ca. 30 vol.% of Ol and Cpx phenocrysts; the sample is taken from a lava block lying on the bottom of the canyon (provided by A. Klügel).

LP7 28°42′20″N 17°51′11″W; small tourist trail starting at the Mirador Cumbrecita toward the NE flank of the Caldera de Taburiente; moderately altered Ol–Cpx-phyric basalt.

LP8 28°42′20″N 17°51′11″W, similar locality; moderately altered Ol–Cpx-phyric basalts but containing less amount of phenocrysts and somewhat higher proportion of Cpx to Ol.

LP13 28°42′44″N, 17°51′11″W; the same tourist trail just below the mountain Pico del Cedro, a few hundred meters to the north from Galeria Aridane, moderately altered cumulative picrite with >30 vol.% of large Ol phenocrysts (up to 15–25 mm in size).

LP14 28°43′00″N, 17°51′04″W, a few hundred meters from the previous stop towards the northern flank of the Caldera de Taburiente; moderately altered Ol–Cpx-phyric picrite similar to LP13.

LP25 28°43′12″N, 17°50′48″W; the same tourist trail, ca. 100–150 m to the north from the Galeria La Faya towards Hoyo de las Pinas; fresh Ol–Cpx-phyric picrite.

LP81 28°43′16″N, 17°50′42″W; the same tourist trail, ca. 300 m from Galeria La Faya towards Hoyo de las Pinos; slightly altered Ol–Cpx-phyric cumulative picrite dike.

B.1.4.2. Outer part of the Caldera de Taburiente

LP43 28°43′24″N 17°46′15″W; the eastern slope of the Taburiente shield; grey, slightly altered Ol–Cpx-phyric basalts exposing in the LP22 road cut between the 5th and 6th km-posts from the town of Miranda towards the Astrophysical Observatory.

LP46 28°43′55N, 17°48′12W; road cut on LP22 ca. ~ 300 m before the 18th km-post, to the north from Montaña Tagoja toward the Astrophysical Observatory; lava flow ca. 20–30 m thick of dark-gray, mostly fresh Ol–Cpx-phyric basalts similar to those collected inside the Caldera de Taburiente.

LP47 28°44′10″N, 17°49′45″W; small tourist trail of a few km long turning from the LP22 road towards Pico de la Nieve; aphyric lava containing single Ol and Cpx crystals.

LP48 28°44′10″N, 17°49′45″W; similar locality; fresh basaltic lava flow containing large Ol and Cpx phenocrysts similar to those collected inside the Caldera de Taburiente.

Appendix C

C.1. Analytical methods

C.1.1. Electron microprobe analyses of rock-forming minerals

Rock-forming minerals (olivine, clinopyroxene, plagioclase, spinel and Fe–Ti oxides) were analyzed with the Cameca SX-50 electron microprobe at IfM-GEOMAR Leibniz Institute. The 15 kV accelerating voltage, 6–20 nA beam current, 20–60 s peak counting times and 10–30 s background counting times were applied during routine analyses of major elements. The Cameca and Smithsonian (Jarosewich et al., 1980) sets of international reference materials, as well as olivine

Table C.1
Precision and accuracy of XRF measurements

Standard [a]	JB-2				JB-3				JA-2				JR-1			
Note	REF	MEAS $N=6$	2RSD %	ΔRV %	REF	MEAS $N=6$	2RSD %	ΔRV %	REF	MEAS $N=4$	2RSD %	ΔRV %	REF	MEAS $N=4$	2RSD %	ΔRV %
Major elements, wt.%																
SiO_2	53.25	53.50	1.2	0.5	50.96	50.97	0.6	0.0	56.42	56.32	0.1	− 0.2	75.45	75.99	0.1	0.7
TiO_2	1.19	1.17	0.9	− 1.7	1.44	1.41	1.1	− 2.1	0.66	0.68	0.0	3.0	0.11	0.11	0.0	0.0
Al_2O_3	14.64	14.89	1.1	1.7	17.20	17.40	0.5	1.2	15.41	15.55	0.2	0.9	12.83	12.97	0.4	1.1
Fe_2O_3	14.25	14.39	1.4	1.0	11.82	11.79	1.4	− 0.3	6.21	6.35	1.7	2.3	0.89	0.88	1.1	− 1.1
MnO	0.22	0.21	1.0	− 4.5	0.18	0.17	6.0	− 5.6	0.11	0.11	0.0	0.0	0.10	0.10	0.0	0.0
MgO	4.62	4.61	3.4	− 0.2	5.19	5.14	2.6	− 1.0	7.60	7.97	1.7	4.9	0.12	ND	–	–
CaO	9.89	10.01	1.6	1.2	9.79	9.82	1.0	0.3	6.29	6.28	0.3	− 0.2	0.67	0.71	3.6	6.0
Na_2O	2.04	2.16	22.9	5.9	2.73	2.72	14.0	− 0.4	3.11	2.94	7.2	− 5.5	4.02	4.09	6.9	1.7
K_2O	0.42	0.43	1.9	2.4	0.78	0.77	1.1	− 1.3	1.81	1.76	0.6	− 2.8	4.41	4.52	0.3	2.5
P_2O_5	0.101	0.102	8.0	1.0	0.29	0.29	0.0	0.0	0.15	0.15	0.0	0.0	0.02	0.02	0.0	0.0
H_2O^+	0.25	ND	–	–	0.18	ND	–	–	1.12	ND	–	–	1.16	ND	–	–
H_2O^-	0.13	ND	–	–	0.07	ND	–	–	1.25	ND	–	–	0.20	ND	–	–
Total	101.00	101.48	–	–	100.63	100.48	–	–	100.14	98.11	–	–	99.98	–	–	–
Trace elements, ppm																
Ba	222	234	14.4	5.4	245	239	11.5	− 2.4	321	314	9.0	− 2.2	50.3	45.7	24.1	− 9.1
Co	38.0	52.3	22.0	37.6	34.3	43.3	6.9	26.2	29.5	24.5	4.7	− 16.9	0.83	BDL	–	–
Cr	28.1	25.0	46.0	− 11.0	58.1	60.7	14.2	4.5	436	511	2.1	17.2	2.83	BDL	–	–
Ga	17.0	15.3	28.2	− 10.0	19.8	18.8	18.3	− 5.1	16.9	15.0	34.4	− 11.2	16.1	18.3	20.7	13.7
Nb	1.58	BDL	–	–	2.5	4.0	31.6	60.0	9.5	10.3	9.8	8.4	15.2	12.0	23.6	− 21.1
Ni	16.6	24.3	39.8	46.4	38.8	41.0	40.9	5.7	130	134	5.2	3.1	1.67	BDL	–	–
Rb	7.4	7.3	28.2	− 1.4	15.1	16.2	18.2	7.3	72.9	73.3	4.1	0.5	257	263	2.3	2.3
Sr	178	178	1.9	0.0	403	406	0.9	0.7	248	244	0.4	− 1.6	29.1	28.9	10.3	− 0.7
V	575	>550	–	–	372	370	1.1	− 0.5	126	124	4.3	− 1.6	7	BDL	–	–
Y	24.9	23.7	12.7	− 4.8	26.9	26.5	10.4	− 1.5	18.3	19.0	8.6	3.8	45.1	31.8	9.4	− 29.5
Zn	108	128	3.1	18.5	100	125	2.1	25.0	64.7	81.8	8.8	26.4	30.6	45.3	9.8	48.0
Zr	51.2	55.3	4.4	8.0	97.8	97.5	3.8	− 0.3	116	101	5.1	− 12.9	99.9	99.8	1.0	− 0.1

[a] International reference materials produced by the Geological Survey of Japan and analyzed as unknown samples during XRF analyses: JB-2 and JB-3 are Basalts, JA-2 is Andesite and JR-1 is Rhyolite (Terashima et al., 1994; Imai et al., 1995). REF = recommended reference values of major and trace element concentrations; MEAS = average measured element concentrations in reference materials analyzed as unknowns together with the samples of interest, where N is a number of replicates; 2RSD = 2-sigma relative standard deviation (given in %) defined as $100 \times 2\sigma$ SD/MEAS, where 2σ SD = 2-sigma standard deviation that characterize the precision of XRF analysis; ΔRV = deviation from the reference values (given in % and defined as 100 × (MEAS/REF − 1) that may characterize not only the accuracy of XRF analyses but also a possible bias introduced during laboratory treatment of samples (production of fused beads, etc.); ND = not determined; BDL = below detection level; – = no value.

Ch-1 and spinel Yb-126 (Lavrent'ev et al., 1974), were used for instrument calibration and stability monitoring. Typical external reproducibility expressed as 2-sigma relative standard deviation (2σ RSD) were better than 3% for SiO_2, Al_2O_3, MgO, CaO, 4–10% for TiO_2, FeO, NiO and Na_2O, ca. 10–20% for MnO, K_2O and Cr_2O_3.

C.1.2. Major and trace elements in whole rocks

Major and selected trace (Ba, Co, Cr, Ga, Nb, Ni, Rb, Sr, V, Y, Zn and Zr) elements in whole-rock samples were analyzed on fused beads using a Phillips X'Unique PW1480 X-ray fluorescence spectrometer (XRF) equipped with a Rh-tube at IfM-GEOMAR Leibniz Institute. The precision and accuracy of XRF measurements were monitored using international reference materials of the Geological Survey of Japan (basalts JB-2 and JB-3, andesite JA-2 and rhyolite JR-1; Terashima et al., 1994; Imai et al., 1995), which were always analyzed as unknown samples together with the samples of interest (Table C.1). The precision (2σ RSD) is better than 2% for SiO_2, TiO_2, Al_2O_3, Fe_2O_3, CaO and K_2O; 1–8% for MnO, MgO and P_2O_5; and 7–23% for Na_2O, while the accuracy (deviation from the reference values) is better than 3% for all major elements, except for MnO and Na_2O (3–6%) (Table C.1). Major element compositions of 19 selected samples were replicated by ICP-AES using the Analytical Service of Rocks and Minerals (original abbreviation SARM) at the Centre de Recherches Pétrographiques et Géochimiques (CRPG-CNRS, Nancy, France). The analytical error announced by SARM is 1–5% for major elements, if their concentrations exceed 1 wt.% and 2–10% for element concentrations below 1 wt.%. Inter-laboratory comparison for selected components SiO_2, CaO and TiO_2 between XRF (IfM-GEOMAR) and ICP-AES (SARM)

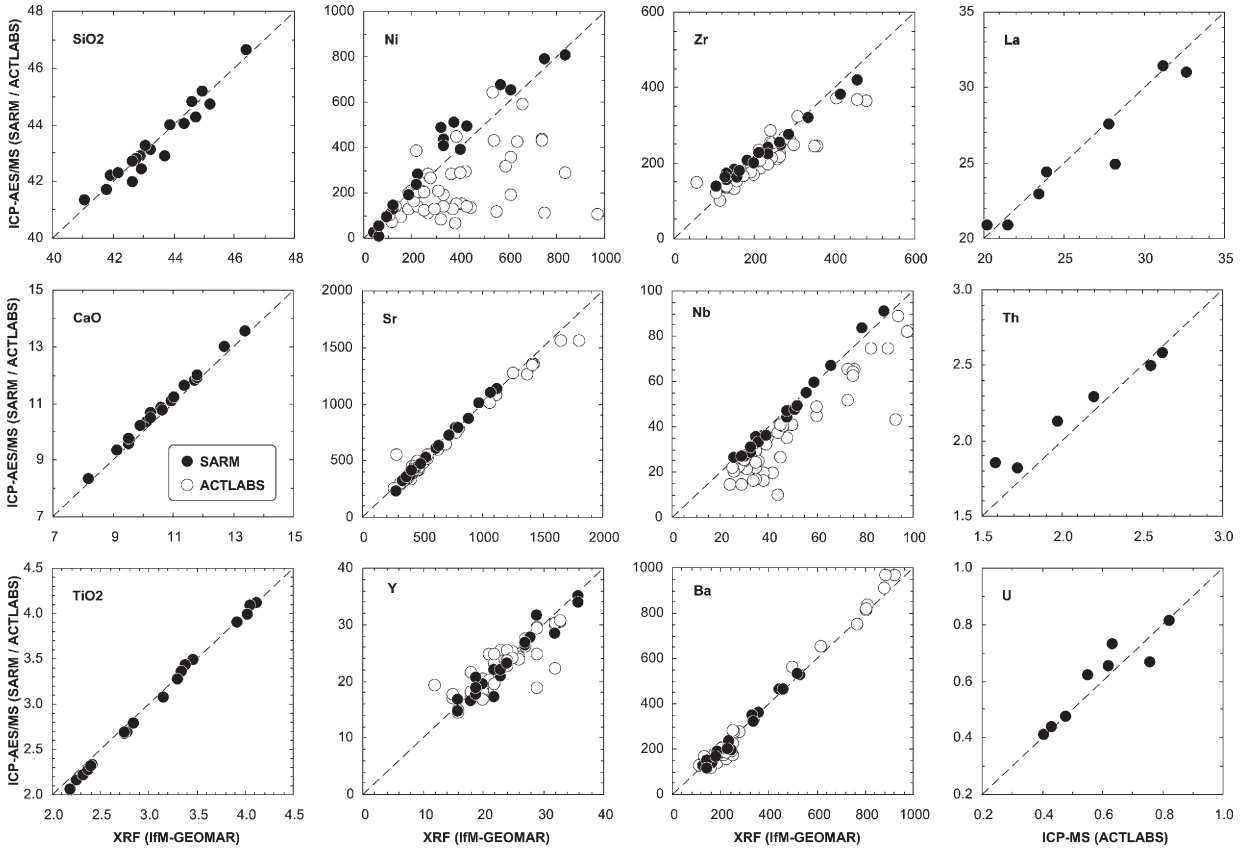

Fig. C.1. Inter-laboratory comparison of the collected analytical data. The whole rock analyses were obtained by XRF method at the IfM-GEOMAR analytical laboratory (labeled as IfM-GEOMAR), by ICP-MS method at the ACTLABS Activation Laboratory (Ancaster, Ontario, Canada) (labeled as ACTLABS) and by ICP-AES (major elements) and ICP-MS (trace elements) methods at the Analytical Service of Rocks and Minerals (CRPG-CNRS, Nancy, France) (labeled as SARM). In most cases, better coherence was obtained between the IfM-GEOMAR and SARM laboratories with respect to Ba, Cr, Ga, Nb, Ni, Rb, Sr, V, Y, Zn and Zr, whereas satisfactory reproducibility was obtained between ACTLABS and SARM for rare earth elements, Sr, Ba, Th, U, Hf and Ta.

methods is presented in Fig. C.1. Similar reproducibility was obtained for other major and minor elements. Averages of the replicate analyses were used for plotting and numerical calculations.

Trace elements analyzed by XRF show varying precision and accuracy which strongly depend on element concentration in the sample. At the concentration level above 100 ppm, i.e., most common concentrations of Ba, Cr, Ni, Sr, V, Zr in the Canary shield stage lavas, the precision and accuracy are better than 20% (Table C.1). Rubidium, Nb and Y, whose concentrations lie between 10 and 50 ppm in the samples studied, were also analyzed with analytical error better than 20% (Table C.1). Analyses of Co were performed with up to 40% analytical error at the concentration level of 20–40 ppm and therefore were considered as unacceptable (Table C.1). Since ΔRV = deviation from the reference values (given in % and defined as 100 × (MEAS/REF − 1) that may characterize not only the accuracy of XRF analyses but also a possible bias introduced during laboratory treatment of samples (production of fused beads, etc.), the analytical data, both XRF and ICP-MS, obtained for the Canary rocks and reported in Table 2 were not corrected for ΔRV values.

Concentrations of trace elements were analyzed by ICP-MS at the ACTLABS Activation Laboratory Ltd. (Ancaster, Ontario, Canada) in accordance with the 4B2-RES protocol (for more detail see website on http://www.actlabs.com) and at SARM. A lithium metaborate/tetraborate fusion technique was employed by ACTLABS, and a set of the United States Geological Survey (USGS) international reference materials (marine mud MAG-1, Icelandic basalt BIR-1, dolerite DNC-1, nepheline syenite STM-1; Flanagan, 1976, 1984; Gladney and Roelandts, 1987, 1988) and the CRPG-CNRS reference biotite Mica-Fe (Govindaraju, 1995) were analyzed together with the samples (Table C.2). Systematic replicate analyses of each 15th sample in the sequence were performed during each analytical session. Although the fusion solution technique provides research quality results for most trace elements, data for chalcophile elements (i.e., As, Co, Cu, Mo, Ni, Pb, Sb, Sn, W and Zn) analyzed in mineralized samples, as announced by ACTLABS, should be considered as semi-quantitative. Analyses of trace elements by ICP-MS at SARM were performed in accordance with the analytical procedure described by Carignan et al. (2001).

The results of inter-laboratory comparison for selected elements Ni, Sr, Y, Zr, Nb, Ba, La, Th and U between XRF (IfM-GEOMAR) and ICP-AES/MS (ACTLABS and SARM) methods are presented in Fig. C.1. We have to emphasize here that the concentrations of Ni, Co, Zn, Cu, Ga, Ge obtained by ACTLABS were not reproduced in other two laboratories using separate splits of the same powder, while the IfM-GEOMAR and CRPG-Nancy laboratories have shown consistent results (Fig. C.1). The concentrations of Zn, Cu, Ga and Ge obtained by ICP-MS at SARM are systematically higher than those by XRF at IfM-GEOMAR. Since it is not clear which of these two data sets better resemble true values, the concentrations of Zn, Cu, Ga and Ge are not discussed in the present study. The results obtained for V, Cr, Rb, Y, Zr, Nb by XRF (IfM-GEOMAR) and ICP-MS (SARM) show better coherence than the ICP-MS results by ACTLABS and SARM (e.g., Y, Zr, Nb; Fig. C.1). We therefore have taken the average of the IfM-GEOMAR and SARM data. When only data from IfM-GEOMAR and ACTLABS were available, the IfM-GEOMAR results were preferentially used. Finally, the analyses of Sr, Ba, rare earth elements (REE), Hf, Ta, Th and U produced similar results in the different laboratories (e.g., Sr, Ba, La, Th, U; Fig. C.1). The averages of the replicate data are taken as the best estimates of the true concentrations.

C.1.3. Sr, Nd and Pb isotopes in whole rocks

The Sr, Nd and Pb isotope ratios were measured on a Finnigan® MAT 262 thermal ionization mass spectrometer (TIMS) at the IfM-GEOMAR operating in static multicollection for Sr and Pb and dynamic multicollection for Nd. Prior to sample dissolution, the powders were leached in hot 6 N HCl for 1 h and thereafter repeatedly rinsed in 18.2 MΩ water. The chemical separation techniques was followed those described in Hoernle and Tilton (1991). The Sr and Nd isotopic ratios were normalized within run to $^{86}Sr/^{88}Sr = 0.1194$ and $^{146}Nd/^{144}Nd = 0.7219$. The long-term reproducibility of NBS 987 is $^{87}Sr/^{86}Sr = 0.710249 \pm 22$ (2 sigma, $N = 160$) and $^{143}Nd/^{144}Nd = 0.511844 \pm 11$ (2 sigma, $N = 68$) for La Jolla. The NBS 981 Pb isotope ratios corrected for the values of isotope fractionation (Todt et al., 1996) are: $^{206}Pb/^{204}Pb = 16.899 \pm 7$, $^{207}Pb/^{204}Pb = 15.437 \pm 9$, $^{208}Pb/^{204}Pb = 36.529 \pm 27$ (2 sigma, $N = 110$). The Pb isotope ratios of the samples studied were also corrected using similar values of isotope fractionation taken from Todt et al. (1996). Based on replicate analyses, the external reproducibility for Pb isotope ratios is estimated to be better than 0.05% per a.m.u. (atomic mass unit) and < 0.000015 for $^{143}Nd/^{144}Nd$ and $^{87}Sr/^{86}Sr$. Total chemistry blanks were < 100 pg for Sr, Nd and Pb and thus considered negligible.

C.1.4. Noble gases and O isotopes in olivine

The experimental conditions of noble gas analyses are reported in Hanyu et al. (1999). In short, olivine

Table C.2
Accuracy of ICP-MS trace element analyses by ACTLAB based on international reference materials

Standard [a]	MAG-1			BIR-1			DNC-1			STM-1			Mica-Fe		
	REF ppm	MEAS ppm	ΔRV %	REF ppm	MEAS ppm	ΔRV %	REF ppm	MEAS ppm	ΔRV %	REF ppm	MEAS ppm	ΔRV %	REF ppm	MEAS ppm	ΔRV %
As	9.2	9.3	1.1	*0.4*	BDL	–	*0.2*	BDL	–	*4.6*	BDL	–	*3*	8.7	–
Ba	480	484	0.8	7.7	5.77	− 25.1	114	106	− 7.0	560	585	4.5	150	144	− 4.0
Ce	88	86	− 2.3	1.95	1.87	− 4.1	*10.6*	8.1	–	259	261	0.8	420	420	0.0
Co	20.4	21.5	5.4	51	47.7	− 6.5	55	55	0.0	*0.9*	BDL	–	23	25	8.7
Cr	97	98	1.0	380	388	2.1	285	280	− 1.8	*4.3*	BDL	–	90	84	− 6.7
Cs	8.6	8.6	0.0	*0.45*	BDL	–	*0.34*	0.17	–	1.54	1.64	6.5	180	180	0.0
Cu	30	28	− 6.7	126	128	1.6	96	94.5	− 1.6	*4.6*	BDL	–	*5*	BDL	–
Dy	5.2	5.3	1.9	2.4	2.7	12.5	2.7	2.8	3.7	8.1	8.3	2.5	11	11	0.0
Er	3	3	0.0	1.8	1.8	0.0	*2*	2	–	4.2	4.5	7.1	3.8	3.5	− 7.9
Eu	1.55	1.48	− 4.5	0.54	0.57	5.6	0.59	0.62	5.1	3.6	3.6	0.0	0.7	0.7	0.0
Ga	*20.4*	21.8	–	16	15.6	− 2.5	15	14	− 6.7	36	36	0.0	95	90	− 5.3
Gd	5.8	5.5	− 5.2	1.85	1.81	− 2.2	2	2	0.0	9.5	9.7	2.1	21	24	14.3
Hf	3.7	3.4	− 8.1	0.58	0.61	5.2	1.01	1.02	1.0	28	28	0.0	26	26	0.0
Ho	1.02	0.99	− 2.9	0.57	0.58	1.8	0.62	0.62	0.0	1.9	1.5	− 21.1	1.6	1.5	− 6.3
La	43	43	0.0	0.62	0.62	0.0	3.8	3.7	− 2.6	150	154	2.7	200	198	− 1.0
Lu	0.4	0.4	0.0	0.26	0.25	− 3.8	0.32	0.3	− 6.3	0.6	0.6	0.0	0.5	0.5	0.0
Mo	*1.6*	BDL	–	*0.5*	BDL	–	*0.7*	BDL	–	5.2	5.4	3.8	*1.2*	BDL	–
Nb	12	12	0.0	*0.6*	0.8	–	*3.0*	1.7	–	268	238	− 11.2	270	242	− 10.4
Nd	38	37	− 2.6	2.5	2.4	− 4.0	4.9	5	2.0	79	81	2.5	180	179	− 0.6
Ni	53	57	7.5	166	161	− 3.0	247	250	1.2	*3*	22	–	35	37	5.7
Pb	24	26	8.3	*3.2*	BDL	–	*6.3*	8.2	–	17.7	18.9	6.8	13	10	− 23.1
Pr	*9.3*	ND	–	*0.5*	BDL	–	–	ND	–	19	20	5.3	*49*	ND	–
Rb	149	151	1.3	*1.0*	BDL	–	*4.5*	3.3	–	118	117	− 0.8	2200	2200	0.0
Sb	0.96	1.01	5.2	0.58	0.52	− 10.3	0.96	1	4.2	1.66	1.63	− 1.8	–	0.43	–
Sm	7.5	7.1	− 5.3	1.08	1.09	0.9	1.38	1.39	0.7	12.6	12.2	− 3.2	33	33	0.0
Sn	3.6	3	− 16.7	*0.65*	BDL	–	–	1.2	–	6.8	8	17.6	70	70	0.0
Sr	146	141	− 3.4	108	108	0.0	145	142	− 2.1	700	698	− 0.3	5	4	− 20.0
Ta	1.11	1.21	9.0	*0.06*	BDL	–	*0.10*	BDL	–	18.6	20.1	8.1	35	35	0.0
Tb	0.96	0.97	1.0	0.41	0.4	− 2.4	0.41	0.43	4.9	1.55	1.5	− 3.2	2.7	2.71	0.4
Th	11.9	11.6	− 2.5	*0.03*	BDL	–	*0.2*	0.2	–	31	32	3.2	150	162	8.0
Tm	0.43	0.41	− 4.7	0.27	0.27	0.0	0.33	0.31	− 6.1	0.69	0.68	− 1.4	0.48	0.482	0.4
U	2.7	2.8	3.7	*0.03*	BDL	–	0.1	0.06	− 40.0	9.03	9.09	0.7	80	86	7.5
V	140	138	− 1.4	313	317	1.3	148	148	0.0	*8.7*	BDL	–	135	131	− 3.0
W	*1.4*	1.3	–	*0.22*	BDL	–	*0.19*	BDL	–	3.6	3	− 16.7	15	17	13.3
Y	28	28	0.0	16	16	0.0	18	18	0.0	46	47	2.2	48	46	− 4.2
Yb	2.6	2.6	0.0	1.7	1.7	0.0	2.01	2.02	0.5	4.4	4.4	0.0	3.5	3	− 14.3
Zn	130	135	3.8	71	70	− 1.4	66	62	− 6.1	235	239	1.7	1300	1300	0.0
Zr	126	116	− 7.9	*15.5*	13.2	–	41	39	− 4.9	1210	1230	1.7	800	777	− 2.9

[a] International reference materials: MAG-1 = marine mud, STM-1 = nepheline syenite (Flanagan, 1976; Gladney and Roelandts, 1988), BIR-1 = Icelandic basalt, DNC-1 = dolerite (Flanagan, 1984; Gladney and Roelandts, 1987) produced by the United States Geological Survey (USGS), Mica-Fe = reference biotite of the Centre de Recherches Pétrographiques et Géochimiques (CRPG-CNRS, Nancy, France; Govindaraju, 1995). REF are recommended reference values, if given by plain font and information values, if given in italic; MEAS = composition of reference materials analyzed as unknown samples together with the samples of interest; ΔRV = deviation from the reference values and defined as in Table C.1.

phenocrysts were handpicked; cleaned sequentially using 2N HNO_3, acetone and ethanol; dried at 120 °C; and finally checked again to ensure the absence of adhering minerals. Prior to analysis, the gas extraction and purification lines were baked overnight at 150–200 °C, whereas the crushing vessel and olivine separates were preheated to 120 °C for ca. 1 h and then were continually heated at 120 °C during crushing. Olivine separates were manually crushed under vacuum using a pressing-type crusher whose sample holder and piston are made out of stainless steel. The crushing process was repeated 10 times for each sample while loading 1–1.5 g of olivine separate under the torque of 250 kg/cm^2 applied to the rotating head. The extracted noble gases were purified by two titanium–zirconium getters heated at 700–800 °C and then separated from each other using cold traps with activated charcoal and cryogenic pump. Isotope

analyses were performed using a mass spectrometer VG-5400 located at the Earthquake Research Institute, University of Tokyo, Japan (analyst H. Dan). The mass resolving power was ~ 600 in order to resolve a $^3He^+$ peak from that of $HD^+$and $^3H^+$. Calibration of measured He isotopic ratios was performed using the Kaminoyama well gas ($^3He/^4He = 5.95 \pm 0.30$ R_A; Yamagata Prefecture, Japan), while those of Ar were calibrated by the repeated measurements of standard diluted air. Crushing blanks were analyzed at the same analytical conditions as sample runs. The isotopic compositions of blanks were indistinguishable from those of the air. The crushing blanks were 5.2×10^{-12}, 8.1×10^{-13} and 7.8×10^{-13} cm^3STP for ^{4}He, ^{20}Ne and ^{36}Ar, respectively.

Olivine phenocrysts analyzed for O isotopes were handpicked under a binocular microscope. Only carefully selected crystals containing no inclusions and adhering groundmass minerals were selected for analyses. Mineral separates were first cleaned in a 10% ultrapure HF-solution for 5–10 min and then repeatedly washed in distilled water in an ultrasound bath. Finally, all olivine crystals were checked again to ensure their cleanliness. Oxygen isotopes in the 15 mg-weight olivine monomineral fractions were analyzed at the ACTLABS Activation Laboratory (Ancaster, Ontario, Canada) that employs thermal ionization mass spectrometry that ensures the analytical uncertainty (2σ standard error) of ± 0.3‰ (for more details information see http://www.actlabs.com/gg_isotope_can.htm).

References

Abdel-Monem, A., Watkins, N.D., Gast, P.W., 1971. Potassium–argon ages, volcanic stratigraphy, and geomagnetic polarity history of the Canary Islands: Lanzarote, Fuerteventura, Gran Canaria, and La Gomera. Am. J. Sci. 271, 490–521.

Ablay, G.J., Carroll, M.R., Palmer, M.R., Martí, J., Sparks, R.S.J., 1998. Basanite–phonolite lineages of the Teide–Pico Viejo volcanic complex, Tenerife, Canary Islands. J. Petrol. 39, 905–936.

Abratis, M., Schmincke, H.-U., Hansteen, T.H., 2002. Composition and evolution of submarine volcanic rocks from the central and western Canary Islands. Int. J. Earth Sci. 91, 562–582.

Albarède, F., van der Hilst, R.D., 1999. New mantle convection model may reconcile conflicting evidence. EOS 80, 537–539.

Allègre, C.J., Staudacher, T., Sarda, P., 1986. Rare gas systematics: formation of the atmosphere, evolution and structure of the Earth's mantle. Earth Planet. Sci. Lett. 81, 127–150.

Amundsen, H.E.F., 1987. Peridotite xenoliths from Gran Canaria, Canary Islands; evidence for metasomatic processes and partial melting in the lower oceanic crust. Neues Jahrb. Mineral. Abh. 156, 121–140.

Ancochea, E., Fuster, J.M., Ibarolla, E., Cendrero, A., Coello, J., Hernan, F., Cantagrel, J.M., Jamond, C., 1990. Volcanic evolution of the island of Tenerife (Canary Islands) in the light of new K–Ar data. J. Volcanol. Geotherm. Res. 44, 231–249.

Ancochea, E., Hernán, F., Cendrero, A., Cantagrel, J.M., Fúster, J.M., Ibarrola, E., Coello, J., 1994. Constructive and destructive episodes in the building of a young oceanic island, La Palma, Canary Islands, and genesis of the Caldera de Taburiente. J. Volcanol. Geotherm. Res. 60, 243–262.

Ancochea, E., Cantagrel, J.M., Fúster, J.M., Huertas, M.J., Arnaud, N. O., Martí, J., Hürlimann, M., Ablay, G., Gudmundsson, A., 1998. Vertical and lateral collapses on Tenerife (Canary Islands) and other volcanic ocean islands: comment and reply. Geology 26, 861–863.

Anderson, D.L., Tanimoto, T., Zhang, Y.-s., 1992. Plate tectonics and hotspots: the third dimension. Science 256, 1645–1651.

Arai, S., 1987. An estimation of the least depleted spinel peridotite on the basis of olivine–spinel mantle array. Neues Jahrb. Mineral., Monatsh. 8, 347–354.

Ballentine, C.J., Barfod, D.N., 2000. The origin of air-like noble gases in MORB and OIB. Earth Planet. Sci. Lett. 180, 39–48.

Burnard, P.G., Graham, D.W., Turner, G., 1997. Vesicle-specific noble gas analyses of "popping rock": Implications for primordial noble gases in the Earth. Science 276, 568–571.

Cantagrel, J.M., Cendrero, A., Fuster, J.M., Ibarrola, E., Jamond, C., 1984. K–Ar chronology of the volcanic eruptions in the Canarian Archipelago: Island of La Gomera. Bull. Volcanol. 47, 597–609.

Carignan, J., Hild, P., Mevelle, G., Morel, J., Yeghicheyan, D.E., 2001. Routine analyses of trace element in geological samples using flow injection and low pressure on-line liquid chromatography coupled to ICP-MS: a study of geochemical reference materials BR, DR-N, UB-N, AN-G and GH. Geostand. Newsl. 25, 187–198.

Carracedo, J.C., 1994. The Canary Islands: an example of structural control on the growth of large oceanic–island volcanoes. J. Volcanol. Geotherm. Res. 60, 225–241.

Carracedo, J.C., 1996. A simple model for the genesis of large gravitational landslide hazards in the Canary Islands. In: McGuire, W., Jones, A.P., Neuberg, J. (Eds.), Volcano Instability on the Earth and Terrestrial Planets. Geol. Soc. London, Spec. Publ., vol. 110, pp. 125–135.

Carracedo, J.C., Day, S.J., Guillou, H., Gravestock, P., 1999. Later stages of volcanic evolution of La Palma, Canary Islands: rift evolution, giant landslides, and the genesis of the Caldera de Taburiente. Bull. Geol. Soc. Am. 111, 755–768.

Cendrero, A., 1971. Estudio geológico y petrológico del Complejo Basal de la Isla de La Gomera (Canarias). Estud. Geol. 27, 3–73.

Class, C., Goldstein, S.L., 1997. Plume–lithosphere interactions in the ocean basins: constraints from the source mineralogy. Earth Planet. Sci. Lett. 150, 245–260.

Cousens, B.L., Spera, F.J., Tilton, G.R., 1990. Isotopic patterns in silicic ignimbrites and lava flows of the Mogan and lower Fataga Formations, Gran Canaria, Canary Islands: temporal changes in mantle source composition. Earth Planet. Sci. Lett. 96, 319–335.

Cubas, C.R., 1978. Estudio de los domos salicos de la Isla de La Gomera (Islas Canarias), I—Vulcanología. Estud. Geol. 34, 53–70.

Eiler, J.M., Crawford, A., Elliott, T., Farley, K.A., Valley, J.W., Stolper, E.M., 2000. Oxygen isotope geochemistry of oceanic-arc lavas. J. Petrol. 41, 229–256.

Farley, K.A., Craig, H., 1994. Atmospheric argon contamination of ocean island basalt olivine phenocrysts. Geochim. Cosmochim. Acta 58, 2509–2517.

Flanagan, F.J., 1976. 1972 compilation of data on USGS standards. USGS Prof. Pap. 840, 131–183.

Flanagan, F.J., 1984. Three USGS mafic rock reference samples, W-2, DNS-1 and BIR-1. USGS Bull. 1623, 54 pp.; updated by Additions and Corrections for USGS Bulletin 1623, 1986. Open-File Report, 86-220.

Foley, S., Tiepolo, M., Vannucci, R., 2002. Growth of early continental crust controlled by melting of amphibolite in subduction zones. Nature 417, 837–840.

Fúster, J.M., Araña, V., Brändle, J.L., Navarro, J.M., Alonso, U., Aparicio, A., 1968. TenerifeGeologa y Volcanologa de las Islas Canarias, Volcanol., Inst. Lucas Mallada, Madrid, Int. Symp., Spec. Publ. 218 pp.

Fúster, J.M., Ibarrola, E., Snelling, N., Cantagrel, J.M., Huertas, M., Coello, J., Ancochea, E., 1994. Cronología K–Ar de la formación Cañadas en el sector Suroeste de Tenerife: implicaciones de los episodios piroclásticos en la evolución volcánica. Sociedad Española de Historia Natural, Madrid, Boletin, Sec. Geologica, vol. 89, pp. 25–41.

Geldmacher, J., Hoernle, K., 2000. The 72 Ma geochemical evolution of the Madeira hotspot (eastern North Atlantic): recycling of Paleozoic (500 Ma) oceanic lithosphere. Earth Planet. Sci. Lett. 183, 73–92.

Geldmacher, J., Hoernle, K., van den Bogaard, P., Zankl, G., Garbe-Schönberg, D., 2001. Earlier history of the 70-Ma-old Canary hotspot based on the temporal and geochemical evolution of the Selvagen Archipelago and neighboring seamounts in the eastern North Atlantic. J. Volcanol. Geotherm. Res. 111, 55–87.

Geldmacher, J., Hoernle, K., van den Bogaard, P., Duggen, S., Werner, R., 2005. New $^{40}Ar/^{39}Ar$ age and geochemical data from seamounts in the Canary and Madeira volcanic province: Support for the mantle plume hypothesis. Earth Planet. Sci. Lett. 237, 85–101.

Gladney, E.S., Roelandts, I., 1987. 1987 compilation of elemental concentration data for USGS BIR-1, DNC-1 and W-2. Geostand. Newsl. 12, 63–118.

Gladney, E.S., Roelandts, I., 1988. 1987 compilation of elemental concentration data for USGS BHVO-1, MAG-1, QLO-1, RGM-1, SCo-1, SDC-1, SGR-1 and STM-1. Geostand. Newsl. 12, 253–362.

Goes, S., Spakman, W., Bijwaard, H., 1999. A lower mantle source for Central European volcanism. Science 268, 1928–1931.

Govindaraju, K., 1995. 1995 working values with confidence limits for twenty-six CRPG, ANRT and IWG-GIT geostandards. Spec. Issue, Geostand. Newsl. 19, 1–32.

Graham, D.W., 2002. Noble gas isotope geochemistry of mid-ocean ridge and ocean island basalts: characterization of mantle source reservoirs. In: Porcelli, D., Ballentine, C.J., Wieler, R. (Eds.), Noble Gases in Geochemistry and Cosmochemistry. Rev. Mineral., vol. 47. Mineralogical Society of America, Washington, DC, pp. 247–317.

Graham, D.W., Humphris, S.E., Jenkins, W.J., Kurz, M.D., 1992. Helium isotope geochemistry of some volcanic rocks from Saint Helena. Earth Planet. Sci. Lett. 110, 121–131.

Guillou, H., Carracedo, J.C., Paris, R., Pérèz Torrado, F.J., 2004. Implications for the early shield-stage evolution of Tenerife from K/Ar ages and magnetic stratigraphy. Earth Planet. Sci. Lett. 222, 599–614.

Gurenko, A.A., Chaussidon, M., 1995. Enriched and depleted primitive melts included in olivine from Icelandic tholeiites: origin by continuous melting of a single mantle column. Geochim. Cosmochim. Acta 59, 2905–2917.

Gurenko, A.A., Hansteen, T.H., Schmincke, H.-U., 1996. Evolution of parental magmas of Miocene shield basalts of Gran Canaria (Canary Islands): constraints from crystal, melt and fluid inclusions in minerals. Contrib. Mineral. Petrol. 124, 422–435.

Gurenko, A.A., Hansteen, T.H., Schmincke, H.-U., 1998. Melt, crystal, and fluid inclusions in olivine and clinopyroxene phenocrysts from the submarine shield stage hyaloclastites of Gran Canaria, Sites 953 and 956. In: Weaver, P.P.E., Schmincke, H.-U., Firth, J.V., Duffield, W. (Eds.), Proceedings of the Ocean Drilling Program, Scientific Results, vol. 157. Ocean Drilling Program, College Station, TX, pp. 375–401.

Gurenko, A.A., Chaussidon, M., Schmincke, H.-U., 2001. Magma ascent and contamination beneath one intraplate volcano: evidence from S and O isotopes in glass inclusions and their host clinopyroxenes from Miocene basaltic hyaloclastites southwest of Gran Canaria (Canary Islands). Geochim. Cosmochim. Acta 65, 4359–4374.

Halliday, A.N., Lee, D.-C., Tommasini, S., Davies, G.R., Paslick, C. R., Fitton, J.G., James, D.E., 1995. Incompatible trace elements in OIB and MORB and source enrichment in the sub-oceanic mantle. Earth Planet. Sci. Lett. 133, 379–395.

Hansteen, T.H., Troll, V.R., 2003. Oxygen isotope composition of xenoliths from the oceanic crust and volcanic edifice beneath Gran Canaria (Canary Islands): consequences for crustal contamination of ascending magmas. Chem. Geol. 193, 181–193.

Hanyu, T., Kaneoka, I., 1997. The uniform and low $^{3}He/^{4}He$ ratios of HIMU basalts as evidence for their origin as recycled materials. Nature 390, 273–276.

Hanyu, T., Kaneoka, I., Nagao, K., 1999. Noble gas study of HIMU and EM ocean island basalts in the Polinesian region. Geochim. Cosmochim. Acta 63, 1181–1201.

Harmon, R.S., Hoefs, J., 1995. Oxygen isotope heterogeneity of the mantle deduced from global ^{18}O systematics of basalts from different geotectonic settings. Contrib. Mineral. Petrol. 120, 95–114.

Hart, S.R., 1984. A large-scale isotope anomaly in the Southern Hemisphere mantle. Nature 309, 753–757.

Hauri, E.H., Whitehead, J.A., Hart, S.R., 1994. Fluid dynamic and geochemical aspects of entrainment in mantle plumes. J. Geophys. Res. 99, 24275–24301.

Hernandez-Pacheco, A., 1971. Nota previa sobre el complejo basal de la isla de La Palma (Canarias). Estud. Geol. 27, 255–265.

Hernandez-Pachero, A., Ibarrola, E., 1973. Geochemical variation trends between the different Canary Islands in relation to their geological position. Lithos 6, 389–402.

Heuschkel, S., 1996. Die miozanen Schildbasalte von Gran Canaria: Stratigraphische and geochemische Untersuchungen zum Aufbau and zur Entwicklung der Schildphase einer ozeanischen Vulkaninsel im Atlantic. Ph. D. thesis, Univ. Kiel.

Hilton, D.R., Macpherson, C.G., Elliott, T.R., 2000. Helium isotope ratios in mafic phenocrysts and geothermal fluids from La Palma, the Canary Islands (Spain): implications for HIMU mantle sources. Geochim. Cosmochim. Acta 64, 2119–2132.

Hoernle, K., 1998. Geochemistry of Jurassic oceanic crust beneath Gran Canaria (Canary Islands): implications for crustal recycling and assimilation. J. Petrol. 39, 859–880.

Hoernle, K., Schmincke, H.-U., 1993a. The petrology of the tholeiites through melilite nephelinites on Gran Canaria, Canary Islands: crystal fractionation, accumulation, and depths of melting. J. Petrol. 34, 573–597.

Hoernle, K., Schmincke, H.-U., 1993b. The role of partial melting in the 15 Ma geochemical evolution of Gran Canaria: a blob model for the Canary hotspot. J. Petrol. 34, 599–626.

Hoernle, K., Tilton, G.R., 1991. Sr–Nd–Pb isotope data for Fuerteventura (Canary Islands) basal complex and subaerial volcanics: application to magma genesis and evolution. Schweiz. Mineral. Petrogr. Mitt. 71, 5–21.

Hoernle, K., Tilton, G., Schmincke, H.-U., 1991. Sr–Nd–Pb isotopic evolution of Gran Canaria: evidence for shallow enriched mantle beneath the Canary Islands. Earth Planet. Sci. Lett. 106, 44–63.

Hoernle, K., Zhang, Y.-S., Graham, D., 1995. Seismic and geochemical evidence for large-scale mantle upwelling beneath the eastern Atlantic and western and central Europe. Nature 374, 34–39.

Hoernle, K., Tilton, G., Le Bas, M.J., Duggen, S., Garbe-Schönberg, D., 2002. Geochemistry of oceanic carbonatites compared with continental carbonatites: mantle recycling of oceanic crustal carbonate. Contrib. Mineral. Petrol. 142, 520–542.

Hofmann, A.W., 1988. Chemical differentiation of the Earth: the relationship between mantle, continental crust and oceanic crust. Earth Planet. Sci. Lett. 90, 297–314.

Hofmann, A.W., White, W.M., 1982. Mantle plumes from ancient oceanic crust. Earth Planet. Sci. Lett. 57, 421–436.

Hofmann, A.W., White, W.M., 1983. Ba, Rb and Cs in the Earth's mantle. Z. Naturforsch. 38a, 256–266.

Hofmann, A.W., Jochum, K.P., Seufert, M., White, W.M., 1986. Nb and Pb in oceanic basalts: new constraints on mantle evolution. Earth Planet. Sci. Lett. 79, 33–45.

Ibarrola, E., 1970. Variation trends in basaltic rocks of the Canary islands. Bull. Volcanol. 33, 729–777.

Imai, N., Terashima, S., Itoh, S., Ando, A., 1995. 1994 compilation of analytical data for minor and trace elements in seventeen GSJ geochemical reference samples, "Igneous Rock Series". Geostand. Newsl. 19, 135–213.

Jarosewich, E.J, Nelen, J.A., Norberg, J.A., 1980. Reference samples for electron microprobe analyses. Geostand. Newsl. 4, 43–47.

Kaneoka, I., 1983. Noble gas constraints on the layered structure of the mantle. Nature 302, 698–700.

Kaneoka, I., Hanyu, T., Yamamoto, J., Miura, Y.N., 2002. Noble gas systematics of the Hawaiian volcanoes based on the analysis of Loihi, Kilauea and Koolau submarine rocks. In: Takahashi, E., Lipman, P.W., Garcia, M.O., Naka, J., Aramaki, S. (Eds.), Hawaiian Volcanoes: Deep Underwater Perspectives. Geophys. Monogr., vol. 128. American Geophysical Union, pp. 373–389.

Kelemen, P.B., Shimizu, N., Dunn, T., 1993. Relative depletion of niobium in some arc magmas and the continental crust: partitioning of K, Nb, La and Ce during melt/rock reaction in the upper mantle. Earth Planet. Sci. Lett. 120, 111–134.

Kellogg, L.H., Hager, B.H., van der Hilst, R.D., 1999. Compositional stratification in the deep mantle. Science 283, 1881–1884.

Kinzler, R.J., Grove, T.L., 1992. Primary magmas of mid-ocean ridge basalts. 1. Experiments and methods. J. Geophys. Res. 97, 6885–6906.

Klügel, A., 1998. Reactions between mantle xenoliths and host magma beneath La Palma (Canary Islands): constraints on magma ascent rates and crustal reservoirs. Contrib. Mineral. Petrol. 131, 237–257.

Klügel, A., Schmincke, H.-U., White, J.D.L., Hoernle, K.A., 1999. Chronology and volcanology of the 1949 multi-vent rift-zone eruption on La Palma (Canary Islands). J. Volcanol. Geotherm. Res. 94, 267–282.

Klügel, A., Hoernle, K.A., Schmincke, H.-U., White, J.D.L., 2000. The chemically zoned 1949 eruption on La Palma (Canary Islands): petrologic evolution and magma supply dynamics of a rift-zone eruption. J. Geophys. Res. 105, 5997–6016.

Kyser, T.K., O'Neil, J.R., Carmichael, I.S.E., 1981. Oxygen isotope thermometry of basic lavas and mantle nodules. Contrib. Mineral. Petrol. 77, 11–23.

LaTourrette, T., Hervig, R.L., Holloway, J.R., 1995. Trace element partitioning between amphibole, phlogopite, and basanite melt. Earth Planet. Sci. Lett. 135, 13–30.

Lavrent'ev, Yu.G., Pospelova, L.N., Sobolev, N.V., 1974. Rock-forming mineral compositions determination by X-ray microanalysis. Zavod. Lab. 40, 657–666 (in Russian).

Lundstrom, C.C., Hoernle, K., Gill, J., 2003. U-series disequilibria in volcanic rocks from the Canary Islands: plume versus lithospheric melting. Geochim. Cosmochim. Acta 67, 4153–4177.

Marcantonio, F., Zindler, A., Elliott, T., Staudigel, H., 1995. Os isotope systematics of La Palma, Canary Islands; evidence foe recycled crust in the mantle source of HIMU ocean islands. Earth Planet. Sci. Lett. 133, 397–410.

Martí, J., Mitjavila, J., Araña, V., 1994. Stratigraphy, structure and geochronology of the Las Cañadas Caldera (Tenerife, Canary Islands). Geol. Mag. 131, 15–727.

Martí, J., Hurlimann, M., Ablay, G.J., Gudmundsson, A., 1997. Vertical and lateral collapses on Tenerife (Canary Islands) and other volcanic ocean islands. Geology 25, 879–882.

Marty, B., Humbert, F., 1997. Nitrogen and argon isotopes in oceanic basalts. Earth Planet. Sci. Lett. 152, 101–112.

Marty, B., Appora, I., Barrat, J.-A., Deniel, C., Vellutini, P., Vidal, P., 1993. He, Ar, Sr, Nd and Pb isotopes in volcanic rocks from Afar: evidence for a primitive mantle component and constraints on magmatic sources. Geochem. J. 27, 219–228.

McKenzie, D., O'Nions, R.K., 1991. Partial melt distributions from inversion of rare earth element concentrations. J. Petrol. 32, 1021–1091.

Middlemost, E.A.K., 1970. San Miguel de La Palma—A volcanic island in section. Bull. Volcanol. 34, 216–239.

Montelli, R., Nolet, G., Dahlen, F.A., Masters, G., Engdahl, E.R., Hung, S.-H., 2004. Finite-frequency tomography reveals a variety of plumes in the mantle. Science 303, 338–343.

Moore, W.B., Schubert, G., Tackley, P., 1998. Three-dimensional simulations of plume–lithosphere interaction at the Hawaiian swell. Science 279, 1008–1011.

Morgan, J.W., 1971. Convection plumes in the lower mantle. Nature 230, 42–43.

Morgan, J., Morgan, W.J., Price, E., 1995. Hotspot melting generates both hotspot volcanism and a hotspot swell? J. Geophys. Res. 100, 8045–8062.

Navarro, J.M., Coello, J., 1989. Depressions originated by landslide processes in Tenerife. ESF, Meeting on Canarian Volcanism, pp. 150–152.

Neumann, E.-R., 1991. Ultramafic and mafic xenoliths from Hierro, Canary Islands: evidence for melt infiltration in the upper mantle. Contrib. Mineral. Petrol. 106, 236–252.

Neumann, E.-R., Wulff-Pedersen, E., 1997. The origin of highly silicic glass in mantle xenoliths from the Canary Islands. J. Petrol. 38, 1513–1539.

Neumann, E.-R., Wulff-Pedersen, E., Johnsen, K., Andersen, T., Krogh, E., 1995. Petrogenesis of spinel harzburgite and dunite suite xenoliths from Lanzarote, eastern Canary Islands: implications for the upper mantle. Lithos 35, 83–107.

Neumann, E.-R., Wulff-Pedersen, E., Simonsen, S.L., Pearson, N.J., Martí, J., Mitjavila, J., 1999. Evidence for fractional crystallization of periodically refilled magma chambers in Tenerife, Canary Islands. J. Petrol. 40, 1089–1123.

Neumann, E.-R., Sørensen, V.B., Simonsen, S.L., Johnsen, K., 2000. Gabbroic xenoliths from La Palma, Tenerife and Lanzarote, Canary Islands: evidence for reactions between mafic alkaline Canary Islands melts and old oceanic crust. J. Volcanol. Geotherm. Res. 103, 313–342.

Nikogosian, I.K., Elliott, T., Touret, J.L.R., 2002. Melt evolution beneath thick lithosphere: a magmatic inclusion study of La Palma, Canary Islands. Chem. Geol. 183, 169–193.

O'Hara, M.J., 1968. The bearing of phase equilibria studies in synthetic and natural systems on the origin and evolution of basic and ultrabasic rocks. Earth Sci. Rev. 4, 69–133.

Ozima, M., Podosek, F.A., 1983. Noble Gas Geochemistry. Cambridge University Press, Cambridge.

Pérez, N.M., Nakai, S., Wakita, H., Sano, Y., Williams, S.N., 1994. $^{3}He/^{4}He$ isotopic ratios in volcanic–hydrothermal discharges from the Canary Islands, Spain: implications on the origin of the volcanic activity. Mineral. Mag. 58, 709–710.

Pérez, N.M., Nakai, S., Wakita, H., Hernandez, P.A., Salazar, J.M., 1996. Helium-3 emission in and around Teide volcano, Tenerife, Canary Islands, Spain. Geophys. Res. Lett. 23, 3531–3534.

Porcelli, D., Ballentine, C.J., Wieler, R., 2002. An overview of noble gas geochemistry and cosmochemistry. In: Porcelli, D., Ballentine, C.J., Wieler, R. (Eds.), Noble Gases in Geochemistry and Cosmochemistry. Rev. Mineral., vol. 47. Mineralogical Society of America, Washington, DC, pp. 1–18.

Rehkämper, M., Hofmann, A.W., 1997. Recycled ocean crust and sediment in Indian Ocean MORB. Earth Planet. Sci. Lett. 147, 93–106.

Revenaugh, J., Meyer, R., 1997. Seismic evidence of partial melt within a possibly ubiquitous low-velocity layer at the base of the mantle. Science 277, 670–673.

Roeder, P.L., Emslie, R.F., 1970. Olivine–liquid equilibrium. Contrib. Mineral. Petrol. 29, 275–289.

Sarda, P., 2004. Surface noble gas recycling to the terrestrial mantle. Earth Planet. Sci. Lett. 228, 49–63.

Schmincke, H.-U., 1976. Geology of the Canary islands. In: Kunkel, G. (Ed.), Biogeography and Ecology of the Canary Islands. Junk, The Hague, pp. 67–184.

Schmincke, H.-U., 1982. Volcanic and chemical evolution of the Canary islands. In: von Rad, U., Hinz, K., Sarnthein, M., Seibold, E. (Eds.), Geology of the Northwest African Continental Margin. Springer, pp. 273–306.

Schmincke, H.-U., 1998. Zeitliche, strukturelle und vulkanische Entwicklung der Kanarischen Inseln, der Selvagens Inseln und des Madeira-Archipels. In: Böhme, W. (Ed.), Handbuch der Reptilien und Amphibien Europas. Die Reptilien der Kanarischen Inseln, der Selvagens Inseln und des Madeira-Archipels. AULA, Wiesbaden, pp. 27–69.

Schmincke, H.-U., Flower, M.J.F., 1974. Magmenevolution auf atlantischen Vulkaninseln. Naturwissenschaften 61, 288–297.

Schmincke, H.-U., Segschneider, B., 1998. Shallow submarine to emergent basaltic shield volcanism of Gran Canaria: evidence from drilling into the volcanic apron. In: Weaver, P.P.E., Schmincke, H.-U., Firth, J.V., Duffield, W. (Eds.), Proceedings of the Ocean Drilling Program. Scientific Results, vol. 157. Ocean Drilling Program, College Station, TX, pp. 141–181.

Schmincke, H.-U., Sumita, M., 1998. Volcanic evolution of Gran Canaria reconstructed from apron sediments: Synthesis of VICAP project drilling (ODP Leg 157). In: Weaver, P.P.E., Schmincke, H.-U., Firth, J.V., Duffield, W. (Eds.), Proceedings of the Ocean Drilling Program. Scientific Results, vol. 157. Ocean Drilling Program, College Station, TX, pp. 443–469.

Schmincke, H.-U., Klügel, A., Hansteen, T.H., Hoernle, K., van den Bogaard, P., 1998. Samples from the Jurassic ocean crust beneath Gran Canaria, La Palma and Lanzarote (Canary Islands). Earth Planet. Sci. Lett. 163, 343–360.

Shaw, D.M., 1970. Trace element fractionation during anatexis. Geochim. Cosmochim. Acta 34, 237–243.

Simonsen, S.L., Neumann, E.-R., Seim, K., 2000. Sr–Nd–Pb isotope and trace-element geochemistry evidence for a young HIMU source and assimilation at Tenerife (Canary Island). J. Volcanol. Geotherm. Res. 103, 299–312.

Sobolev, A.V., Hofmann, A.W., Sobolev, S.V., Nikogosian, I.K., 2005. An olivine-free mantle source of Hawaiian shield basalts. Nature 434, 590–597.

Staudigel, H., Schmincke, H.-U., 1984. The Pliocene seamount series of La Palma/Canary Islands. J. Geophys. Res. 89, 11195–11215.

Sun, S.S., 1980. Lead isotopic study of young volcanic rocks from mid-ocean ridges, ocean islands and island arcs. In: Bailey, K., Tarney, J., Dunham, K. (Eds.), The Evidence for Chemical Heterogeneity in the Earth's Mantle. Royal Society of London, pp. 409–445.

Taylor, S.R., McLennan, S.M., 1985. The Continental Crust: Its Composition and Evolution. Blackwell, Oxford.

Terashima, S., Imai, N., Itoh, S., Ando, A., Mita, N., 1994. 1993 compilation of analytical data for major elements in seventeen GSJ geochemical reference samples, "Igneous Rock Series". Bull. Geol. Surv. Jpn. 45, 305–381.

Thirlwall, M.F., 1997. Pb isotopic and elemental evidence for OIB derivation from young HIMU mantle. Chem. Geol. 139, 51–74.

Thirlwall, M.F., Jenkins, C., Vroon, P.Z., Mattey, D.P., 1997. Crustal interaction during construction of oceanic islands: Pb–Sr–Nd–O isotope geochemistry of the shield basalts of Gran Canaria, Canary Islands. Chem. Geol. 135, 233–262.

Thirlwall, M.F., Singer, B.S., Marriner, G.F., 2000. $^{39}Ar–^{40}Ar$ ages and geochemistry of the basaltic shield stage of Tenerife, Canary Islands, Spain. J. Volcanol. Geotherm. Res. 103, 247–297.

Todt, W., Cliff, R.A., Hanser, A., Hofmann, A.W., 1996. Evaluation of a $^{202}Pb–^{205}Pb$ double spike for high precision lead isotope analyses. In: Basu, A., Hartm, S. (Eds.), Earth Processes: Reading the Isotope Code. Geophys. Monograph., vol. 95. American Geophysical Union, pp. 429–437.

Trieloff, M., Kunz, J., Clague, D.A., Harrison, D., Allègre, C.J., 2000. The nature of pristine noble gases in mantle plumes. Science 288, 1036–1038.

Van der Hilst, R., Widiyantoro, R.S., Engdahl, R., 1997. Evidence for deep mantle circulation from global tomography. Nature 386, 578–584.

Vroon, P.Z., Lowry, D., van Bergen, M.J., Boyce, A.J., Mattey, D.P., 2001. Oxygen isotope systematics of the Banda Arc: low $\delta^{18}O$ despite involvement of subducted continental material in magma genesis. Geochim. Cosmochim. Acta 65, 589–609.

Walter, T.R., Schmincke, H.-U., 2002. Rifting, recurrent landsliding and Miocene structural reorganization on NW-Tenerife (Canary Islands). Int. J. Earth Sci. (Geol. Rundsch.) 91, 615–628.

Walter, T.R., Troll, V.R., Cailleau, B., Belousov, A., Schmincke, H.-U., Amelung, F., van den Bogaard, P., 2005. Rift zone reorganization through flank instability in ocean island volcanoes: an example from Tenerife, Canary Islands. Bull. Volcanol. 67, 281–291.

Watson, S., McKenzie, D., 1991. Melt generation by plumes: a study of Hawaiian volcanism. J. Petrol. 32, 501–538.

Weaver, B.L., 1991. The origin of ocean island basalt end-member compositions: trace element and isotopic constraints. Earth Planet. Sci. Lett. 104, 381–397.

White, W.M., 1997. Geochemistry. An On-Line Text-Book. Cornell University. Available at http://www.geo.cornell.edu/geology/classes/geo455/Chapters.HTML.

Widom, E., Hoernle, K.A., Shirey, S.B., Schmincke, H.-U., 1999. Os isotope systematics in the Canary Islands and Madeira: lithospheric contamination and mantle plume signatures. J. Petrol. 40, 297–314.

Widom, E., Farquhar, J., 2003. Oxygen isotope signatures in olivines from Sao Miguel (Azores) basalts: implications for crustal and mantle processes. Chem. Geol. 193, 237–255.

Williams, Q., Garnero, E.J., 1996. Seismic evidence for partial melt at the base of the Earth's mantle. Science 273, 1528–1530.

Williams, Q., Revenaugh, J., Garnero, E., 1998. A correlation between ultra-low basal velocities in the mantle and hot spots. Science 281, 546–549.

Wulff-Pedersen, E., Neumann, E.-R., Vannucci, R., Bottazzi, P., Ottolini, L., 1999. Silicic melts produced by reaction between peridotite and infiltrating basaltic melts: ion probe data on glasses and minerals in veined xenoliths from La Palma, Canary Islands. Contrib. Mineral. Petrol. 137, 59–82.

Wyllie, P.J., 1988. Solidus curves, mantle plumes, and magma generation beneath Hawaii. J. Geophys. Res. 93, 4171–4181.

Yoder, H.S., Tilley, C.E., 1962. Origin of basaltic magmas: an experimental study of natural and synthetic rock systems. J. Petrol. 3, 342–532.

Zindler, A., Hart, S., 1986. Chemical geodynamics. Annu. Rev. Earth Planet. Sci. 14, 493–571.